Schwann cells restrict axonal diameters via CMTM6

Dissertation

for the award of the degree

"Doctor rerum naturalium"

of the Georg-August-Universität Göttingen

within the doctoral program Biology

of the Georg-August University School of Science (GAUSS)

submitted by

Maria Eichel

from Pirna

Göttingen, 13.03.2020

Thesis Committee

Dr. Hauke B. Werner (1st Reviewer)

Department of Neurogenetics

Max-Planck-Institute of Experimental Medicine

Prof. Dr. Alexander Flügel (2nd Reviewer)

Institute for Neuroimmunology and Multiple Sclerosis Research

University Medical Center Göttingen

Prof. Dr. Ralf Heinrich

Department of Cellular Neurobiology

Georg-August University Göttingen

Further member of the Examination Board

Prof. Dr. Dr. Hannelore Ehrenreich

Clinical Neuroscience

Max-Planck-Institute of Experimental Medicine

Prof. Dr. Manual Schmidt

Somatosensory Signaling and Systems Biology

Max-Planck-Institute of Experimental Medicine

Prof. Dr. Christine Stadelmann-Nessler

Institute for Neuropathology

University Medical Center Göttingen

Declaration

I hereby declare that the Ph. D. thesis entitled, “Schwann cells restrict axonal diameters via CMTM6”, was written independently and with no other sources and aids than quoted.

Göttingen, 13.3.2020

Maria Eichel

“Curiosity is in great and generous minds the first passion and the last”
- *William Samuel Johnson*

Acknowledgements

First and foremost, I would like to thank my supervisor Dr. Hauke B. Werner for all the lively scientific but also non-scientific discussions we had and for the trust and freedom he gave me during my time as a doctoral researcher in his group. I really appreciated the chance to work on joint projects and the familiar working atmosphere which made it possible for me to grow scientifically and personally. Thank you for your patience, respect and endurance regarding all questions and opinions I had even if they sometimes appeared out of the normal.

Secondly, I want to thank Prof. Dr. Klaus-Armin Nave for giving me the opportunity to work in his department. Thank you for your respect, critical advices and sharing of scientific expertise.

I would like to thank both my thesis advisory committee members, Prof. Dr. Alexander Flügel and Prof. Dr. Ralf Heinrich for insightful comments and discussions during my presentations as well as advice on how to proceed with my projects within the timeframe of this thesis. I would also like to thank my thesis examination committee, namely Prof. Dr. Dr. Hannelore Ehrenreich, Prof. Dr. Manuela Schmidt and Prof. Dr. Christine Stadelmann-Nessler. Thank you for taking the time on this special day.

I am sincerely grateful to both Dr. Robert Fledrich and Dr. Theresa Kungl who took the time to discuss many scientific outcomes and strongly motivated me with their high interest in this project. Thank you for teaching me electrophysiology and peripheral nerve dissections.

A big thank you also to our collaborators Dr. Elisa D´Este, Dr. Robert Fledrich, Dr. Kathrin Kusch, Dr. Wiebke Möbius, Dr. Ute Distler, Prof. Dr. Swen Hülsmann and Prof. Dr. Stefan Tenzer for their supportive contributions towards this project.

I would especially like to thank previous and recent members of the AG Werner: Julia Patzig, Michelle Erwig and Katja Lüders for being there at my first steps and teaching me all the necessities. A big thank you to Ramona Jung, Sophie Siems, Vasiliki-Ilya Gargareta and Tobias Buscham for all the discussions, everything we worked on, laughter filled chocolate breaks and your utmost encouraging spirit – this would not have happened without your support! Thanks also to Anna Bretschneider for taking care of the genotyping of mice.

I am grateful to the outstanding students I had the pleasure to supervise: Silya thank you for tackling new hypotheses together with me, to Cristina Miracle, Gesa Albers and Benedict Atzler for their contributions to this project and beyond during your lab rotation and bachelor thesis.

Special thanks goes to the Max Planck PhDnet and especially Jana Lasser, the Steering group of 2018 and Niklas Michel for encouraging me to engage in sometimes challenging situations and your inspiring attitude to shape a better future for scientist! Also, thank you to the Offspring magazine team of the last 3 years for this amazing time and the many lovely articles we produced.

Many thanks also go to…

…Michaela Schmalstieg for all the administrative support and the lovely and chatty balcony coffee times in the morning.

… our animal caretakers Marion Peine, Sarah Schulze and Kerstin Claus for always keeping an eye on my mice and that our work together always went smoothly.

… Dr. Sarah Kimmina, Dr. Ursula Fünfschilling and Dr. Anke Schräpler for providing an excellent mouse house, transgenic animal facility and support when it comes to animal licences.

… the EDV team: Martin, Rolf, Hajo, Lothar and Beate for their continuous support when something technical crashed or did not work as expected.

… Dr. Wiebke Möbius, Torben Ruhwedel and Boguslawa Sadowski for introduction and the friendly support in the electron microscopy facility.

… Ulli Bode, Anette Fahrenholz and Uschi Kutzke for your technical support.

…The “GOT & Neurogen Stuff group” and former lab members: Stefan Berghoff, Swati Subramanian, Lisa Linhoff, Lena Spieth, Tim Düking, Jan Winchenbach, Martin Meschkat, Ting Sun, Constanze Depp, Doris Hermes, Alejandro Restrepo: Thanks for the unforgettable times, the delicious lunches, the scientific and sometimes rebellious discussions, spontaneous wine evenings and late-night dinners!

… Der Harte Kern and beyond: Verena, Lisa, Tina and Jule for being the best Master Crew ever, making me leave the lab earlier to meet with you and the fun times we had. Verena for your continuous support even if you are literally on the other side of the world!

…Elisa for being the best flat mate ever, for all the wine & late-night chats, your constant open ears when I was complaining about whatsoever and your encouragement when we were trying to figure out what to do with our lives!

…Chris Weiß for being there literally every step along the way since our bachelors.

… #Crewlove – thank you for being there since a long time and accepting the sometimes-crazy scientist in your rows.

… Alice and Tina for all the encouraging chats we had about future, for your genuine interest in what life will bring next for me, for trying to understand what I indeed do and for making me laugh. Also, to Benni for not even trying to understand what I do but being there anyways.

… Maria for already letting chemical reagents explode with me back in school and for the most honest and longest friendship one can wish for.

… Riesengroßer Dank geht an meine Mom Andrea. Danke für deine stetige mentale Unterstützung, dafür dass du immer da bist und mich zu dem Menschen erzogen hast der ich bin. Danke, dass du stets an mich geglaubt hast und ein Vorbild bist: Es geht immer weiter nach vorn egal wo man herkommt! Diese Arbeit ist dir gewidmet.

... Ein großer Dank für all die Unterstützung, euer Interesse und die tollen Momente in den letzten Jahren geht auch an meine Oma, an Andras, meine Schwestern, Neffen und Nichten, sowie an Andreas und Manon.

... Danke an meinen Partner in Crime und besten Freund Tobias. Danke für deine Unterstützung, deine Geduld, die tollen Reisen und deinen Glauben an mich vom ersten Tag meines Studiums bis zu diesem Moment und garantiert noch viel weiter!

Content

List of Figures and Tables

Abbreviations

AEF	Axogliasome-enriched fraction
ATP1a1	ATPase 1 alpha 1
cKo	Conditional knockout
CAMS	Cell-adhesion molecules
CASPR	Contactin-associated protein
CD274/PD-L1	Programmed-death ligand 1
CKLF	Chemokine-like factor
CMAP	Compound muscle action potential
CMT	Charcot-Marie-Tooth
CMTM	Chemokine-like factor-like MARVEL transmembrane domain-containing family
CNS	Central nervous system
CNP	2'3'-cyclic nucleotide 3'phosphodiesterase
Dhh	Desert hedgehog
E	Embryonic day
ECM	Extracellular matrix
e.g.	*Exempli gratia*
EM	Electron microscopy
ErbB	Epidermal growth factor receptor
Fig.	Figure
GPR126	G-protein coupled receptor 126
iSCs	Immature Schwann cells
JXP	Juxtaparanode
kDa	Kilodalton
Ko	Knockout
log_2FC	Log_2 fold change
MAG	Myelin associated glycoprotein
MBP	Myelin basic protein
mNCV	Motor nerve conduction velocity
mo	month
MPI-EM	Max Planck Institute of Experimental Medicine
mRNA	messenger RNA
n	biological replicate number

NCV	Nerve conduction velocity
NEFH/NF-H	Neurofilament-heavy chain
NF	Neurofilaments
Nf155/NFASC155	Neurofascin 155
Nrg1 type III	Neuregulin 1 type III
n.s.	non-significant
P0/MPZ	Myelin protein zero
P	Postnatal day
PLP	Proteolipid protein
PMP2	Peripheral myelin protein 2
PMP22	Peripheral myelin protein of 22 kDa
PNS	Peripheral nervous system
ppm	Parts per million
q-RT PCR	Quantitative real-time PCR
RSC	Remak-associated Schwann cell
SC	Schwann cell
SCP	Schwann cell precursor
SD	Standard Deviation
SLI	Schmidt-Lantermann incisure
SNAP	Sensory nerve action potential
sNCV	Sensory nerve conduction velocity
STED	Stimulated-emission-depletion microscopy
WT	Wild-type

Material & methods: compounds, quantities and units

°C	Degree Celsius
µm	micro-meter
ANOVA	Analysis of variance
bp	base pairs
cDNA	Complementary DNA
DAPI	4'-6-Diamidino-2-phenylindole
ddH20	Double-destilled water/H2O
dNTP	Deoxyribonucleoside triphosphate

EMMA	European Mouse Mutant Archive
g	Gravity
g	Gramm
h	Hour(s)
K&S	Karlsson-Schultz fixative
M	Molar
m	Meter
min	Minutes
mm	Millimeter
nm	Nanometer
o/n	over-night
p	P-value
PBS	Phosphate-buffered saline
PCR	Polychain reaction
PFA	Paraformaldehyde
PVDF	Polyvinylidene difluoride
RT	Room temperature
SDS PAGE	Sodium dodecyl sulfate-polyacrylamide gel electrophoresis
sec	Seconds
TRIS	Tris-buffered saline
v/v	Volume per volume
V	Volt
w/v	Weight per volume

1 Abstract

Myelination of axons accelerates nerve impulse propagation 20-100-fold, theoretically allowing rapid nerve conduction with reduced axonal diameters. However, to our knowledge no myelin dependent signal has been described to restrict axonal diameters. Indeed, the only myelin-to-axon signal known to affect axonal size, myelin associated glycoprotein (MAG), actually increases radial axonal growth of myelinated axons in the peripheral nervous system. We hypothesized that many signaling molecules mediating cross-talk between axons and myelinating Schwann cells remain unknown. Thus, we used label-free proteomics of a biochemically fraction enriched for axon/myelin interface to identify novel signaling candidates. By STED-microscopy, immunoblotting and cryo-immuno electron microscopy we confirmed the localization of a novel Schwann cell protein CMTM6 (chemokine-like factor-like MARVEL-transmembrane domain-containing protein 6) at the adaxonal Schwann cell membrane and thus identified a novel myelin constituent in the peripheral nervous system. Genetic disruption of *Cmtm6* expression in Schwann cells causes a substantial increase of axonal diameters in various peripheral nerves without impairing myelin biogenesis or axonal integrity. Diameters of non-myelinated axons are also increased when CMTM6 is lacking from Schwann cells. Importantly, radial sorting of axons and myelin biogenesis are not compromised. Notably, increased axonal diameters correlate with accelerated sensory nerve conduction velocity, enhanced sensory responses and perturbed motor performance. It was previously suggested that expression of CMTM6 in cancer cells and interaction with PD-L1 (programmed death ligand 1) limits anti-tumor immunity. Our data however do not support interactions of CMTM6 with PD-L1 in the peripheral nervous system. We could demonstrate that CMTM6-loss of function leading to larger axonal diameters overrides MAG-loss of function, which by itself causes a shift towards reduced axonal diameters. Together we find that Schwann cells utilize adaxonal proteins such as MAG and CMTM6 to regulate radial axonal growth and optimize nervous system function.

2 Introduction

2.1 Myelin and the axon/myelin unit

The complexity of the nervous system comprised of the central nervous system (CNS, brain and spinal cord) and peripheral nervous system (PNS, peripheral nerves) requires rapid impulse propagation along axons to fully perform sensory and motor capabilities as well as cognitive functions (Nave and Werner 2014). Two strategies evolved to provide faster conduction and more rapid information processing being either increase in axonal fiber size or the insulation of axons with myelin (Hartline and Colman 2007, Nave and Werner 2014).The ensheathment of axons by a multilayered myelin membrane in vertebrates (and some invertebrates) increases the transverse resistance and reduces the transverse capacitance of the axonal plasma membrane. The action potential is restricted to short unmyelinated segments, termed nodes of Ranvier, by insulating internodes (axonal segments between two nodes of Ranvier) and thus provides the structural basis for saltatory nerve impulse propagation. Consequently, the nerve conduction velocity is accelerated 20-100-fold compared to non-myelinated axons of the same diameter (also see Fig.4) (Tasaki 1939, Huxley and Stämpfli 1949, Huxley and Stämpfli 1951, Moore, Joyner et al. 1978, Hartline and Colman 2007, Nave and Werner 2014). Myelin is formed by so called myelinating glial cells: oligodendrocytes in the CNS and Schwann cells (SCs) in the PNS. Both cells wrap their membrane around the axon and thus form myelin sheaths. Nevertheless, oligodendrocytes and SCs differ not only in the number of axonal segments (internodes) one cell can myelinate (1:60 for oligodendrocytes, 1:1 for SCs), but also in their origin (Hildebrand, Bowe et al. 1994, Arroyo and Scherer 2000, Nave and Werner 2014). Even though myelin is known to contain up to 70% lipids, being mainly cholesterol, phospholipids and glycosphingolipids (Norton and Autilio 1965, Norton and Poduslo 1973) the protein composition between CNS and PNS myelin differs resulting in distinctive molecules that regulate the structure of the axon/myelin unit and control myelination (Patzig, Jahn et al. 2011, De Monasterio-Schrader, Jahn et al. 2012, Nave and Werner 2014).

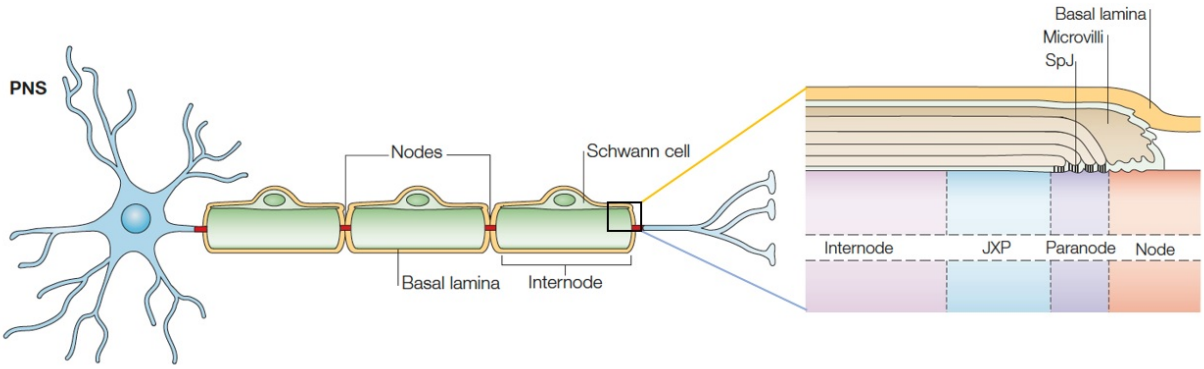

Figure 1 Structure of a myelinated axon of the peripheral nervous system (PNS). The myelinating glial cells of the PNS, namely Schwann cells (SCs), wrap their membrane around an axon and thus form the multilayered myelin sheath. Non-myelinated segments between myelinated internodes are called nodes of Ranvier, contain Na^+ channels and thus are the areas to which the action potentials are restricted to. The longitudinal cut (right) illustrates one heminode and the different axonal domains. Segments divide into the node of Ranvier to which SC microvilli attach, paranodes with septate-like junctions (SpJ), juxtaparanode (JXP) and the internode. Noteworthy, in the PNS the myelin/axon unit is covered by a basal lamina. (Fig.1 adapted from Poliak & Peles, 2003)

Figure 1 displays the distinct functional domains of myelinated axons illustrating the aforementioned node of Ranvier, the paranode as well as juxtaparanode (JXP) and the myelinated internodal segments which are organized and maintained via different mechanism involving numerous proteins (Poliak and Peles 2003). Briefly, in the peripheral nervous system microvilli extent from SCs and contact the node of Ranvier which contain a high density of voltage-gated Na^+ channels mediating saltatory conduction as well as transmembrane and cytoskeleton proteins such as cell-adhesion molecules (CAMs), ankyrin G and spectrin βIV (Kordeli, Davis et al. 1990, Davis, Lambert et al. 1996, Berghs, Aggujaro et al. 2000, Poliak and Peles 2003). The nodes are flanked by two paranodes forming a close association between myelin lamellae and the axon septate-like junctions, attaching the myelin to the axons. Here, mainly but not exclusively, contactin and contactin-associated protein (CASPR) and protein 4.1B in the axolemma as well as neurofascin 155 (Nf155) and ankyrin B in the SC membrane are essential molecular components of the paranodal junction (Peles, Nativ et al. 1997, Charles, Tait et al. 2002, Poliak and Peles 2003, Zollinger, Baalman et al. 2015). The juxtaparanodal segment, followed by the internode, are both laying beneath compact myelin layers. A high density of voltage-gated K^+ channels is the most prominent feature of juxtaparanodal domains which most likely play a role in maintaining the internodal resting potential (Chiu and Ritchie 1984, Poliak and Peles 2003). Mainly CASPR2 and transient-axonal glycoprotein1 (TAG1), as well as protein 4.1B and postsynaptic density protein 95 (PSD95) stabilize the juxtaparanodal complex and regulate clustering of K^+ channels (Poliak and Peles 2003, Poliak, Salomon et al. 2003, Traka, Goutebroze et al. 2003). The internode extends next to

the juxtaparanodes and also lies beneath compact myelin. The outermost layer is referred to as the abaxonal myelin membrane while the innermost layer is referred to as the adaxonal membrane. Both are comprised of non-compact myelin. The abaxonal membrane is opposing the basal lamina which is covering the axon/myelin unit in the PNS (Arroyo and Scherer 2000). Another distinct feature of the organization of myelinated axons in the PNS is the presence of Schmidt-Lantermann incisures (SLI) which are thought to provide cytosolic channels through the compact myelin and are also part of non-compact myelin (Arroyo and Scherer 2000). Besides SLI also the innermost adaxonal SC membrane connecting to the underlying axon is part of the non-compact myelin (Arroyo and Scherer 2000, Nave and Werner 2014). Interestingly, optimized biochemical purification methods and mass spectrometric analysis allow investigations of the protein content of myelin as well as of the contact zone between axon and myelin/myelinating glia cells, also referred to as axon/myelin unit, in more detail (see chapter 1.4) (Jahn, Tenzer et al. 2009, Patzig, Jahn et al. 2011, Erwig, Hesse et al. 2019). Note that aforementioned molecules involved in structural domain organization can differ between CNS and PNS or change during development. Further, deletion of some of these proteins can disrupt the described domain organization leading to various changes and functional impairment. However, the molecular basis for this structural organization is not yet fully understood. Refer to the following reviews for more information: (Arroyo and Scherer 2000, Poliak and Peles 2003, Salzer 2003, Zollinger, Baalman et al. 2015).

Besides insulating axons with myelin, it was shown that oligodendrocytes and SCs provide additional trophic support to axons and thus maintain axonal integrity (Nave and Werner 2014). Particularly, mouse models with specific mutations in myelinating glial genes as well as human patients suffering from either peripheral neuropathies caused by SC-specific gene mutations or neurological diseases e.g. Multiple sclerosis or leukodystrophies affecting oligodendrocytes, suggest that myelinating glial cells support axon function and survival (Pellerin, Pellegri et al. , Riethmacher, Sonnenberg-Riethmacher et al. 1997, Nave and Trapp 2008, Nave 2010, Nave 2010, Fünfschilling, Supplie et al. 2012, Lee, Morrison et al. 2012, Domènech-Estévez, Baloui et al. 2015, Stassart, Möbius et al. 2018). The following chapters will focus in more detail on the interaction of Schwann cells and axons and beyond to ensure proper nervous system development and maintenance. For more

information about the communication between oligodendrocytes and axons in the CNS one can refer to the following reviews: (Nave and Trapp 2008, Nave and Werner 2014, Stassart, Möbius et al. 2018).

2.2 Schwann cells and axo-glial interactions

2.2.1 Schwann cell development

During development of the nervous system the Schwann cell lineage progression follows well-defined steps displaying crucial interdependence of axons and SCs (Jessen and Mirsky 2005). The following chapter will outline the major steps of the SC lineage as illustrated schematically in Figure 2 and highlight the most important but not all, key players.

During early embryonic development multipotent neural crest cells give rise to Schwann cell precursors (SCPs) at around embryonic day 12/13 (Douarin, Dulac et al. 1991). These have the ability to further differentiate into immature Schwann cells (iSCs) but also to endoneurial fibroblasts, melanocytes and parasympathetic neurons in embryonic peripheral nerves (Jessen, Mirsky et al. 2015, Jessen and Mirsky 2019). This feature is similar to radial glia in the CNS which give rise to neurons, astrocytes, oligodendrocytes and ependymal cells (Merkle et al., 2004). In addition, SCP are crucial for nerve fasciculation and survival of sensory DRG neurons as well as spinal cord motoneurons (Woldeyesus, Britsch et al. 1999, Birchmeier 2009, Jessen, Mirsky et al. 2015). Interestingly, it was shown *in vivo* that SCPs die without axonal contact and further depend on axonal survival signal Neuregulin 1 type III (Nrg1 type III) and its interaction with epidermal growth factor receptors (Erb2B2/ErbB3) on the SC side (Dong, Brennan et al. 1995, Meyer and Birchmeier 1995, Riethmacher, Sonnenberg-Riethmacher et al. 1997). One of the main roles of neuregulin 1 type III is the suppression of neurogenesis and promotion of gliogenesis which supports the switch from SCP towards immature Schwann cells (iSCs) and illustrates nicely the interdependence of SC and axons (Shah, Marchionni et al. 1994, Birchmeier and Nave 2008, Jessen, Mirsky et al. 2015). Note, that the Nrg1/ErbB axis plays a pivotal role during SC development and differentiation, but also peripheral myelination and repair and the following reviews cover the diverse role of Neuregulin in more depth: (Birchmeier and Nave 2008, Mei and Nave 2014, Fledrich, Kungl et al. 2019). Further, also the SC lineage specific transcription factor Sox 10 is crucial as it maintains ErbB3

receptors on SCs, demonstrating that SC lineage is also reliant on each other (Britsch, Goerich et al. 2001). Noteworthy, also negative signals are involved at this step of SC lineage progression. Two examples are endothelin and the transcription factor AP2α which both delay the differentiation of SCPs into immature SCs (Brennan, Dean et al. 2000, Stewart, Brennan et al. 2001, Jessen, Mirsky et al. 2015).

At E15/E16 all SCP differentiated into iSCs, a step which is irreversible. At this point iSCs engulf axons and form defined axon/SC bundles covered by a basal lamina (Jessen and Mirsky 1999, Jessen, Mirsky et al. 2015, Jessen and Mirsky 2019). Importantly, from this step onwards SC survival, but not fate, is independent of axons because they establish an autocrine survival loop. This survival loop involves the expression of various growth factors, e.g. platelet-derived growth factor beta (PDGFβ), leukemia inhibitory factor (LIF), neurotrophin 3 (NT3) and insulin-like growth factor 2 (IGF2) (Jessen and Mirsky 1999, Meier, Parmantier et al. 1999, Jessen and Mirsky 2005). Nonetheless, survival of SCs can still be impaired upon injury in neonatal and adult nerves when SCs loose axonal contact over a prolonged period of time (Grinspan, Marchionni et al. 1996, Syroid, Maycox et al. 1996, Höke 2006, Jessen, Mirsky et al. 2015). Further, signals from iSCs also promote organization and differentiation of perineurial (e.g via secreting Desert hedgehog; Dhh) and endoneurial connective tissue (via SC secreted VEGF) as well as blood vessels (Webster, Martin et al. 1973, Parmantier, Lynn et al. 1999, Mukouyama, Gerber et al. 2005, Fledrich, Kungl et al. 2019). Most importantly, the process of radial sorting, a prerequisite for myelination, starts during this phase. Thus, a 1:1 ratio of axon/SC is established via sorting out of axons being larger than 1 µm in diameter. This crucial step is important for building up the mature nerve architecture for a functional peripheral nervous system and can lead to neuropathies when impaired (Feltri, Poitelon et al. 2016). Axonal signals, which trigger radial sorting and are involved in initiating myelination are for example brain-derived neurotrophic factor (BDNF), Nrg1 and IGF1 (Cheng, Reinhardt et al. 2000, Meintanis, Thomaidou et al. 2001, Taveggia, Zanazzi et al. 2005, Nave and Salzer 2006). Notably, also signals between iSCs and ECM/basal lamina molecules, including collagen, laminins and G protein-coupled receptor 126 (Gpr126/Adgrg6) affect radial sorting which is reviewed in more detail in (Monk, Feltri et al. 2015, Feltri, Poitelon et al. 2016, Mogha, D'Rozario et al. 2016).

After establishing a 1:1 ratio with axons larger than 1 µm SC reach the stage of a promyelinating Schwann cell. While promyelinating SCs still react to the aforementioned axonal signals and trophic factors they also change their own expression profiles of several transcription factors such as Krox-20/Egr2, Oct6, Sox10 and NfkB which is described in more detail in reviews by (Taveggia, Zanazzi et al. 2005, Monk, Feltri et al. 2015). Amongst those, Krox20/Egr2 is considered to be an important key player to initiate differentiation from promyelinating to myelinating SCs by inducing for example the expression of P0/MPZ, the most abundant peripheral myelin protein
(Parkinson, Bhaskaran et al. 2004, Mager, Ward et al. 2008, Monk, Feltri et al. 2015).

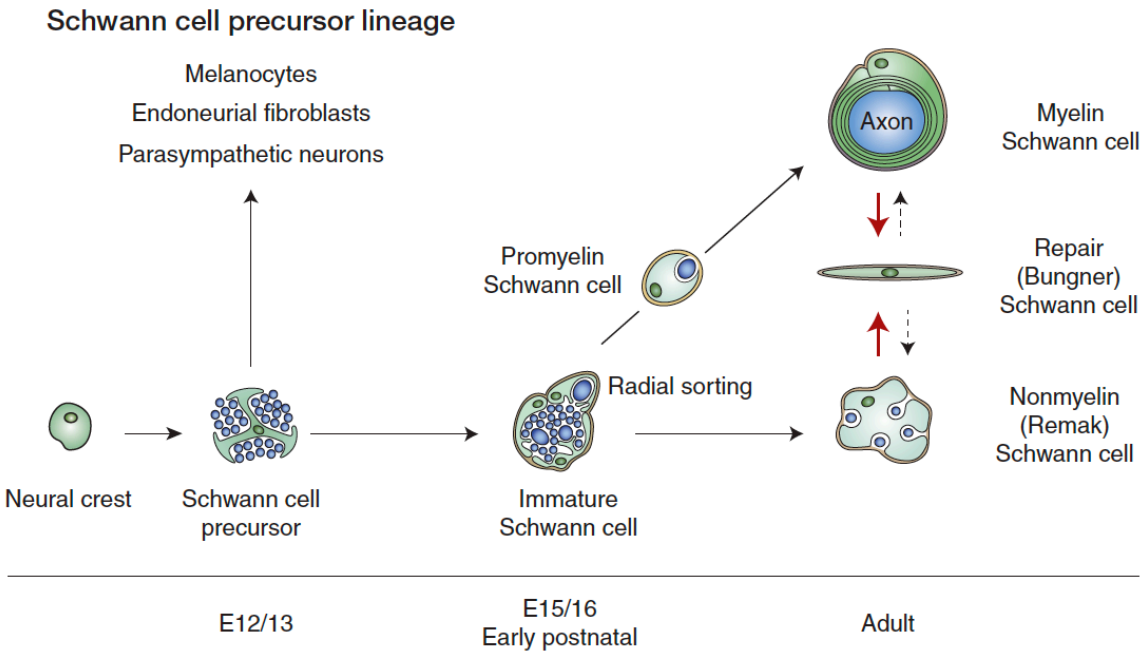

Figure 2 The Schwann cell lineage. This drawing illustrates the main transitions of the SC lineage from migrating neural crest cells into Schwann cell precursors (SCP) which group with several unsorted axons at embryonic day E12/E13. SCP differentiate into immature SCs (iSCs) but also give rise to melanocytes, endoneurial fibroblasts and parasympathetic neurons. iSC engulf several axons within Remak bundles and sort axons larger than 1µm out of bundles (radial sorting). When SC are in 1:1 contact with an axon which is large enough they transition from promyelinating SC to myelinating SC. Black uninterrupted arrows display normal development. Upon injury, both myelinating SCs and non-myelinating Remak-SCs can transdifferentiate into Repair (Bungner) SC (red arrow) and re-differentiate back to myelinating or Remak SC after repair (dashed arrow). Image taken from Jessen and Mirsky 2015.

2.2.2 Non-myelinating and repair SC

In the peripheral nervous system not all axons are myelinated post development. Thus, another class of SCs, referred to as non-myelinating SCs is present in peripheral nerves associating either with bundles of small caliber axons

(Remak SCs engulfing so called Remak-bundles); with neuromuscular junctions (terminal SCs) or Pacini and Meissner corpuscles (Griffin and Thompson 2008, Monk, Feltri et al. 2015). Non-myelinating Remak-associated Schwann cells (RSCs) are less investigated and it is not fully understood how their fate is exactly determined. Nevertheless, Figure 2 already indicates that SC differentiation is rather plastic and conversion between myelinating-, non-myelinating RSC and Repair SC is possible. This was especially demonstrated in nerve grafting studies by Aguayo. He could show that nerve segments with myelinating SC do not myelinate when grafted into unmyelinated nerve segments and *vice versa* transplantation of RSCs in myelinated nerve segment resulted in dedifferentiation and generation of myelin (Aguayo, Peyronnard et al. 1973, Aguayo, Attiwell et al. 1977, Murinson and Griffin 2004). On morphological level it was shown that RSC engulf several axons in a single bundle but that the number of axons surrounded by RSC processes differs between and along peripheral nerves (Aguayo, Peyronnard et al. 1973, Murinson and Griffin 2004). Nevertheless, defects in SCs and RSCs can lead either to impairment of radial sorting (axons larger than 1µm are not sorted out of Remak-bundles) or “naked axons” which are not ensheathed by RSCs (Feltri, Poitelon et al. 2016). Notably, many molecules and signaling pathways between myelinating SCs and RSCs overlap, such as Nrg1-type II/ErbB2/3, PI3K/Akt as well as Gpr126/Adgrg6, which is further reviewed in (Harty and Monk 2017).

Upon injury, SCs and RSCs have the ability to transdifferentiate to so-called Repair Schwann cells, which is until now thought to be mainly controlled by the transcription factor c-Jun (Arthur-Farraj, Latouche et al. 2012, Fontana, Hristova et al. 2012, Jessen and Mirsky 2016). Further, SCs in the distal stump respond to the injury even before axons degenerate suggesting a yet unknown SC/axon signal triggering the phenotypical changes that SCs undergo rapidly (Jessen, Mirsky et al. 2015). These prompt changes include for example upregulation of molecules from the iSCs stage (e.g. NCAM, P75NTR, GFAP, L1) and down-regulation of myelin genes such as *Mpz*, *Mbp* and *Mag*. Further, they upregulate neurotrophic factors (such as GDNF, artemin, BDNF, VEGF) to support neuronal survival and cytokines including TNFα, LIF and interleukins for macrophage recruitment (Jessen and Mirsky 2008, Jessen, Mirsky et al. 2015). Interestingly, it was also reported that SCs degrade their own myelin after injury via a process recently termed myelinophagy and further change their length and

morphology during repair (Gomez-Sanchez, Carty et al. 2015, Gomez-Sanchez, Pilch et al. 2017). The SC reprogramming in regenerating nerves is highly diverse involving several molecules and transcription factors which is reviewed in more detail in: (Jessen and Mirsky 2016). Even though the regenerative capacity of the PNS is comparably high full functional recovery in humans is rarely the case (Höke 2006). It will be interesting how future research focusing on the role and regulation of Repair SCs and their interactions might have a beneficial effect on recovery after nerve injury.

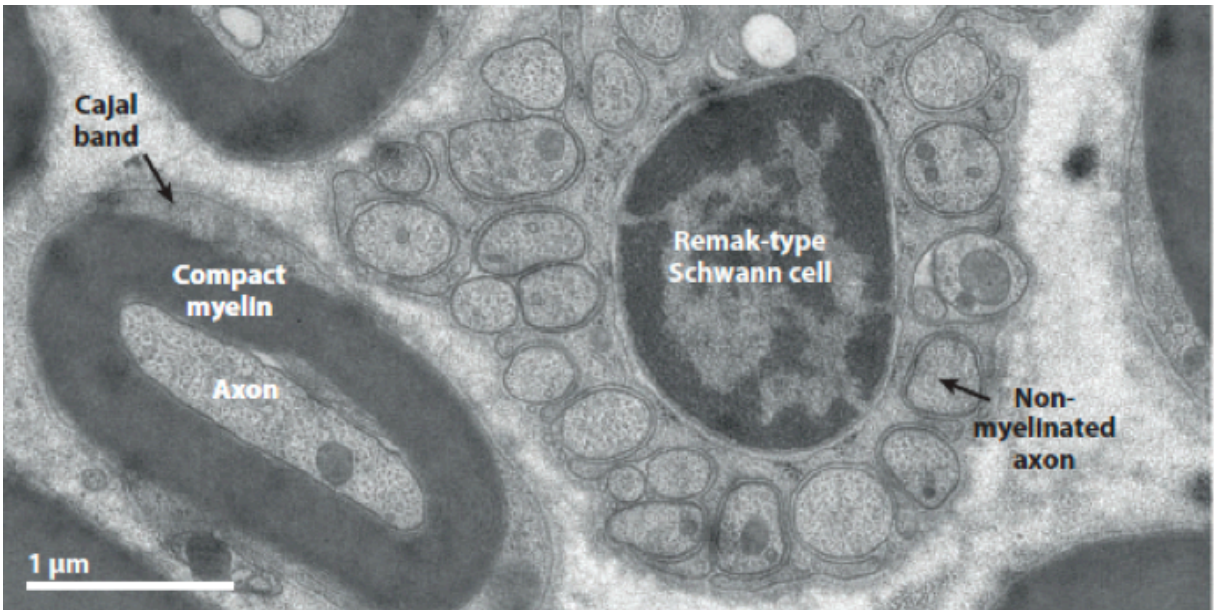

Figure 3 Ultrastructure of myelinated axons and non-myelinating Remak Schwann cell. Electron microscopic image of a cross-sectioned sciatic nerve illustrates a myelinated axon being surrounded by one myelinating SC which ensheathed the axon with a multilayered compacted myelin membrane. On the lower half a non-myelinating Remak SC engulfs several non-myelinated axons being smaller than 1 µm. The adaxonal SC membrane, axolemma and a non-myelinated axon are indicated by arrows. Scale bar = 1µm. Image taken from Nave & Werner, 2014.

2.2.3 Myelinating SCs: axo-glial interactions in peripheral nerves post development

As mentioned above axons with a threshold diameter of above 1µm are sorted out of Remak bundles and associate with promyelinating SC indicating that axonal signals steer myelination. Thus, it was shown that Nrg1 type III expressed on the axonal surface is sensed by ErbB2/B3 receptors on SCs controlling the amount of myelin in dependence on the axonal size (Michailov, Sereda et al. 2004, Taveggia, Zanazzi et al. 2005, Nave and Salzer 2006). This leads to activation of several pathways mainly involving PI3/Akt and MAPK signaling (Pertusa, Morenilla-Palao et al. 2007, Pereira, Lebrun-Julien et al. 2012, Glenn and Talbot 2013). Further, it was revealed that deletion of either axonal Disintegrin and metalloproteinase domain-

containing protein 22 (ADAM22) or SC expressed leucine rich repeat LG family member 4 (LGI4) lead to myelin formation defects underlining its importance for peripheral myelination (Kegel, Jaegle et al. 2014, Monk, Feltri et al. 2015). Several other molecules such as Notch1 interaction with axonal Jagged1, neurotrophins like BDNF, NGF and NT3 or cell adhesion molecules of the Nectin-like family (mainly NECL-1/CADM3 and NECL4/CADM4) are involved in steering peripheral myelination (reviewed in (Monk, Feltri et al. 2015). Even though axon to SC signaling plays a major role in myelination of peripheral nerves the interaction between SCs and the ECM is also crucial for radial sorting and subsequent myelination. Thus, studies have shown that G-protein coupled receptor GPR126/ADGRG6 controls radial sorting and similar to Nrg1 type III also initiates myelination. This occurs mainly by incorporating signals from laminins and collagens of the ECM and the abaxonal membrane leading to an elevation of second messenger cAMP (Paavola, Sidik et al. 2014, Petersen, Luo et al. 2015, Feltri, Poitelon et al. 2016, Mogha, D'Rozario et al. 2016). Particularly for the axonal prion protein (PrPc), which interacts with Gpr126/ADGRG6 in SCs, it was demonstrated that ablation leads to impaired myelin maintenance resulting in a late-onset neuropathy (Bremer, Baumann et al. 2010, Küffer, Lakkaraju et al. 2016).

Concluding, several axonal and other extrinsic factors besides the above-mentioned signaling molecules regulate the SC lineage and their ability to myelinate. Notably, only little is known about *vice versa* signaling from SCs towards the axon. How myelination is maintained throughout life and which factors and signaling cascades are involved is still not fully understood making axo-glial investigations a promising field of research.

2.2.4 Additional function of SCs

Schwann cells not only myelinate axons of the peripheral nervous system but also metabolically support the axons and preserve axonal integrity. This concept was already shown for the CNS with oligodendrocytes and astrocytes (Pellerin, Pellegri et al. , Fünfschilling, Supplie et al. 2012, Lee, Morrison et al. 2012). Fünfschilling et al. also showed that impairing mitochondrial complex IV in SCs by deleting *Cox10* leads to a severe peripheral neuropathy underlining that SCs are important for the support axons (Fünfschilling, Supplie et al. 2012). Beyond this, recent studies could demonstrate the presence of glycogen in Schwann cell cytoplasm and could show that

it supports the excitability of myelinated but not unmyelinated axons. Their data indicates that SCs break down glycogen into lactate upon metabolically challenging situations such as aglycemia and can even keep up this metabolic support for large myelinated axons 6-fold longer than what was seen in CNS white matter (Brown, Evans et al. 2012). Latest studies could even show a conversion of fructose to lactate and subsequent shuttling to myelinated fibers both mediated by SCs, whereas unmyelinated fibers seem to directly take up fructose. This additionally suggests specific metabolic differences and function depending on the variety of axonal subtypes (Rich and Brown 2018). Apart from this SCs are also involved in sodium and potassium channel clustering at the node of Ranvier and in shaping axonal architecture during development (see chapter 1.1) (reviewed by (Poliak and Peles 2003, Salzer, Brophy et al. 2008)). Their role in nerve injuries is partially described in chapter 1.2.2 and reviewed in much more detail in (Jessen and Mirsky 2016). Apart from this, a recent study provides indications for cutaneous Schwann cells expressing nociceptive capabilities and forming a glia-neural complex mediating pain sensation (Abdo, Calvo-Enrique et al. 2019).

2.3 About rapid nerve conduction and axon diameter regulation

For both, invertebrates and vertebrates, fast signal propagation is a prerequisite for proper nervous system function. Positive effects on the conduction speed along axons within the nervous system are achieved by decreasing the interior resistance and/or by decreasing trans-fiber capacitance. Thus, two solutions emerged in evolution being axonal gigantism and myelination (Hartline and Colman 2007). The following chapter will focus on the concept of rapid conduction and axon diameter regulation while some of the involved molecules for myelination are described in chapter 2.1. and 2.2.3.

Over the last decades it was continuously shown that conduction speed increases rather proportionally to the square root of the interior diameter of an axon, which decreases the interior resistance of the fiber (Hodgkin 1954). Thus, so called `Axonal Gigantism` evolved preferably in species which need rapid impulses for example the squid escape mechanisms or the tail flip of lobster or crayfish. Nonetheless, also Drosophila species and some crustaceans developed giant axons (Eaton 1984, Allen, Drummond et al. 1998, Lenz, Hartline et al. 2000, Hartline and

Colman 2007). However, it has been calculated by Hartline and Colman that axons would need to be 100 times larger to achieve an only 10-fold faster signal propagation which would result in immense space problems within the nervous system and body (Hartline and Colman 2007). Strikingly, myelin evolved in vertebrates and allowed for rapid nerve conduction velocities with smaller axonal diameters (Nave and Werner 2014). Upon wrapping of a multilamellar membrane around axons the trans-fiber capacitance is decreased. The flowing currents reach the next unmyelinated and Na^+ channel dense node of Ranvier without delay and thus the adjacent internodal membrane is excited more rapidly, which speeds up signal propagation (Hartline and Colman 2007). This led to the concept of action potentials “jumping” across internodal segments. Further, the number of myelin layers increases proportionally to the respective axon diameter. In consequence, the internodal capacitance reduces with axon diameter in myelinated axons, which results in a first power dependence of conduction velocity on axonal diameter (Rushton 1951, Moore, Joyner et al. 1978, Hartline and Colman 2007, Perge, Niven et al. 2012). Notably, Kole and colleagues could recently show that the periaxonal space between the axolemma and myelin sheath as well as the paranodal space is also conductive and important for spatiotemporal action potential propagation at least in myelinated pyramidal axons of the CNS (Cohen, Popovic et al. 2019). The theoretical relation between nerve conduction velocity and diameters of myelinated and non-myelinated axons is schematically depicted in Figure 4. Besides myelination and radial axonal size, several studies could show that the conduction velocity is additionally influenced by internodal length and nodal parameters in both CNS and PNS, though to a more moderate extend (Wu, Williams et al. 2012, Ford, Alexandrova et al. 2015, Arancibia-Cárcamo, Ford et al. 2017).

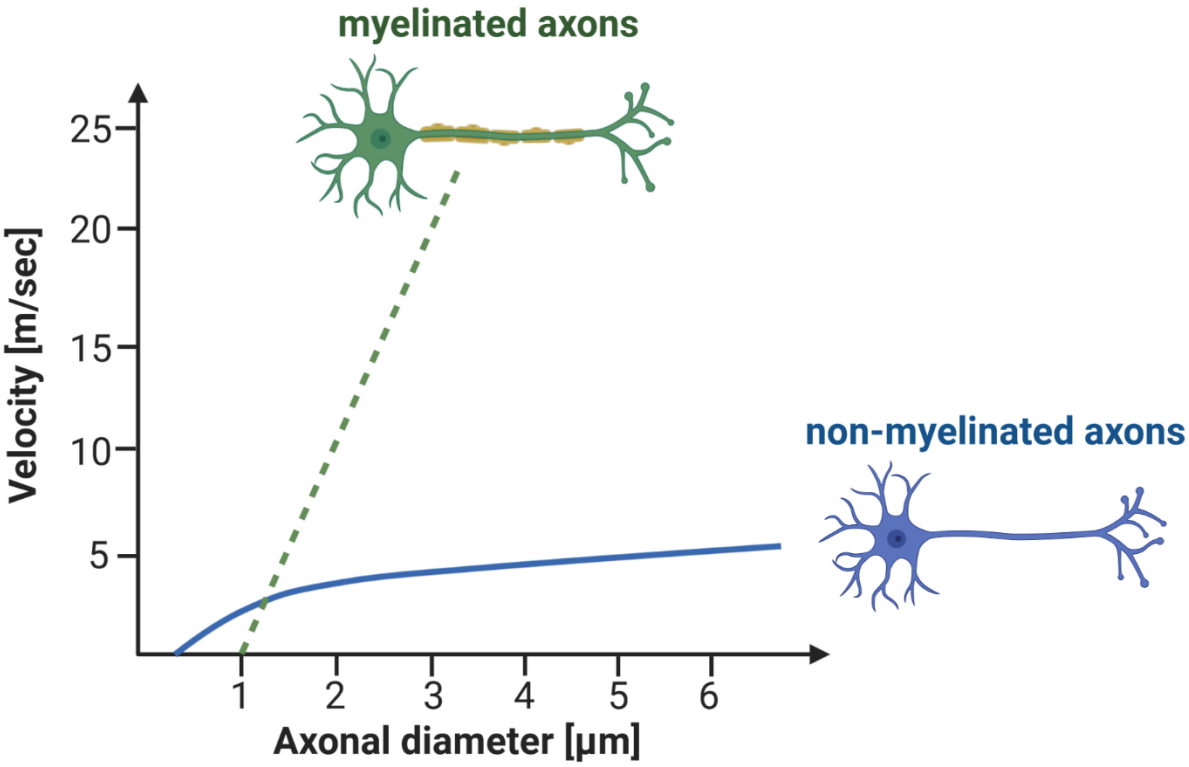

Figure 4 Theoretical relation between nerve conduction velocity and axon diameter for myelinated vs. non-myelinated axons. Stippled green line represents the relation between axonal diameter and nerve conduction velocity of myelinated axons larger than 1µm. Blue line represents relation between axonal diameter and nerve conduction velocity for non-myelinated axons. Representation and graph adapted from Rushton et al. 1951. Scheme created with Biorender.com.

But how is radial axonal growth actually regulated? It has been recently reported that loss of axonal α-adducin leads to enlarged axonal diameters preceding axonal degeneration in both CNS and PNS (Leite, Sampaio et al. 2016). They suggest that α-adducin controls the diameter growth of actin rings within axons to maintain axonal diameters and axonal integrity (Leite, Sampaio et al. 2016). However, one of the first detailed studies tackling the question of how axonal diameters are regulated was already published in 1970 by Friede & Samorajski. They demonstrated a positive correlation between axonal diameter and neurofilament (NF) numbers predominantly in large myelinated fibers and a mild effect of microtubule number before the onset of myelination (Friede and Samorajski 1970). Noteworthy, other studies suggest that organization of the axonal cytoskeleton is also locally regulated since some studies observed a varying density of NF depending on the investigated axon type (Price, Paggi et al. 1988, Szaro, Whitnall et al. 1990). In addition, not only the number and density of NF but also NF phosphorylation is crucial for radial axonal growth and is mainly regulated by myelinating SCs (de Waegh, Lee et al. 1992, Barry, Stevenson et

al. 2012). The proposed “outside-in” signaling is thought to be regulated by the interaction of myelin-associated-glycoprotein (MAG) with the p75NTR receptor on the axonal side (Yin, Crawford et al. 1998, Garcia, Lobsiger et al. 2003). Since deletion of MAG results in reduced axonal diameters and moderate axonal degeneration in the PNS a role in promoting radial axonal growth is implied (Li, Tropak et al. 1994, Yin, Crawford et al. 1998). Thus, MAG is one of a few examples for signaling from Schwann cells to axons. Nonetheless, first proof of the concept that SCs also directly affect radial axonal growth comes from experiments by Aguayo and colleagues in 1977. They investigated *Trembler* mice, which have a point mutation in the peripheral myelin protein 22 (PMP22) resulting in dys- and demyelination, increased number of Schwann cells, decreased axonal diameters and slower nerve conduction velocity. Interestingly, they demonstrated that by grafting wildtype sciatic nerve segments into *Trembler* mice axons became myelinated and larger in size. *Vice versa*, normal wild-type axons regrowing through a *Trembler* sciatic nerve graft showed reduced axonal diameters (Aguayo, Attiwell et al. 1977). Defects involving PMP22 account for diseases such as hereditary neuropathy with liability to pressure palsy (HNPP) as well as CMT1A, the most common form of Charcot-Marie-Tooth (CMT) disease (De Waegh and Brady 1990, Suter, Moskow et al. 1992, Suter, Welcher et al. 1993, Adlkofer, Frei et al. 1997, Pareyson and Marchesi 2009). Another relevant Schwann cell protein is myelin protein zero (P0/MPZ), which is the most abundant peripheral myelin protein maintaining proper myelin compaction in the PNS (Giese, Martini et al. 1992, Martini, Zielasek et al. 1995, Shapiro, Doyle et al. 1996, Martini and Schachner 1997, Patzig, Kusch et al. 2016). Consequently, total loss of MPZ results in a dysmyelinating phenotype and reduced axonal diameters and serves as a model for Dejerine-Sottas syndrome (Giese, Martini et al. 1992, Warner, Hilz et al. 1996, Frei, Mötzing et al. 1999). In contrast, mice heterozygous for MPZ display myelin decompaction and demyelination only after 4 months of age modelling human CMT1B (Martini, Zielasek et al. 1995). Unlike for MAG, studies about the role of MPZ suggest a more complex and diverse role in maintaining healthy myelin rather than axon diameter regulation. However, these models suggest that understanding of signaling events from Schwann cells to axons are of great importance since impairment of SC genes or proteins can lead to peripheral nerve disorders such as neuropathies. The lack or impairment of the aforementioned proteins leads to a decrease in axonal diameter although exact

mechanisms of how Schwann cells regulate axonal diameters and if there are SC-dependent mechanisms that restrict radial axonal growth remains poorly understood.

2.4 How to study axo-glia interaction in more detail?

Bidirectional interactions between Schwann cells and axons are crucial for establishing and maintaining nervous system function (Nave and Werner 2014). The close association of peripheral axons and Schwann cells (described in previous chapters) suggest that the axon/myelin interface is prone to be the major site of communication. Since many mechanisms are still not fully understood we hypothesize that functionally relevant but yet unknown proteins are localized at either the axolemma or innermost adaxonal SC membrane. Myelin is biochemically purified to investigate functionally relevant proteins, neglecting that proteins of the axolemma and partially of the non-compact myelin compartment are often not detected using the existing purification methods (Norton and Poduslo 1973, Patzig, Jahn et al. 2011, Erwig, Hesse et al. 2019). Nonetheless, two labs established protocols for enriching specifically the axon/myelin interface for the CNS and termed the respective membrane fraction either `myelin-axolemmal complex` or `axogliasome` (Menon, Rasband et al. 2003, Dhaunchak, Huang et al. 2010). The protocols were adapted from common myelin purification procedures and are also based on a sucrose density gradient centrifugation approach. Within the department of Neurogenetics, MPI-EM, the purification protocol was modified for application to peripheral nerves, illustrated in Figure 5 and described in more detail in Methods Section 3.2.5.2.

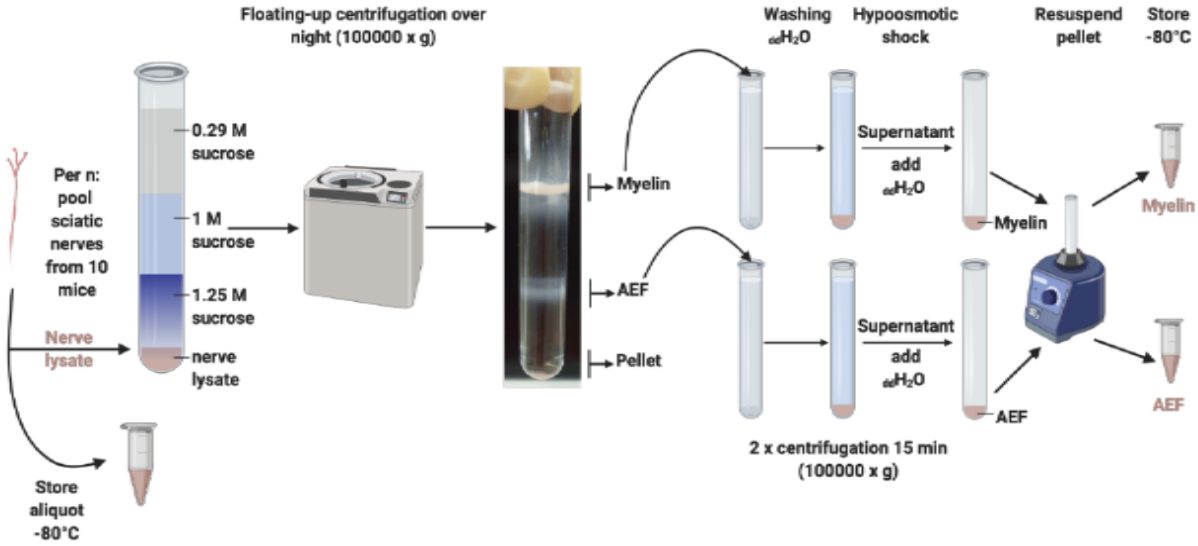

Figure 5 Biochemical purification of the axon/myelin interface. Scheme illustrates the biochemical purification of the light-weight membrane fraction of the axolemma and adaxonal myelin previously termed `axogliasome. The protocol was adapted from CNS protocols by Menon and Dhaunchak. Sciatic nerve lysates from 10 mice were pooled and overlaid with a sucrose gradient of three different molarities. Floating up ultra-gradient centrifugation was performed overnight and subsequent washing steps and osmotic shock were performed resulting in purified myelin and axogliosome-enriched fractions. For further detail on the method see chapter 3.2.5.2. Scheme created with Biorender.com

2.5 Aim of this study

For the establishment of functional axon/myelin units and the maintenance of long-term integrity of axons, glial cells and axons need to interact. This cellular association involves complex and not yet fully understood signaling processes. We hypothesize that relevant, but yet unknown proteins mediating interactions between axons and myelinating Schwann cells remain to be identified. To this aim we will biochemically purify a light-weight membrane fraction enriched for the axon/myelin interface from pools of wild-type murine sciatic nerves using a sucrose gradient centrifugation approach, as previously established for the central nervous system. Subsequently, the purified fraction, previously referred to as axogliasome, will be subjected to gel-free, quantitative mass spectrometric analysis. Besides known markers of non-compact myelin compartment we expect to identify known proteins of the axonal membrane and those yet unknown to be present at the axon/myelin interface. From this dataset we will select proteins for functional characterization applying the following criteria: I) Robust proteomic identification in all samples, II) novel protein with yet unknown role in the peripheral nervous system, III) predicted function as ligand, receptor, transporter or ion channel IV) preferably expressed in Schwann cells (SCs) rather than neurons and V) availability of embryonic stem cells or mice harboring a floxed allele at a mouse genome consortium for SC specific deletion. Upon selecting an appropriate candidate, we will analyze its abundance and expression in peripheral nerves applying mainly biochemical approaches e.g. immunoblots. Using imaging techniques such as confocal microscopy on sciatic nerve teased fibers, cryo-immuno-electron microscopy and Stimulated-emission-depletion microscopy (STED), we will determine the selected candidate's localization preferably to the adaxonal SC membrane or axolemma. Further, we intend to understand the functional relevance of the selected candidate *in vivo.* Thus we will delete its expression specifically in SC by expressing Cre recombinase under control of *Dhh* promoter and confirm efficient deletion of the floxed allele of the candidate gene by using biochemical approaches. Hypothesizing a possible role in mediating SC-axon interaction we will analyze morphological changes affecting the axon/myelin unit by electron- and light microscopy of various peripheral nerves at selected time-points. If relevant abnormalities of mutant mice occur we will also characterize behavioral as well as functional capabilities using appropriate behavioral tests and nerve conduction velocity measurements.

3 Material and Methods

3.1 Material

3.1.1 General Material

General laboratory materials were purchased from BD Falcon (Heidelberg, Germany), Bio-Rad (München, Germany), Gilson (Limburg-Offheim, Germany), Brand (Radebeul, Germany), Sarstedt (Nümbrecht, Germany) and Eppendorf (Hamburg, Germany). All chemicals used, were from Sigma-Aldrich GmbH (Munich, Germany), Merck KGaA (Darmstadt, Germany) and SERVA (Heidelberg, Germany).

3.1.2 Commercial Assays & Kits

Description	Manufacturer
RNA purification 'RNeasy mini prep'	Qiagen (Portland, USA); Cat#74104
DC Protein Assay (Lowry)	Bio-Rad (Munich, Germany); Car#5000111
Agilent RNA6000 Nano kit	Agilent Technologies Cat#5067-1511
Western Lightning® Plus-ECL	PerkinElmer (xxx), Cat#NEL105001EA
SuperSignal™ West Femto Maximum Sensitive Subrate	Thermo Fischer Scientific (xxx);Cat#34095

3.1.3 Primary antibodies

Antibody	Application	Dilution	Species	Source
Actin	IB	1:2000	Monoclonal mouse	Chemicon; Cat#MAB1501
Alpha-Tubulin	IB IHC	1:5000	Polyclonal rabbit	Sigma; Cat#SAB2102603
ATPaseα1	IB	1:2000	Monoclonal mouse	Abcam; Cat#ab7671
betaII-spectrin	STED	1:200		BD Biosciences, Cat#612563
CASPR	IHC	1:500		Neuromabs; Cat#clone K65/35
CD274/PDL1	IB	1:1000		Abcam; Cat#ab213480

	IHC	1:500		
CNP	IB	1:1000	Monoclonal mouse	Sigma; Cat#C5922
CMTM6	IB IHC IEM	1:500 1:200 1:100	Polyclonal rabbit	Origene; Cat#TA322304
MAG (clone 513)	IB IHC	1:1000 1:50	Monoclonal mouse	Chemicon
MPZ	IB IHC	1:2000	Monoclonal mouse	J. Archelos-Garcia
Nav1.6	IHC	1:500		Almonelabs; Cat#ASC-009
NFASC155	IB	1:1000		Prof. Peter Brophy
PMP2	IB	1:1000		PTG; Cat#12717-1-AP
SMI31	IB	1:500		Covance; Cat#SMI31P
SMI32	IB	1:500		Covance; Cat#SMI32-P

3.1.4 Secondary antibodies

Antibody	Application	Dilution	Species	Source
HRP-goat-α-rabbit-IgG	IB	1:10000	Goat	Dianova; Cat#111035-003
HRP-goat-α-mouse-IgG	IB	1:10000	Goat	Dianova; Cat#11503-003
Donkey α-mouse-Alexa 488	IHC	1:1000	Donkey	Invitrogen; Cat#A21202
Donkey α-rabbit-Alexa 488	IHC	1:1000	Donkey	Invitrogen; Cat#A21206
Donkey α-mouse-Alexa 555	IHC	1:1000	Donkey	Invitrogen; Cat#A31570

Donkey α-rabbit-Alexa 555	IHC	1:1000	Donkey	Invitrogen; Cat#A31572
STAR580	STED	1:100		Abberior; Cat#ST580-0002
STAR 635P	STED	1:100		Abberior, Cat#ST635P-002
Sheep- α-mouse	STED	1:100		Dianova; Cat#515-005-003
Goat-α-rabbit	STED	1:100		Dianova; Cat#111-005-003

3.1.5 Materials for genotyping

Description	Content	
Digestion buffers	5 M NaOH	67 mM
	Tris/HCl pH 8.0	
Tris-borat-EDTA (TBE) buffer	Tris Base	40 mM
	Boric acid	20 mM
	EDTA	1 mM
10 mM dNTP (50x stock)	dATP	2.5 mM
	dCTP	2.5 mM
	cGTP	2.5 mM
	cTTP	2.5 mM
	200 µM final concentration in a PCR reaction (50 µM each nucleotide)	

Description	Manufacturer
GoTaq DNA polymerase	Promega (Mannheim, Germany)
GoTaq buffer 5x	Promega (Mannheim, Germany)
Superscript III-reverse transcriptase	Invitrogen (Karlsruhe, Germany)
dNTPs	Boehringer GmbH (Mannheim, Germany)
GeneRuler 100 bp DNA ladder	Thermo Fisher Scientific (St. Leon-Rot, Germany)

3.1.6 Genotyping primer

Description	Number	Sequence
Cmtm6 genotyping	33516	5'-GCTGCTGTTT CTCATTGCTG-3'
	33517	5'-TGTGTCAAAC GCTAAGACTCAG-3'
Recombined Cmtm6 genotyping	33516	5'-GCTGCTGTTT CTCATTGCTG-3'
	32202	5'-GAGCTCAGAC CATAACTTCG-3'
Mag recombinase genotyping	1864	5'-TTGGCGGCGA ATGGGCTGAC-3'
	7649	5'-ACGGCAGGGA ATGGAGACAC-3'
	7650	5'-ACCCTGCCGC TGTTTTGGAT-3'
Cd274 genotyping	37526	5'-AGAACGGGAGCTGGACCTGCTTGCGTTAG-3'
	37527	5'-GCCTTCTTGA CGAGTTCTTC-3'
	12370	5'-ATTGACTTTC AGCGTGATTCGCTTGTAG-3'
Plp^{CreERT} genotyping	10099	5'-TGGACAGCTG GGACAAAGTAAGC-3'
	7963	5'-CGTTGCATCG ACCGGTAATGCAGGC-3'
Dhh Cre recombinase genotyping	10967	5'- CCTGCGGAGATGCCCAATTG-3'
	15793	5'- CAGCCCGGACCGACGATGAA-3'
Flp recombinase genotyping	15300	5'- CACTGATATTGTAAGTAGTTTGC-3'
	15301	5'- CTAGTGCGAAGTAGTGATCAGG-3'
LacZ/neo genotyping	15048	5'-CAACGGGTTCTTCTGTTAGTCC-3'

3.1.7 Genotyping PCRs

PCR reaction	Content	Amount	Bandsize
$Cmtm6^{fl/fl}$	Go-Taq buffer (5x)	4.2 µl	Wt ~ 292 bp
	dNTP (2nM)	2.1 µl	Flox ~ 450 bp
	Primer 33516	0.5 µl	
	Primer 33517	0.5 µl	
	GoTaq DNA polymerase	0.07 µl	
	$_{dd}H2O$	12.63 µl	
Recombined Cmtm6	Go-Taq buffer (5x)	4.2 µl	~ 350 bp
	dNTP (2nM)	2.1 µl	
	Primer 33516	0.5 µl	
	Primer 32202	0.5 µl	
	GoTaq DNA polymerase	0.07 µl	
	$_{dd}H2O$	12.63 µl	

Mag^{null}	Go-Taq buffer (5x)	4.2 µl	Wt ~ 300 bp
	dNTP (2nM)	2.1 µl	*Mag*^{null} ~ 600 bp
	Primer 1864	0.5 µl	
	Primer 7649	0.6 µl	
	Primer 7650	0.25 µl	
	GoTaq DNA polymerase	0.08 µl	
	$_{dd}$H2O	12.35 µl	
Cd274^{null}	Go-Taq buffer (5x)	4.2 µl	Wt ~ 250 bp
	dNTP (2nM)	2.1 µl	*Cd274*^{null} ~ 450 bp
	Primer 37526	0.5 µl	
	Primer 37527	0.5 µl	
	Primer 12370	0.5 µl	
	GoTaq DNA polymerase	0.07 µl	
	$_{dd}$H2O	12.13 µl	
Plp^{CreERT}	Go-Taq buffer (5x)	4.2 µl	~ 250 bp
	dNTP (2nM)	2.1 µl	
	Primer 10099	0.2 µl	
	Primer 7963	0.2 µl	
	GoTaq DNA polymerase	0.07 µl	
	$_{dd}$H2O	13.23 µl	
Dhh^{Cre}	Go-Taq buffer (5x)	4.2 µl	~ 400 bp
	dNTP (2nM)	2.1 µl	
	Primer 10967	0.5 µl	
	Primer 15793	0.5 µl	
	GoTaq DNA polymerase	0.06 µl	
	$_{dd}$H2O	12.64 µl	
Cmtm6$^{LacZ/neo}$	Go-Taq buffer (5x)	4.2 µl	Wt ~ 292 bp
	dNTP (2nM)	2.1 µl	LacZ ~ 366 bp
	Primer 33516	0.5 µl	Flox ~ 450 bp
	Primer 33517	0.5 µl	
	Primer 15048	0.5 µl	
	GoTaq DNA polymerase	0.07 µl	
	$_{dd}$H2O	12.13 µl	
Flp	Go-Taq buffer (5x)	4.2 µl	
	dNTP (2nM)	2.1 µl	
	Primer 15300	1 µl	
	Primer 15301	1 µl	

	GoTaq DNA polymerase	0.07 µl
	$_{dd}$H2O	11.63 µl

3.1.8 Quantitative real-time PCR primer

Gene	Direction	Sequence
Cmtm3	Forward	5`-GAGGACACCA CGTAGCAGATG -3'
	Reverse	5`-GAGGACACCA CGTAGCAGATG -3'
Cmtm4	Forward	5`-GAGGATCCCC CAGATCAACT -3'
	Reverse	5`-GGCGATAAAG AAAAAGAAAGTGC -3'
Cmtm5	Forward	5`-TTCCTGTCTT CCCTCAAAGG -3'
	Reverse	5`-GCCGTGAAGC AAATGAAGAT -3'
Cmtm6	Forward	5`-GATACTGGAA AAGTCAAGTCATCG -3'
	Reverse	5`-AATGGGTGGA GACAAAAATGA -3'
Cmtm7	Forward	5`-TCGCCTCCAT AGTGATAGCC -3'
	Reverse	5`-CTCGCTAGGC AGAGGAAGC -3'
Cmtm8	Forward	5`-CAGAGAAGGA AGGGCACAAC -3'
	Reverse	5`-TGACCAGGAA GGCAAAGAAC -3'
Rps13	Forward	5`-CGAAAGCACCTTGAGAGGAA -3'
	Reverse	5`-TTCCAATTAGGTGGGAGCAC -3'
Ube2l3	Forward	5`-AGCAGCACCAGATCCAAGAT -3'
	Reverse	5`-CACATTTGCGGATCTCTTCA -3'

3.1.9 Protein Biochemistry, SDS PAGE and immunoblot

Description	Content	
10x Phosphate-buffered saline (PBS)	NaCl	1.7 M
	KCl	34 mM
	Na_2HPO_4 x $2H_2O$	40 mM
	K_2HPO_4	18 mM
		pH 7.2 with 1N NaOH
10x Tris-buffered saline (TBS)	Tris/HCl, pH 7.5	500 mM
	NaCl	1.5 M
Modified RIPA buffer	TBS	1x
	EDTA	1 mM

	Sodium deoxycholate	0.5% [w/v]
	Triton X-100	1.0% [v/v]
	Protease inhibitor	1 tablet/10 ml
SDS separating gel	Acrylamid/Bisacrylamid 29:1	15%, 12% or 10% [v/v]
	Tris/HCl pH 8.8	0.4 M
	SDS	0.1% [w/v]
	APS	0.03% [w/v]
	TEMED	0.08% [v/v]
SDS stacking gel	Acrylamid/Bisacrylamid 29:1	4% [v/v]
	Tris/HCl pH 8.8	
	APS	125 mM
	TEMED	0.05% [w/v]
		0.1% [v/v]
4x SDS sample buffer	Glycerol	40% [v/v]
	Tris/HCl pH 6.8	240 mM
	SDS	8% [w/v]
	Bromphenol blue	0.04% [w/v]
10x SDS running buffer	Tris base	250 mM
(Laemmli buffer)	Glycine	1.92 mM
	SDS	1% [w/v]
Transfer buffer	Tris base	96 mM
(semi-dry blot)	Glycine	78 mM
	Methanol	10% [v/v]
	SDS	0.03% [w/v]
20x Tris buffered saline (TBS)	Tris/HCl, pH 7.4	1 M
	NaCl	3 M
1x TBS with Tween-20 (TBST)	Tris/HCl, pH 7.5	50 mM
	NaCl	150 mM
	Tween-20	0.05% [v/v]
Immunoblot blocking buffer	Non-fat dry milk powder	5% [w/v]
		in TBST

Description	Manufacturer
Complete Mini protease inhibitor	(Roche Diagnostics GmbH, Mannheim, Germany)

PageRuler™ Plus Prestained Protein Ladder	Thermo Fisher Scientific (St. Leon-Rot, Germany)
PVDF Membrane Amersham Hybond P0.45 µm	GE Healthcare Life Science (Chicago, USA)
PVDF Membrane Imobilon®-FL P0.45 µm	Merck Millipore Ltd. (Darmstadt, Germany)

3.1.10 Fixation solutions

Description	Content	
16% Paraformaldehyde (PFA)	PFA	16% [w/v]
	NaOH	5N
	PFA cooked at 65 °C for 20min while stirring, NaOH droplets until solution was cleared and then filtered	
0.2 M Phosphate buffer	Sodiumdihydrogenphosphate (NaH_2PO_4 x H_2O)	0.36% [w/v]
	di-Sodiumhydrogenphosphate (Na_2HPO_4 x $2H_2O$)	3.1% [w/v]
	NaCl	1% [w/v]
4% Paraformaldehyde (PFA)	PFA	4% [w/v]
	Phosphate buffer	0.1 M
Karlsson-Schultz fixative (K&S)	PFA	4% [w/v]
	Glutaraldehyde	2.5% [v/v]
	Phosphate buffer	0.1 M
Immuno Karlsson-Schultz fixative	PFA	4% [w/v]
	Glutaraldehyde	0.25% [v/v]
	Phosphate buffer	0.1 M

3.1.11 Immunohistochemistry and staining solutions

Description	Content	
Phosphate buffer (0.2 M, pH 7.4)	Sodiumdihydrogenphosphate (NaH_2PO_4 x H_2O)	0.04 M
	di-Sodiumhydrogenphosphate (Na_2HPO_4 x $2H_2O$)	0.16 M

PBS/BSA	Sodiumdihydrogenphosphate (NaH_2PO_4 x H_2O)	0.04 M
	di-Sodiumhydrogenphosphate (Na_2HPO_4 x $2H_2O$)	0.16 M
	NaCl	1.8% [w/v]
	Bovines serum albumin (BSA)	1.0% [w/v]
Blocking buffer (cryosections)	Goat serum or horse serum	10% [v/v]
	Triton X-100	0.5% [v/v]
	Dissolved in BSA/PBS	
Blocking buffer (teased fibers)	Horse serum	10% [v/v]
	Tween-20	0.1% [v/v]
	Dissolved in 1x PBS	
X-Gal staining buffer	Potassium ferrycyanid	5 mM
	Potassium ferrocyanid	5 mM
	MgCl2	2 mM
	5-bromo-4-chloro-indolyl-β-D-galactopyranoside (X-gal)	1.2 mg/ml
	Adjusted in 1 x PBS	

Description	Manufacturer
Eukitt	Kindler (Freiburg, Germany)
Aqua-Poly/Mount	Polysciences (Eppelheim, Germany)
Mowiol Mounting Media	Sigma Aldrich (Darmstadt, Germany)
DABCO	Sigma Aldrich (Darmstadt, Germany)

3.1.12 Electron Microscopy

Description	Content	
Epon	Glycidether 100	171.3 g
	Dodecenyl succinic anhydride (DDSA)	115 g
	Methyl nadic anhydride (MNA)	89 g
	Mixed using magnet stirrer for 10 min	
	DMP-30	6.5 ml
	Mixed using magnet stirrer for 20 min	

Methylene blue	Na-tetraborat (Borax) Methylenblau	1% [w/v] 1% [w/v]
Azure II	Azure II	1% [w/v]
Methylene blue - Azure II staining solution	Methylene blue Azure II Freshly mixed before use	50% [v/v] 50% [v/v]
Contrasting solution	UranyLess (Science Services, Munich, Germany).	

3.1.13 Mouse lines

Genotype	Description	Reference/Origin
Cmtm6$^{fl/fl}$	Mice carrying *Cmtm6*$^{tm1c(EUCOMM)Wtsi}$ allele	*Cmtm6*$^{tm1c(EUCOMM)Wtsi}$ (EUCOMM)
Dhh^{Cre}	Mice expressing *Cre* recombinase under *Dhh* promotor	Jaegle et al. 2003
Cmtm6LacZ	Mice harboring *Cmtm6*$^{LacZ/neo}$ allele	This study
Cmtm6$^{fl/fl}$*;Dhh*^{Cre}	Mice lacking *Cmtm6* in SCs (termed *Cmtm6* cKo)	This study
Cd274^{null}	CD274/PDL1 null mice (termed *Cd274* Ko)	Dong et al 2004
Mag^{null}	MAG null mice (termed *Mag* Ko)	Montag et al. 1994
Plp^{CreERT2}	Mice expressing *Cre* recombinase under *Plp* promotor	Leone et al 2003
Cmtm6$^{fl/fl}$*;Plp*^{CrERT2}	Inducible deletion of CMTM6 in SCs after Tamoxifen administration	This study

Cmtm6$^{fl/fl}$;*Dhh*^{Cre};*Mag*^{null}	Mice lacking CMTM6 from SCs and MAG constitutively (termed *Cmtm6* cKo;*Mag* Ko)	This study

3.1.14 Software and RStudio script

Description	Manufacturer	Link
GraphPad Prism 6	GraphPad Software, Inc.	https://www.graphpad.com/
ImageJ	Schindelin et al.,2012	https://imagej.nih.gov/ij/
RStudio	RStudio, Inc.	https://www.rstudio.com/
LAS AF lite	Leica	http://leica-las-af-lite.software.com
Adobe Photoshop	Adobe	http://www.adobe.com
bioRENDER	bioRENDER	http://biorender.com
ZEN2011	Zeiss	https://www.zeiss.de

3.2 Methods

3.2.1 Animals

All animal experiments were performed in accordance with the animal policies of the Max Planck Institute of Experimental Medicine and were approved by the German animal protection law of the federal state of Lower Saxons (License numbers: 16/2168 and 15/1833). All animals used in experiments were bred and kept in the mouse facility of the Max Planck Institute of Experimental Medicine. Animals were group-housed 3-5 mice per cage in a 12-hour dark/light cycle with ad libitum access to food and water. Experimental mice were male unless indicated otherwise and were analyzed together with littermate controls as far as possible. All mice were sacrificed by cervical dislocation or by perfusion using anesthetics.

3.2.2 Generation of *Cmtm6* conditional knockout mice

To generate CMTM6 conditional knockout mice *(Cmtm6* cKo) frozen mouse sperm comprising the *Cmtm6*$^{tm1a(EUCOMM)Wtsi}$ allele (also termed *Cmtm6*$^{lacZ/neo}$) was obtained from the European Mouse Mutant Archive (EMMA, Neuherberg/Munich, Germany). The sperm was used for *in vitro*-fertilization, yielding mice which harbor the *Cmtm6*$^{lacZ/neo}$ allele. *Cmtm6-lacZ* mice were identified via genotyping PCR, used for experiments or further interbred with mice expressing FLIP recombinase (129S4/SvJaeSor-*Gt(ROSA)26Sor*$^{tm1(FLP1)Dym}$*/J*; backcrossed into C57BL/6N). Hence, the lacZ/neo cassette was excised *in vivo,* yielding mice carrying the *Cmtm6*$^{tm1c(EUCOMM)Wtsi}$ allele (also termed *Cmtm6*^{flox}). Upon appropriate interbreeding of homozygous *Cmtm6* floxed mice (*Cmtm6*$^{fl/fl}$*)* and mice expressing *Cre* under the control of the *Dhh* promotor (*Dhh*^{Cre}*)*, exon 2 and 3 of *Cmtm6* were excised *in vivo* and *Cmtm6* expression was inactivated in Schwann cells. For simplicity, *Cmtm6*$^{flox/flox}$*;Dhh*^{Cre} mice are also termed *Cmtm6* conditional knockout (*Cmtm6* cKo) throughout this thesis. Routine genotyping of *Cmtm6* cKo mice was performed by genotyping PCR (see Fig 9).

3.2.2.1 Tamoxifen induced recombination

To conditionally inactivate the expression of *Cmtm6* in adult Schwann cells *Cmtm6*$^{fl/fl}$*;Plp*^{CrERT2} (termed *Cmtm6* iKo) were generated. Therefore, *Cmtm6*$^{fl/fl}$ mice

were interbred with mice expressing tamoxifen inducible *Cre* recombinase under control of the *Plp* promotor (*Plp*^{CreERT2} mice). Tamoxifen was always freshly prepared for 5 days of injection. Thus, Tamoxifen was diluted in corn oil (both Sigma Aldrich) and mixed on a vortexer in the dark for at least 30 min RT. A concentration of 1mg tamoxifen dissolved in 100µl corn oil per mouse per day and was injected intraperitoneally (i.p.) in both, *Cmtm6*$^{fl/fl}$ (termed control) and *Cmtm6* iKo, at the age of 8 weeks for 10 days with a break of two days after the first 5 consecutive days of injection (scheme in Fig. 21**;** protocol adapted from (Leone, Genoud et al. 2003)).

3.2.3 Genotyping PCR

For genotyping of mice, small ear punches of P21 old mice were taken and digested. Thus, 300 µl 5M NaOH were added and biopsies were incubated at 90°C for 1-2h. After samples cooled down, 300µl of Tris/HCl pH 8.0 were added, tubes were inverted once and stored at 4°C until further processing. To amplify genotype specific DNA fragments, polymerase chain reaction (PCR) was performed (Saiki, Gelfand et al. 1988, Mullis, Faloona et al. 1992). Respective primers were selected and synthesized by the service facility of the MPI-EM. 20µl of the respective PCR reaction mix was added to 1 µl DNA and PCRs were run in a T3 or Gradient Thermocycler (Biometra GmbH, Göttingen,Germany). PCR products were separated using respective gels (2% [w/v] agarose in TBE buffer). Before loading, 5µl Gel Red Nucleic Acid Stain (BioTrend, Cologne, Germany) was added to each sample for DNA visualization and 25µl were loaded onto the gel along with the marker GeneRuler 100 bp ladder (Thermo Fischer Scientific). Samples were separated at a maximum of 120V for 60-90 minutes in TBE buffer. For documentation pictures were obtained using an Intas UV system (Intas Science Imaging, Göttingen, Germany).

3.2.4 RNA isolation and analysis

For RNA isolation and analysis, sciatic nerves of n=4-5 male mice per genotype at the age of 8 weeks were collected, snap frozen on dry ice and stored at -80°C until further processing. All consecutive steps (RNA isolation, cDNA synthesis and qRT-PCR) were done by Ursula Kutzke and is briefly described below.

3.2.4.1 RNA extraction

Small scale RNA isolation and purification was performed using Qiagen`s "RNeasy Mini Prep" kit following the manufacturer`s instructions. Beforehand, the tissue was homogenized in Trizol (Life Technologies™, Thermo Fischer Scientific, St. Leon-Rot, Germany) followed by chloroform extraction. RNA quality and concentrations were tested using Agilent RNA 6000 Nano Kit, the Agilent 2100 Bioanalyzer (Agilent Technologies, Santa Clara, California, United States) and the NanoDrop 2000 spectrophotometer (Thermo Fischer Scientific, St. Leon-Rot, Germany) following manufacturer's instructions. Thereafter, concentration of all samples was adjusted to 100ng/µl.

3.2.4.2 cDNA synthesis

For quantitative comparisons of mRNA equal amounts of the isolated RNA was transcribed to complementary single stranded DNA (cDNA) using the SuperScript III reverse transcriptase (Invitrogen, Karlsruhe, Germany) and below mentioned protocol for cDNA synthesis.

cDNA synthesis
8 µl RNA (800 ng in total)
2 µl dT mic Primer (0.6pmol/µl)
2 µl N9 (random nonamers 120 pmol/µl)
Mixture was incubated for 10 min at 70°C and 1 min on ice to denature RNA and primers
The following premix was added to the reaction:
4 µl 5x first strand buffer
1 µl dNTP (10mM)
2 µl DDT (100mM)
1 µl SuperScript III reverse transcriptase (200 U/µl)
Mix was incubated in thermocycler using the following setting:
25°C 10 min
50°C 45 min

55°C 45 min

Synthesized cDNA was diluted 1:30 with $_{dd}H_2O$ and stored at -20°C until further processing via q-RT PCR.

3.2.4.3 q-RT PCR

Quantitative real-time PCR was performed using a pipetting robot epMotion 5075 (Eppendorf, Hamburg Germany) for pipetting, the Power SYBR Green PCR Master Mix (Promega, Fitchburg, Wisconsin, United States) and the Light Cycler 480II (Roche Diagnostics GmbH, Mannheim, Germany). Primer sequences for respective genes can be found under Materials. For every reaction 4 technical replicates were used and pipetted as follows:

Mix for gene expression analysis
2 µl cDNA (2 ng/µl)
5 µl SYBR Green PCR Master Mix
0.1 µl forward primer
0.1 µl reverse primer
2.8 µl ddH2O

PCR program for 50 cycles:
15 sec 95°C
1 min 60°C

Data analysis was carried out using Microsoft Excel 2013. mRNA abundances were normalized in relation to the mean of standard genes (*Rps13* and *Ube2l3*) which did not differ between genotypes. The average of all biological replicates was calculated and related to wild-type levels which were set to 1. Graphical illustration of statistical testing was performed by using GraphPad Prism 6.

3.2.5 Biochemical protein analyses

3.2.5.1 Sample collection

Male mice of indicated genotypes and ages were sacrificed by cervical dislocation and sciatic nerves were carefully dissected. Dorsal and ventral root preparations for immunoblotting were performed by Theresa Kungl. Sciatic nerves of wild-type mice for proteomic analysis of the AEF fraction were dissected from Katja Lüders. Freshly dissected nerves were immediately frozen on dry ice and stored at -80°C until further processing.

3.2.5.2 Biochemical purification of the axogliosome-enriched fraction (AEF)

To purify a light-weight membrane fraction enriched for the plasma membrane of peripheral axons and the adaxonal Schwann cell membrane (also termed axogliosome-enriched fraction; AEF), protocols from Dhaunchak et al. 2010 and Menon et al. 2003 were adapted (Menon, Rasband et al. 2003, Dhaunchak, Huang et al. 2010). For each biological replicate sciatic nerves dissected from 10 mice of indicated age and gender were pooled and collected in a centrifugation tube containing 1.25M sucrose supplemented with complete protease inhibitor tablets (Roche Diagnostics GmbH, Mannheim, Germany). Nerves were homogenized using Polytron PT3000 (Kinemetica, Eschbach, Germany) and 100µl lysate was directly frozen on dry ice for later comparison. The remaining nerve lysate was carefully overlaid with first 1M and then 0.29M sucrose (see scheme in Fig. 5). Further, floating-up centrifugation was carried out using an XL-70 ultracentrifuge with Optima™ TLX rotor (Beckman Coulter, Krefeld, Germany) at 100.000g for 16 h at 4°C with slowest possible acceleration/deceleration settings.

Using a Pasteur pipette, the myelin-enriched fraction at the 0.29M/1M interphase and subsequently the axogliasome-enriched fraction (AEF) at the 1M/1.25M interphase was collected (see Fig. 5) and transferred into a fresh centrifugation tube. While the myelin fraction was stored on ice, the AEF was further processed and two subsequent washing steps and osmotic shocks were performed as previously described in detail for the myelin-enriched fraction (Erwig et al., 2019). Briefly, ice-cold $_{dd}H_2O$ was added to the AEF and tubes were centrifuged at 100.000g for 15 min at 4°C. The supernatants were carefully poured off and each pellet was resuspended in ice-cold $_{dd}H_2O$ and centrifuged at 12000 g for 15 min at 4 °C. Again,

the supernatants were poured off, remaining fluid was taken up using tissue paper and the AEF-pellet was taken up in 50µl 10X TBS with protease inhibitor (Roche), snap-frozen and stored at -80°C. The myelin-enriched fraction was processed the same way and the pellet was taken up in 100µl 10X TBS including protease inhibitor (Roche), snap-frozen and stored at -80°C. Purification of the AEF of wild-type mice was performed by Katja Lüders.

3.2.5.3 Proteome Analysis

For wild-type proteome analyses the AEF was purified from nine pools of sciatic nerves from 10 mice, considered as nine biological replicates. For comparing control and *Cmtm6* cKo mice the AEF was purified from three pools per genotype of sciatic nerves from 10 mice per pool, considered as three biological replicates per genotype. All samples were analyzed with silver staining beforehand, to ensure equal qualities and quantitative mass spectrometry (MS) was performed by Dr. Stefan Tenzer, Institute for Immunology, University Mainz as previously described in (Distler, Kuharev et al. 2014, Distler, Kuharev et al. 2016). Briefly, respective AEF samples with a protein concentration of at least 100µg each were sent to Stefan Tenzer and were analyzed using ultraperformance Liquid Chromatography –Mass Spectrometry (LC-MS). Proteolytic digestion of isolated AEF fractions was performed beforehand, using filter-aided sample preparation (FASP) as described in (Wiśniewski, Zougman et al. 2009, Distler, Kuharev et al. 2016). LC-separation was performed using the nanoAquity UPLC system (Waters Corporation) and MS analysis was done using a nano-ESI-Q-TOF mass spectrometer (Waters Corporation Synapt G2-S HDMS) equipped with an ion-mobility separation (IMS) device. Data was collected in data-independent acquisition mode using MS^E combined with $UDMS^E$ and raw data was processed and searched with ProteinLynx Global SERVER (PLGS, Version 3.02. Waters Corporation) against UniProtKB/SwissProt Mouse Reference Proteome and known contaminants. Post-processing and quantification were performed using ISOQuant and absolute sample amounts were estimated using the TOP3 quantification method as described in (Silva, Gorenstein et al. 2006). In general, peptides had to be identified in at least three biological replicates with at least 2 peptides per protein and only peptides with a PLGS identification score equal or above 5.5 were considered. For depicted data, further statistical analysis and data representation in graphs was prepared using Microsoft Excel 2013 and GraphPad Prism 6.

3.2.5.4 Sample preparation

Snap frozen peripheral nerve tissue (sciatic nerves, dorsal or ventral roots) were taken from -80°C, cut in small pieces on dry ice and added to Precellys tubes on ice. Further, tissue was homogenized in 400µl (sciatic nerves) or 200µl (dorsal and ventral roots) RIPA buffer containing protease inhibitor using Precellys 24 (Peglab, Erlangen, Germany) two times at 6500rpm for 3x 10sec + 10 sec break. Lysates were kept on ice for 15 min and foam was removed by short centrifugation (Heraus Biofuge Pico table centrifuge, 13000 rpm). If samples were not fully homogenized a third homogenization step using the Precellys was performed. Afterwards the lysate was transferred into a 1.5 ml tube and centrifuged at 13000 rpm 10 min at 4°C. The supernatant was transferred into a new tube and stored at -80°C until further processing.

To determine protein concentrations of respective samples the Lowry assay (Lowry 1951 Peterson 1979) was performed using the Bio-Rad DC Protein Assay kit and following manufacturer`s instruction. The optical density was measured at 650 nm using the Eon™ High Performance Microplate Spectrophotometer (BioTek, Vermont, USA). Samples were further diluted to 0.1µg/µl and 1µg/µl in 1x SDS sample buffer and 5%β-mercaptoethanol [v/v] to denature proteins. For detecting MAG non-reduced conditions without 5%β-mercaptoethanol were used. Samples were kept at -20°C.

3.2.5.5 SDS PAGE

Protein separation was performed by SDS-PAGE. Thus, Acrylamid gels (10-15%) were freshly prepared using the Mini-PROTEAN Handcast system (Bio-Rad, Munich, Germany). Before usage samples were always heated for 10 min at 40°C. Depending on respective protein and antibody, between 2-25µg per sample, as well as 5µl pre-stained protein ladder (PageRuler™, Thermo Fischer Scientific) were carefully loaded onto the gel. Protein separation was carried out using the BioRad Protein Electrophoresis device with a constant current of 200V for 1 h. Afterwards gels were removed and incubated in transfer buffer for 15 min before performing the immunoblot.

3.2.5.6 Immunoblot

For immunodetection, proteins were transferred to a PVDF membrane (GE Healthcare, Buckinghamshire, UK; Cat#10600023) using the Novex® Semi-Dry Blotter (Invitrogen, Karlsruhe, Germany). Beforehand, the PVDF membranes were activated with 100% ethanol for 1 min, washed 2 times in $_{dd}H_2O$ and kept in transfer buffer for up to 10 minutes until further processing. Additionally, eight Whatman™ papers (GE Healthcare Life Sciences, Buckinghamshire, UK) were soaked in ice cold transfer buffer for about 20 min. On the anode plate four Whatman™ papers were stacked and air bubbles were carefully removed with a blotting roller. Next, the activated PVDF membrane was placed on top of the stack, followed by the gel and four additional Whatman™ papers. Proteins were transferred at 20V for 30-45 min (depending on protein size) using Bio-Rad power supply. After blotting, membranes were incubated in blocking buffer (5% non-fat dry milk in 1 x TBS containing 0.05% Tween-20 (Promega, Fitchburg, USA)) for 30 min-1 h at RT. Primary antibodies were diluted in 5 ml blocking buffer and the membrane was incubated overnight at 4°C on a rotor. For CD274/PDL1 better results were achieved with additional 1-2h incubation at RT the following day. Afterwards the membranes were washed 3 x 5 min with 1xTBS-T and then incubated with appropriate horseradish peroxidase (HRP)-coupled secondary antibodies (diluted in blocking buffer) for 1 h at RT. Afterwards, membranes were again washed 3 x 5 min in 1xTBS-T.

Bands were visualized using enhanced chemiluminescent detection (ECL) according to the manufacturer's instructions and depending on the intensity of the signal (Western Lightning® Plus-ECL or SuperSignal™ West Femto Maximum Sensitive Subrate for CD274/PDL1; Thermo Fischer Scientific, St. Leon-Rot, Germany). Immunoblots were scanned using ECL Chemostar (Intas Science Imaging, Göttingen, Germany). Membranes were incubated with internal standards like actin or alpha-tubulin to control for equal loading.

Quantifications for NEFH- and phosphorylated NEFH abundances were performed by measuring band intensity using ImageJ software (https://imagej.nih.gov/ij/) and normalizing to band intensities of actin detected on the same membrane (n=3). In general, immunoblots were replicated 3 times with an n=3 per genotype whenever possible.

3.2.6 Immunohistochemistry

3.2.6.1 Teased fiber preparation

For immunolabeling of teased fiber preparations, sciatic nerves dissected from mice of the indicated genotypes at 8-10 weeks were transferred into ice-cold PBS. Using two fine forceps (Dumont No.5) the epineurium was carefully removed, nerves were split longitudinally and smaller nerve pieces were transferred onto a new coverslip. Thereafter, fiber bundles were carefully pulled apart with both forceps resulting in axons being completely separated from each other. Afterwards, slides were dried and stored at -20°C for up to a maximum of 12 month.

3.2.6.2 Cryosections

Mice were sacrificed by cervical dislocation and the sciatic nerves of 8-weeks-old mice were carefully dissected and post-fixed with 4% PFA [w/v] for 1 h and 1 % PFA [w/v] o/n at 4°C. The following days the tissue was transferred to 10% [w/v] sucrose, 20% [w/v] sucrose and 30% [w/v] sucrose in 0.1 phosphate buffer, each o/n at 4°C. Afterwards, the tissue was embedded in small plastic chamber on dry ice using Tissue-Tek® O.C.T.™ Compound (Sakura, Staufen, Germany) and stored at -20°C. Using a cryostat (Reichert Jung® Cryocut 18000, Leica, Wetzlar, Germany) 10µm thick transverse sections were cut and collected on Superfrost® Plus microscope slides (Thermo Fischer Scientific, t. Leon-Rot, Germany), dried at RT and stored at -20°C until further processing.

3.2.6.3 Fluorescent Staining

For immunolabeling, teased fiber preparations or sciatic nerve cross-sections were incubated for 5 min in 4%PFA followed by 5 min 100% Methanol and 3 x 5 min washing in PBS. Samples were blocked for 1 h in blocking buffer (PBS, 10% horse serum and 0.1% Tween-20) at RT consecutively. Next, primary antibodies were diluted in blocking buffer and slides were incubated overnight at 4°C. Samples were washed 3 x 5 min in PBS and appropriate secondary antibodies diluted in blocking buffer were applied for 1 h at RT. After washing with PBS 3 x 5 min and 2 x 30 sec in $_{dd}$H2O slides were mounted using Aqua-Poly/Mount (Polysciences, Eppelheim, Germany).

3.2.6.4 Imaging and analysis

Fluorescent images of sciatic nerve teased fiber preparations were obtained randomly at 10x or 40x magnification using Axio Observer Z2 (Zeiss) and, if required, stitched using Zeiss Zen2011. Obtained images were used for quantifications. For representative images, slides were imaged using the confocal microscope Leica SP5. Here, the signal was collected with the objective HCX PL APO lambda blue 63.0.x1.20. DAPI staining was excited with 405 nm and collected between 417 nm - 480 nm. Alexa488 fluorophore was excited with an Argon laser for which the excitation was set to 488 nm and the emission to 500 nm - 560 nm. Alexa555 was excited by using the DPSS561 at an excitation of 561 nm and the emission was set to 573 nm - 630 nm. For obtaining, exporting and processing the images LAS AF lite and Adobe Photoshop were used. Node and paranode length and diameter were quantified on 40x magnified images using ImageJ. For node assessment the diameter and length of each Nav1.6 positive node was measured (as displayed in Fig.18) and the overall mean per animal was calculated. For paranodes, the diameter and length of both CASPR positive paranodes besides a Nav1.6 positive node was measured (as displayed in Fig.18), the mean of both paranodes beside one node and the overall mean per animal was calculated. For internodal length the distance between one Nav 1.6 positive node and the next was measured using Image J software on stitched images obtained at 10x magnification.

3.2.6.5 STED nanoscopy

STED nanoscopy on free-floating partially teased fibers of wild-type mice was performed by Elisa D`Este (Max Planck Institute for Medical Research, Heidelberg) as described in (D'Este, Kamin et al. 2017). Primary antibodies were specific for CMTM6 (OriGene, Cat# TA322304*,* 1:100) and betaII spectrin (BD Biosciences, San Jose, United States, Cat# 612563, 1:200). Secondary antibodies (sheep anti-mouse, Dianova, Hamburg, Germany, Cat# 515-005-003; goat-anti-rabbit, Dianova, Cat# 111-005-003) were labeled with STAR580 (Abberior, Göttingen, Germany, Cat# ST580-0002) or STAR635P (Abberior, Cat# ST635P-002) and used at 1:100 dilution.

3.2.6.6 LacZ staining and imaging

To visualize cells with *Cmtm6* gene activity, teased fibers of heterozygous *Cmtm6*$^{LacZ/neo}$ mice were obtained and lacZ immunohistochemistry was performed. Thus, slides were incubated with X-gal staining buffer at 37°C for 2-3.5 h in the dark. To stop the reaction, samples were rinsed with PBS 1-2 times and mounted using Aqua-Poly/Mount (Polysciences, Eppelheim, Germany). Images were captured at 40x magnification using the Zeiss AxioImager Z1 (Zeiss, Oberkochern, Germany).

3.2.7 Electron microscopy

3.2.7.1 Sample collection

Animals of indicated age and genotype were sacrificed by cervical dislocation. Subsequently, sciatic nerves and phrenic nerves as well as dorsal and ventral roots were carefully dissected and postfixed in Karlsson-Schultz fixative (4% PFA, 2.5% glutaraldehyde in 0.1M phosphate buffer) solution at 4°C until further processing.

3.2.7.2 Epon embedding

For electron microscopic imaging, the fixed nerves were embedded in Epon using an automated system (EMPT, Leica, Wetzlar, Germany). Beforehand, nerves were rinsed with 0.1M phosphate buffer and placed into small plastic chambers. Thereafter, the tissue was processed according to the following protocol:

Solution	Incubation time	Temperature
Phosphate buffer	3x10 min	4°C
2% [w/v] OsO_4	4 h	4°C
$_{dd}H_2O$	3x10 min	4°C
30% [v/v] Ethanol	20 min	4°C
50% [v/v] Ethanol	20 min	4°C
70% [v/v] Ethanol	20 min	4°C

90% [v/v] Ethanol	20 min	4°C
100% [v/v] Ethanol	4x10 min	4°C
Propylenoxid	3x10 min	RT
Propylenoxid/Epon 2:1	2 h	RT
Propylenoxid/Epon 1:1	2 h	RT
Propylenoxid/Epon 1:2	4 h	RT
Epon	4 h	RT

Afterwards the tissue was carefully placed into molds filled with Epon, labelled accordingly and left o/n at 60°C for polymerization of Epon.

3.2.7.3 Sectioning, staining and imaging of semi- and ultra-thin sections

Semithin (500nm) cross sections of epon embedded samples were obtained using a PTPC Powertome Ultramicrotom (RMC, Tuscon Arizona, USA) and a diamond knife (Diatome Ultra 45°). The sections were transferred to a glass slide, dried on a warm plate (60°C) and stained with methylene blue/azur II (1:1) for approximately 1 min followed by rinsing with $_{dd}H_2O$ for 1 min (Richardson et al., 1960). Thereafter, the samples were mounted using Eukitt and images were acquired with a 100x oil objective of the Zeiss AxioImager Z1 (Zeiss, Oberkochern, Germany) and stitched by Zeiss Zen 1.0 software.

For transmission electron microscopy ultrathin section (50nm) were cut using the same equipment and collected on formvar polyvinyl coated double sized slot grids (AGAR scientific, Essex, UK). Grids carrying ultrathin sections were contrasted with UranyLess (Electron Mircoscopy Science, Hatfield, Panama) for 15-30 min and washed 6 x with $_{dd}H_2O$. For quantitative analyses 8-20 random, non-overlapping images were taken at a magnification of 3000x (sciatic nerves, dorsal roots), 4000x (phrenic nerves) or 7000x (Remak bundles) using a Zeiss EM900 electron microscope (Zeiss, Oberkochen, Germany). To analyze neurofilament density, at least 30 images of cross-sectioned, non-angled sciatic nerve axons were obtained at a magnification of 6300x using the EM912AB-Omega (Zeiss, Oberkochen, Germany).

3.2.7.4 Analysis

To investigate axonal diameters a semi-automatically method using the ROI based analyze particle function of ImageJ (Fiji) was applied followed by careful visual inspection. Thus, myelinated axons that escaped automated quantification were manually encircled. Further, tilted axons which were not cross sectioned accordingly were not included in analysis of axonal diameters. All myelinated axons were included in the number of myelinated axons irrespective if the axonal diameter was measured or not, resulting in 3000-5000 axons per sciatic nerve, 1800-2600 per dorsal root and between 200-300 per phrenic nerve. Schwann cell (SC) nuclei were quantified as described in (Patzig, Kusch et al. 2016) by only counting those SC nuclei which are in close contact to an axon in a 1:1 ratio. All other nuclei in close proximity to other cells (mainly macrophages or fibroblasts) or nuclei away from axons where not counted. All quantifications on semi-thin levels were performed blinded to the genotype and between n=3-5 animals per genotype at respective time points were analyzed (exact values indicated in figure or figure legends).

On electron microscopic level g-ratio, axonal degeneration, number of non-myelinated axons and Remak bundles were assessed as previously described in (Fledrich, Stassart et al. 2014, Patzig, Kusch et al. 2016) using ImageJ (Fiji) and Microsoft Excel 2013 for calculations of g-ratio. The g-ratio was measured by encircling the circumference of an axon without myelin divided by the encircled circumference of the same axon including the myelin sheath. Only normal appearing myelinated axons were measured. At least 58 axons per phrenic nerve and 180 axons per sciatic nerve per animal with n=3-5 per genotype were analyzed on 8-20 non-overlapping images. To evaluate axonal degeneration, every myelin/axon unit in which the axon was either gone (just myelin sheath) or appeared degenerating was counted. For assessing axons in Remak bundles at least 200 axons per animal were analyzed using images with 7000x magnification. Thus, the circumference of each unmyelinated axon within a bundle was measured. Additionally, the number of axons per bundle was counted. It should be taken into account that axons smaller than 0.2µm could not be assessed using the obtained images. Further, for the number of pro-myelinated axons only axons which are larger than 1µm were measured, counted and set in relation to the overall number of axons within the total quantified area. For measuring neurofilament density 30 cross-sectioned, non-angled sciatic nerve axons of n=3 per genotype were

analyzed by overlaying a 0.2µm^2 grid and counting the number of neurofilaments within a minimum of 3 grids/axon using ImageJ (Fiji). Afterwards, the mean of the neurofilament number per axon was calculated. All quantifications were performed blinded to the genotype.

3.2.7.5 Immunogold-labeling

Immunogold labeling of cryosections was performed by Ramona Jung as described in (Tait, Gunn-Moore et al. 2000, Werner, Kuhlmann et al. 2007). Cross-sectioned sciatic nerves from 2-month-old WT mice were used and antibodies were specific for CMTM6 (OriGene, Cat# TA322304; 1:100). Images of respective samples were obtained using the EM912AB-Omega (Zeiss, Oberkochen, Germany) coupled to a wide-angled dual speed 2k CCD-camera (TRS, Moorenweis, Germany).

3.2.8 Behavioral Analysis and Plethysmography

All behavioral experiments as well as Plethysmography and subsequent analyses were performed by the same investigator, blinded to the genotype and with standardized methods generally used in the department. All experiments were performed one mouse at a time, only once per mouse and without any prior habituation to the test itself (except for open-field assay and Plethysmography, further information see below). Mice were generally placed in the experimental room at least 30 minutes before the testing. Number of animals per genotype and ages are indicated in the respective graphs and legends. Calculations and illustration of data was done using Microsoft Excel 2013 and GraphPad Prism 6.

3.2.8.1 Grid walking test

For assessing motor coordination, mice were placed on a metal grid (1 cm grid size) and allowed to run a distance of 2m while being videotaped. The number of complete fore-and hind limb slips through the grid was assessed on a slow-motion video.

3.2.8.2 Hot plate assay

For sensory assessment (Fledrich, Schlotter-Weigel et al. 2012) animals were placed on a hot plate (Leica HI 1220; Nussloch, Germany) which was heated to constant 52°C and surrounded by a clear acrylic cage (open top). A timer was started once the mouse was placed on the hot plate and the time until it responded with either licking or retracting one of their hind limbs was stopped and measured as retraction latency. Afterwards, mice were always immediately removed from the hot plate and placed back in the home cage.

3.2.8.3 Rotarod test

For motor assessment animal were tested on the Rotarod system 3375.5 (TSE systems). Therefore, mice were placed on a rotating rod that was accelerated from 5 to 40 rpm in 300 sec. Mice were tested for 2 consecutive days following 1 day of training. Mice had to perform 3 consecutive runs per trial with 3 trials each day and a 10 min break between trials and the holding time (sec) per run was recorded. Afterwards, the mean holding time (sec)/Latency to fall (sec) per trial as well as the mean of the maximum value per trial was calculated using Microsoft Excel 2013.

3.2.8.4 Open-field assay

For assessing motor capabilities and exploratory behavior mice were tested in the open-field assay as previously described in (Dere, Dahm et al. 2014, Dere, Winkler et al. 2015, Netrakanti, Cooper et al. 2015). Prior testing mice were placed in the front room of the testing room for 1-2 hours for habituation. The open-field set-up is an apparatus with a gray circular Perspex area (120 cm diameter, 25 cm height) and contains a light intensity of 140 lux in the center of the box. One mouse at a time was placed in the center of the box and allowed to explore the box for 10 min freely. An automated tracking software (Viewer2, Biobserve, Bonn, Germany) tracked the following parameters: latency (s) to cross from center to periphery, time spent (s) in the peripheral, intermediate and center zones of the box as well as the total distance (m) and mean running velocity (mm/s) mice travelled in the box. After each mouse, the box was cleaned with ethanol, wiped with $_{dd}H_2O$ and after 3 min the next mouse was placed inside the open-field box. Mice were only tested once.

3.2.8.5 Plethysmography

Breathing was analyzed by unrestrained whole-body-plethysmography essentially as originally established (Drorbaugh and Fenn 1955). Experiments and analyses were performed by Swen Hülsmann (UMG Göttingen). Briefly, mice were placed in a plexiglass chamber and could habituate for at least 12 minutes and breathing cycles from a subsequent period of 3 min were analyzed. Overall, intervals longer than 750 ms were considered as breathing pauses, and the number per minute was calculated. Plethysmography and analyses were done blinded to the genotype.

3.2.9 Electrophysiology

Standard electroneurography was performed by Robert Fledrich on mice of indicated genotypes at P75 using a Toennies Neuroscreen® (Jaeger, Joechsberg, Germany) (Fledrich, Akkermann et al. 2019). Briefly, mice were anesthetized with intraperitoneal (i.p.) injection of Ketaminehydrochloride/Xylazinhydrochloride (100mg kg^{-1} BW / 8 mg kg^{-1} BW) to perform recordings under deep anesthesia. Sensory nerve conduction velocity (sNCV) measurements were performed on the tail of the mice. Therefore, a pair of fine steel needle recording electrodes (Schuler Medizintechnik, Freiburg, Germany) was placed upright at the tail base on either side of the tail followed by 2 proximal stimulation electrodes exactly 50 mm distally. Additionally, the ground electrode was placed subcutaneously between the two needle pairs. Thereafter, increasing current pulses were delivered until supramaximal stimulation was achieved and the compound nerve action potential (SNAP) reached a plateau. SNAP measurements were averaged over 20 stimuli and the sensory nerve conduction velocities (sNCV) were calculated from sensory action potential latency measurements over the 50 mm distance. For motor recordings the first pair of needle electrodes (proximal) was placed close to the sciatic notch, the other pair (distal) in vicinity to the ankle next to the tibial nerve and motor recording electrodes in the small foot muscle of the plantar surface. The distance of the stimulation electrodes was measured. Again, proximal and distal supramaximal stimulation of the sciatic and tibial nerve was applied and the compound muscle action potentials (CMAPs) were recorded. Together with the distance of the stimulation electrodes and the difference of the responses the motor nerve conduction velocity (mNCV) was calculated.

3.2.10 Quantification and statistical analysis

Quantifications, statistical analyses and data visualization were mainly performed with Microsoft Excel 2013, GraphPad Prism (GraphPad Software, Inc., San Diego, United States) and RStudio (https://www.rstudio.com/, Version 3.4.1). Data in this thesis is mainly shown as bar graphs or dot plots as mean ± SD (error bars). The overall data distribution was always assumed to be normal but was not formally tested, except for Plethysmography data performed by Swen Hülsmann. Sample sizes were not predetermined but are similar to those commonly used in the field. Exact sample size as well as the number of mice used for the different experiments is shown in the figures and/or indicated in the figure legends. In addition, outlier tests were performed on all data except axonal diameter values using GraphPad (https://www.graphpad.com/quickcalcs/Grubbs1.cfm). Only for nerve conduction velocity measurements one outlier in the control group was detected but no further outliers were identified. For comparing two groups, unpaired two-tailed Student`s t test was applied. For qRT-PCR two-way analysis of variance (ANOVA) with Sidak`s multiple comparisons test was performed. For rotarod data two-way ANOVA with Bonferroni multiple comparison test was used. Since data of the breathing pauses are not normally distributed, the nonparametric Mann-Whitney Rank Sum Test was applied. For statistically assessing the relative frequency distribution of axonal diameters RStudio was used. The script has been generated by Drini Morina and is deposited at https://github.com/MariaEichel/FrequencyDistributions.R or can be found in the addendum. For this statistical analysis, data was used in data frames and a simple linear model was applied. The two-tailed Kolmogorow-Smirnow test was used to judge the change in distribution between two groups but was only applied if the previously applied two-tailed Student`s t test gave a significant result. The visualization of axonal diameter frequency distributions was performed in GraphPad Prism. Therefore, all measured axonal diameter values per animal were grouped respective to their genotype and the built-in analysis of frequency distribution in % was performed applying a bin width of 0.5 µm or 0.1 µm and binning each replicate. Overall, a p-value of <0.05 was considered significant in all tests. Significance levels are represented as n.s. =non-significant, *P<0.05, **P<0.01, ***P<0.001 with exact p-values mentioned in the respective figure legends.

4 Results

4.1 Identifying CMTM6 as a novel adaxonal Schwann cell protein

To closer investigate the association between myelinating Schwann cells and peripheral axons and to reveal yet unknown but functionally relevant novel molecules at the axon/myelin interface, we biochemically purified a light-weight membrane fraction from pools of sciatic nerves of wild-type mice. The method itself was originally established by Menon and Dhaunchak for purifying the so called “axogliasome” (Dhaunchak, Huang et al. 2010) or “axolemmal complex” (Menon, Rasband et al. 2003) in the CNS but was adapted in this study as depicted in Figure 5. The purified fractions were subjected to quantitative mass spectrometry (performed by Stefan Tenzer, Univ. Mainz) and resulted in 755 identified proteins. Amongst those were markers of the axolemma and adaxonal myelin membranes depicted in Figure 6A. Further, proteins of the extracellular matrix and basal lamina, compact myelin as well as axonal cytoskeleton were detected (Fig. 27 and Table 2 Addendum). Since proteins known to be located in other compartments than the axon/myelin interface were detected in the purified fractions, we will further refer to the fraction as the “axogliasome-enriched fraction” (AEF).

Amongst the identified proteins we tried to select candidates for future *in vivo* investigations by applying the following selection criteria: I) robust abundance in all purified AEF samples, II) possible function as ligand or receptor III) novel protein or protein family with a yet unknown role for the nervous system, IV) preferably expressed on SCs rather than neurons and V) availability of embryonic stem cells or mice harboring a floxed allele at a mouse genome consortium for SC specific deletion. Based on these criteria, we selected CMTM6 (chemokine-like factor-like MARVEL transmembrane-domain-containing family member 6), a tetra span protein from the under investigated CMTM protein family, for further analysis. *Cmtm6* was previously also detected in microarray analysis of murine sciatic nerves displaying higher mRNA abundance compared to other CMTM-family members in adult mice (unpublished data by Chris Hummel, MPI-EM Neurogenetics). By applying immunoblot analysis we validated the increased abundance of CMTM6 in the AEF compared to biochemical purified myelin and lysate, respectively. Also, other axolemma and adaxonal membrane proteins like MAG, NFASC and ATP1A1 showed an increased abundance

in the AEF, whereas myelin markers (MPZ and PMP2) were clearly enriched in the myelin fraction. Axonal cytoskeleton protein NEFH could only be reliably detected in the lysate fraction (Fig. 6B).

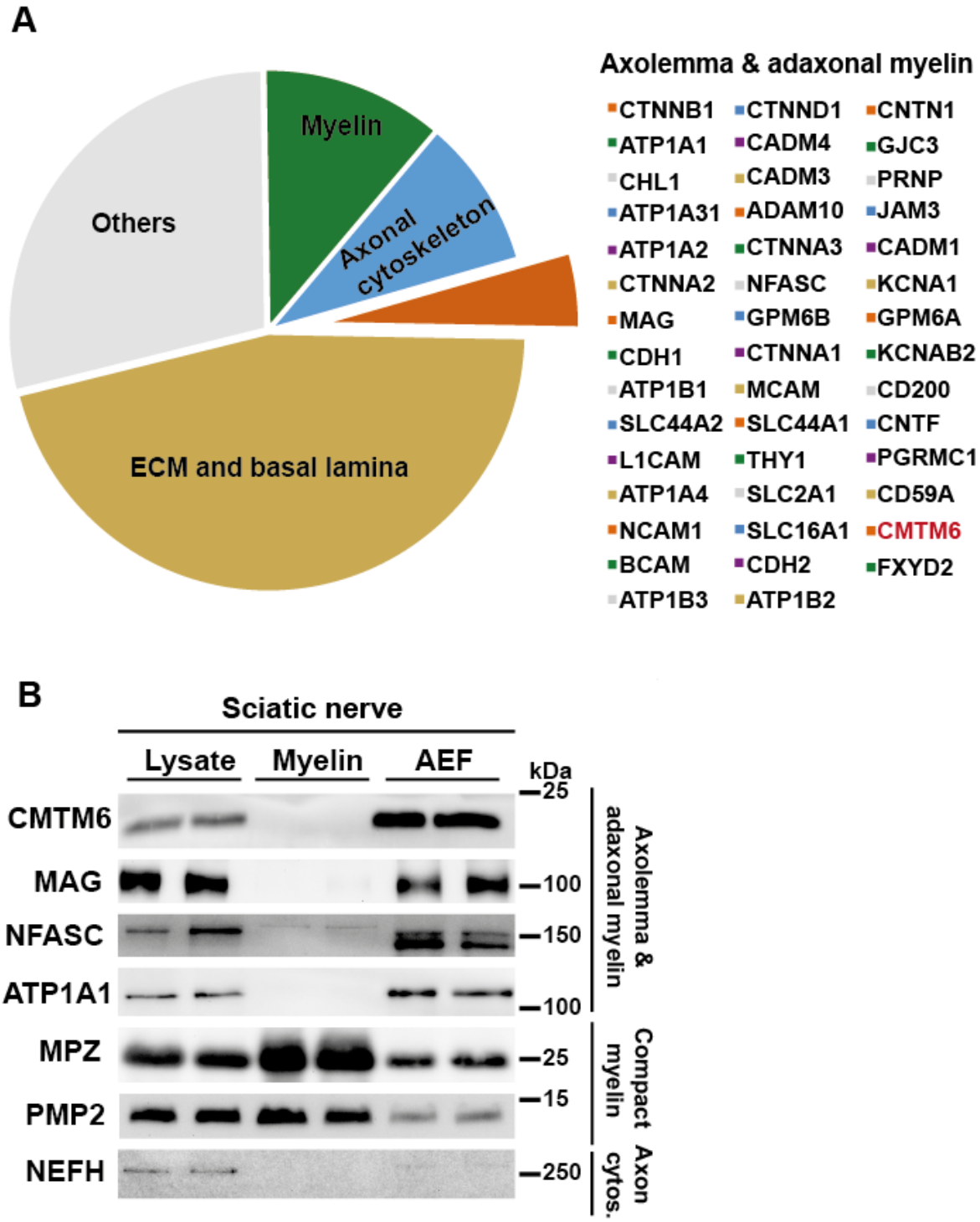

Figure 6 Identification of CMTM6 as a novel adaxonal Schwann cell protein. A) Pie chart showing protein composition of axolemma and adaxonal myelin enriched fraction (AEF) from pools of sciatic nerves of adult WT mice. Proteins of the axolemma and adaxonal myelin compartment are depicted on the right side. CMTM6 was discovered as novel constituent. Protein composition of the other compartments and exact ppm values can be found in the addendum (Fig. 27 and Table 2) **B)** Immunoblot-analysis identifies CMTM6 enrichment in AEF compared to myelin and nerve lysate. Marker for axolemma & adaxonal myelin (MAG, NFASC, ATP1A1), compact myelin (MPZ, PMP2) and axonal cytoskeleton (NEFH) serve as controls.

To further investigate if CMTM6 could indeed play a role in Schwann cell to axon signaling we used STED microscopy on sciatic nerve teased fiber preparations to determine the exact localization of CMTM6. Indeed, we showed that CMTM6 (red) can be found at the adaxonal SC membrane adjacent to the axolemma labeled with betaII-spectrin (green) as well as in Schmidt-Lantermann incisures (SLI) (Fig. 7A, B indicated by white arrowheads). Further, it was shown that CMTM6 displays a periodic distribution along the internode with an autocorrelation peak at 200 nm (Fig. 7C, black arrow). Additionally, cryo-immuno electron microscopy on cross-sectioned sciatic nerves of 2-month-old WT mice confirmed the adaxonal localization of CMTM6 (Fig. 7D, indicated by black arrowheads).

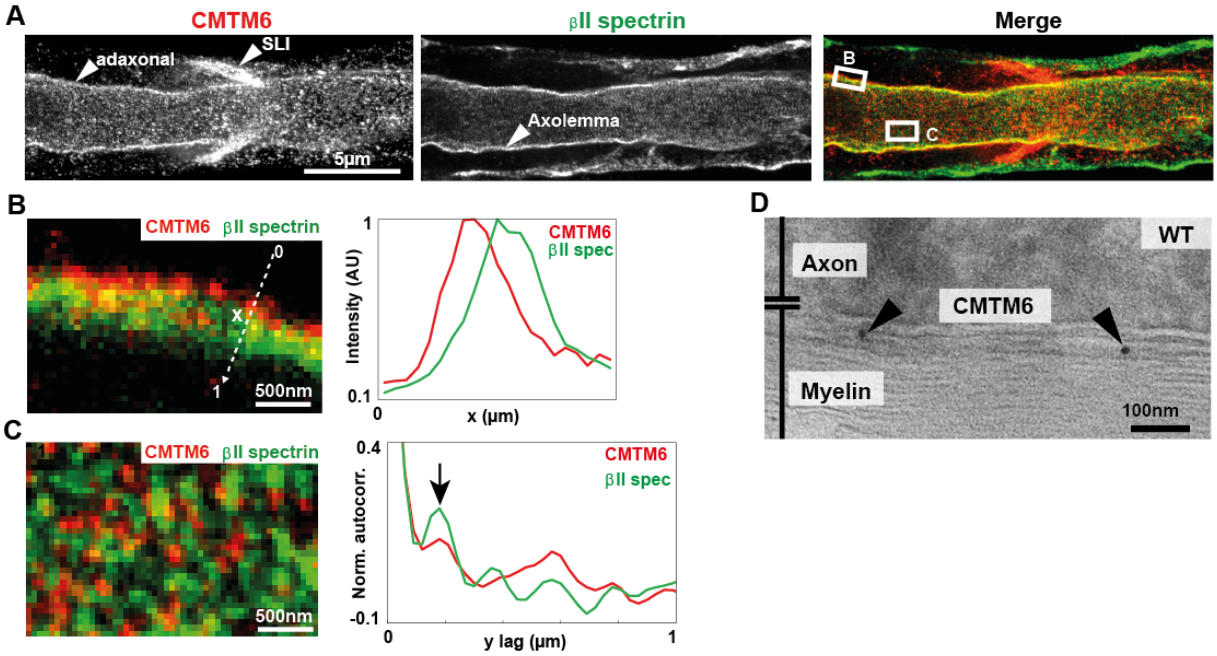

Figure 7 CMTM6 is localized to the adaxonal membrane. **A)** STED-micrographs of teased sciatic nerve preparations immunolabeled for CMTM6 (red) and betaII-spectrin (green). Arrowheads indicate adaxonal myelin membrane, Schmidt-Lantermann incisures (SLI) and axolemma. Boxes on merged image indicate areas enlarged for line-profile of intensities (**B**) and autocorrelation analysis (**C**). Scale bar, 5 µm. **B)** Line profile shows that CMTM6 immunolabeling (red) is detected adjacent to the axolemma, identified by betaII-spectrin immunolabeling (green). Scale bar, 500 nm. **C)** Autocorrelation-analysis reveals a peak of periodic distribution of CMTM6-immunolabeling (red) longitudinal along the axon/myelin unit, similar to betaII-spectrin, indicated by black arrows. Scale bar, 500 nm. **D)** Immunogold-labeling of cross-sectioned sciatic nerves (WT, 2 mo) shows CMTM6-labeling (arrowheads) at the adaxonal myelin. Scale bar, 100 nm.

To further elucidate if *Cmtm6* is expressed in Schwann cells we performed X-Gal histochemistry on sciatic nerve teased fibers of adult *Cmtm6*$^{lacZ/neo}$ mice and indeed demonstrated a labeling pattern in the soma of Schwann cell nuclei (Fig. 8A). To discover the appearance of CMTM6 developmentally, its abundance was analyzed by immunoblotting of WT sciatic nerve lysates at different time-points ranging from P1 to

P30. Here, we showed a developmentally increasing abundance of CMTM6 from P5 onwards which is similar to common myelin proteins such as MPZ, MAG and CNP (Fig. 8B).

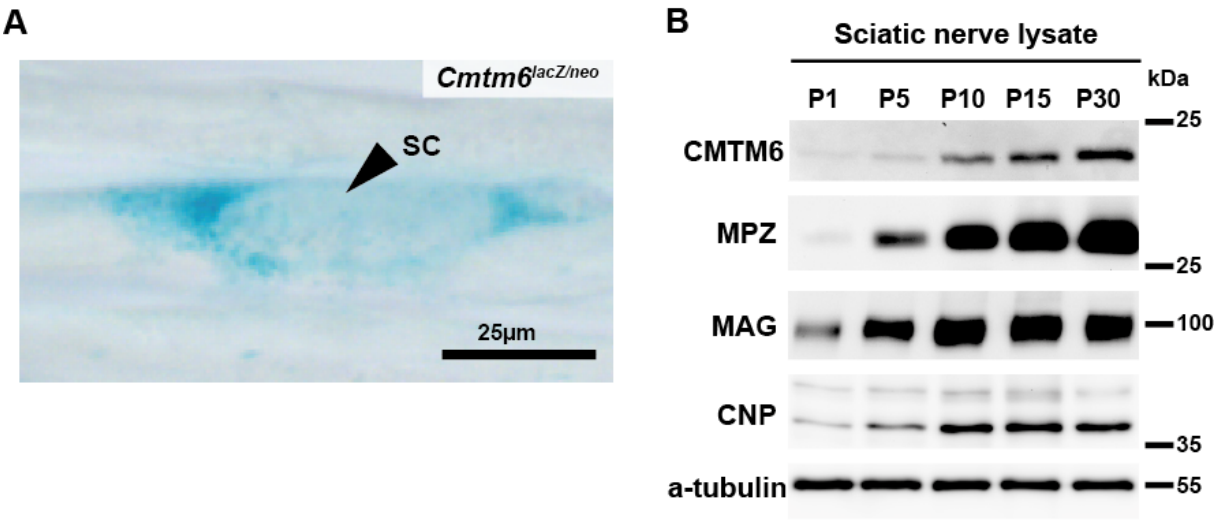

Figure 8 Cmtm6 is expressed by SC and protein abundance increases with nerve development. **A)** X-gal-histochemistry on sciatic nerve teased fiber preparations of *Cmtm6*$^{lacZ/neo}$ mice shows LacZ activity in the Schwann cell soma. Scale bar, 25µm. **B)** Immunoblot analysis of sciatic nerve lysate of 1, 5, 10, 15- and 30-days old WT mice shows developmentally increasing CMTM6 abundance similar to known myelin markers (MPZ, MAG, CNP). a-tubulin serves as control.

Taken together, these results demonstrate that the newly identified protein CMTM6 is indeed a Schwann cell protein which is localized adjacent to the axolemma suggesting it is an interesting candidate for mediating Schwann cell to axon interaction.

4.2 Characterization of mice lacking CMTM6 from Schwann cells

To investigate possible relevant function of the newly identified adaxonal Schwann cell protein CMTM6 for the axon/myelin unit of the PNS we generated mice lacking CMTM6 from Schwann cells. The following chapters will show the results of the characterization of these conditional mutant mice ranging from morphological and biochemical analysis to functional and behavioral readouts.

4.2.1 Generation and validation of *Cmtm6* cKo mice

To identify a potential role of CMTM6 *in vivo*, conditional mutant mice lacking CMTM6 specifically from Schwann cells (*Cmtm6*$^{fl/fl}$**Dhh*^{Cre}, further referred to as *Cmtm6* cKo) were generated as described under Material & methods, chapter 3.2.2. Figure 9A illustrates the scheme for conditional inactivation of the engineered *Cmtm6*

gene and respective primer binding sites which were used for genotyping (depicted in Fig. 9B). The upper image in Figure 9B depicts a 292 bp band for the WT and a 450 bp band for the *Cmtm6*^{flox} allele whereas the lower image in 9B depicts that only in presence of *Dhh*-Cre recombinase (Fig. 9B, middle image, 400 bp) a product of 350 bp is generated identifying the recombined *Cmtm6* allele.

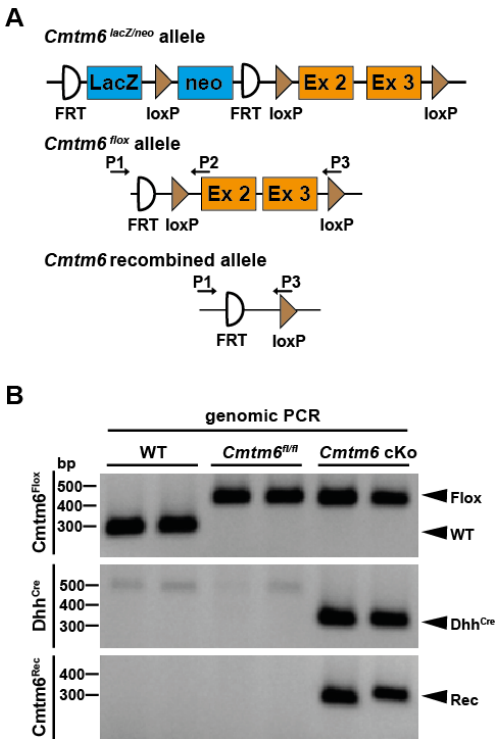

Figure 9 Conditional inactivation of Cmtm6 in Schwann cells. **A)** Scheme of the engineered *Cmtm6* allele. Exon 2 and 3 of the *Cmtm6*^{flox} allele are flanked by loxP-sites for *Cre*-mediated recombination. Primers for genotyping (**B**) are indicated within the scheme. **B)** Genotyping PCR of DNA isolated from mouse ear tags at P21. Upper image shows *Cmtm6*^{flox} allele and WT PCR product. Middle image shows *Dhh*^{Cre} specific PCR product and lower image shows PCR product identifying recombined *Cmtm6* allele in *Cmtm6* cKo. Gel shows n=2 mice per genotype.

Further, we applied immunoblot analysis and confocal microscopy to validate if deletion of CMTM6 from Schwann cells was functional. Indeed, immunoblot analysis on sciatic nerves lysates of 2 month (2 mo) old control and *Cmtm6* cKo mice confirmed absence of CMTM6 in mice lacking CMTM6 from Schwann cells. (Fig. 10A). Additionally, the immunoblot showed that the abundance of classical myelin markers MPZ and MAG are unaltered upon the deletion of CMTM6. Immunolabeled sciatic nerve teased fiber preparations and cross-sections displayed a preferentially co-localization of CMTM6 and MAG at the adaxonal membrane and SLI but absence of CMTM6 from the abaxonal membrane (Fig. 10B, white arrowheads). Notably, the abaxonal localization of MAG appears diminished in *Cmtm6* cKo even though the

overall abundance is unchanged. Nonetheless, when comparing MAG labeling between adult control and *Cmtm6* cKo sciatic nerve cross-sections the abundance of MAG appeared unchanged similar to MBP which is labeling the compact myelin (Fig. 10C). Both, Figure 5B and C confirm the absence of CMTM6 in *Cmtm6* cKo nerves.

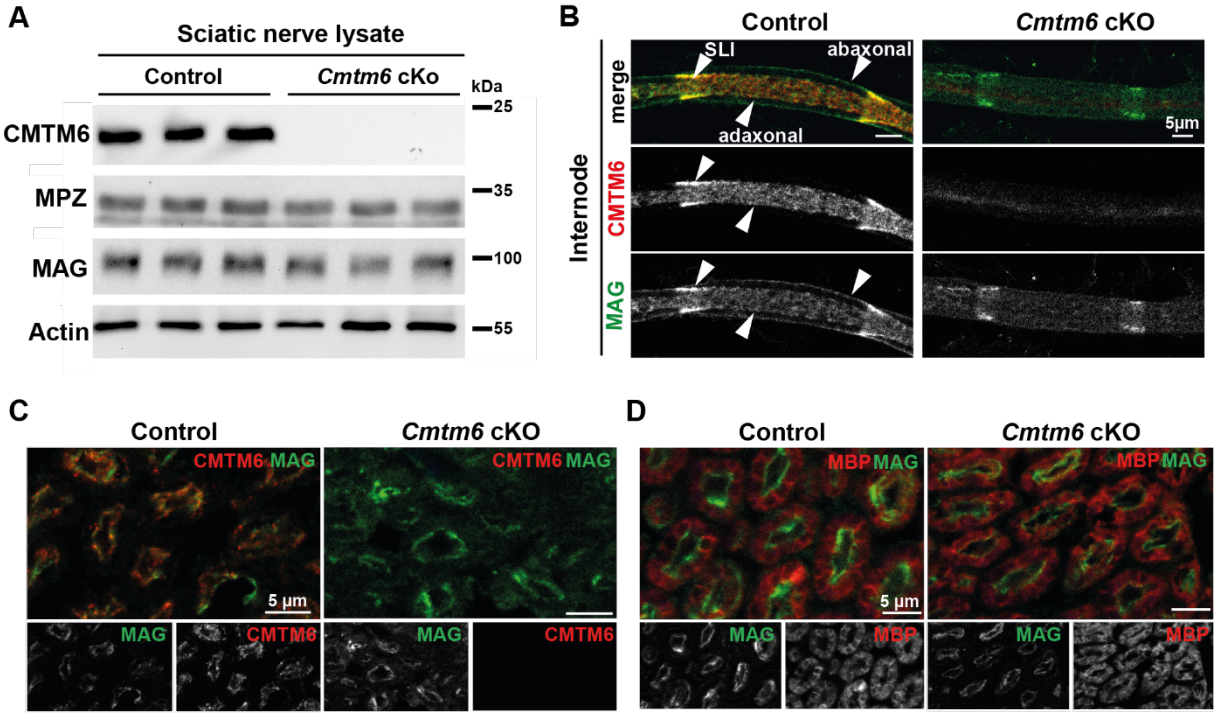

Figure 10 CMTM6 is absent in Cmtm6 cKo. A) Immunoblot analysis of sciatic nerve lysates from control and *Cmtm6* cKo mice (2 mo) reveals absence of CMTM6. MPZ, MAG and actin serve as controls. **B)** Immunolabeling of teased sciatic nerve preparations immunolabeled for CMTM6 (red) and MAG (green) validates adaxonal myelin localization of CMTM6 and absence in *Cmtm6* cKo mice. SLI, adaxonal and abaxonal myelin membrane are indicated by white arrowheads. Scale bar, 5µm. **C)** Immunolabeling of cross-sectioned sciatic nerves reveals partially co-labeling of CMTM6 (red) and MAG (green) at the adaxonal myelin membrane and SLI in control mice and absence of CMTM6 in *Cmtm6* cKo. Scale bar, 5µm **D)** Immunolabeling of MBP (red) and MAG (green) of adult control and *Cmtm6* cKo cross-sectioned sciatic nerves indicates normal appearing MBP and MAG localization. Scale bar, 5µm.

To investigate if the expression of classical myelin and SC markers as well as other CMTM family members is changed upon CMTM6 deletion, mRNA abundances on sciatic nerve tissue of respective mice were quantified using qRT-PCR (Fig. 11). The quantification showed, that only *Cmtm6* is virtually undetectable, whereas mRNAs encoding other CMTM family members are unchanged (Fig. 11A). Further, the expression of typical myelin marker genes (Fig. 11B) and transcription factors of the Schwann cell lineage (Fig. 11C) are not altered when CMTM6 is lacking from SCs.

Concluding, these experiments validate that the genotype dependent depletion of CMTM6 from Schwann cells is functional on both, mRNA and protein level, whereas the abundance of typical myelin and SC lineage markers is unaltered in *Cmtm6* cKo.

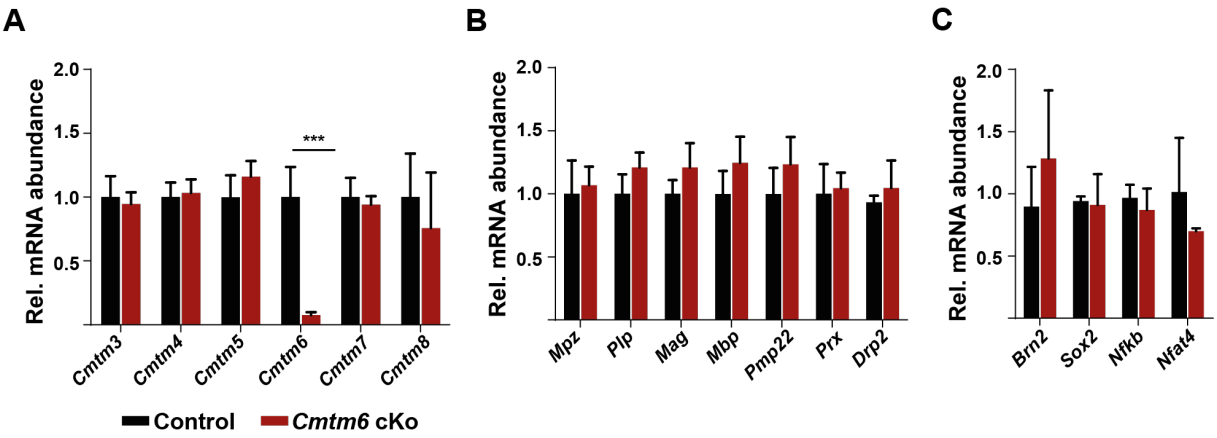

Figure 11 Conditional inactivation of Cmtm6 in Schwann cells does not result in abundance changes of mRNAs encoding typical myelin genes, SC transcription factors or other CMTM family member genes. **A)** Quantitative PCR analysis assessing the abundance of mRNAs encoding CMTM family members in sciatic nerves dissected from control and *Cmtm6* cKo mice at 2 mo indicates no changes except for *Cmtm6* which is virtually undetectable in *Cmtm6* cKo. **B)** The abundance of typical myelin marker transcripts is unchanged between control and *Cmtm6* cKo sciatic nerves. **C)** Assessing the abundance of mRNAs encoding typical transcription markers of the SC lineage indicates no changes between control and *Cmtm6* cKo nerves. All data are n=4-5; Mean +/-SD (error bars); ***P<0.001 by two-way analysis of variance (ANOVA) with Sidak`s multiple comparisons test.

4.2.2 *Cmtm6* cKo mice display abnormally increased diameters of myelinated axons

Hypothesizing a functional impact of CMTM6 deletion on the Schwann cell-axon unit we assessed consequences of its deletion on several cross-sectioned peripheral nerves dissected from 2-month-old control and *Cmtm6* cKo mice using light- and electron microscopy. First, we measured the diameters of all cross-sectioned myelinated axons within the phrenic nerve of five animals per genotype on light-microscopic level (for further details on quantification and statistics see Material and Methods, chapter 3.2.7.4 and 3.2.10). Strikingly, we detected significantly increased axonal diameters in *Cmtm6* cKo mice compared to control mice as displayed in representative electron microscopic images in Figure 12A and in frequency distributions of axonal diameters in Figure 12C. Notably, the number of myelinated axons within the phrenic nerve is unchanged between control and *Cmtm6* cKo mice (Fig. 12E). Further, the g-ratio (diameter of the axon divided by the respective myelinated fiber diameter) was calculated on electron microscopic images to assess myelin sheath thickness. g-ratio analysis shows unchanged values of around 0.6 for

both control as well as *Cmtm6* cKo mice (Fig. 12G) suggesting that larger axons within *Cmtm6* cKo also have appropriately thicker myelin sheaths.

The phrenic nerve is a mixed nerve containing smaller sensory and larger motor axons. Hence, we next quantified the axonal diameters of myelinated, sensory axons in the dorsal root of control and *Cmtm6* cKo mice since it is easy to identify and contains various sensory fibers ranging from small unmyelinated, Remak-associated C-fibers to larger A-alpha, beta and delta afferent fibers (FitzGerald, Gruener et al. 2012). Indeed, we showed a similar significant increase in diameters of myelinated axons (Fig. 12B and D) without a loss of the number of myelinated axons in *Cmtm6* cKo compared to control dorsal roots (Fig. 12F). These results imply a novel role for CMTM6 in restricting axonal diameter growth.

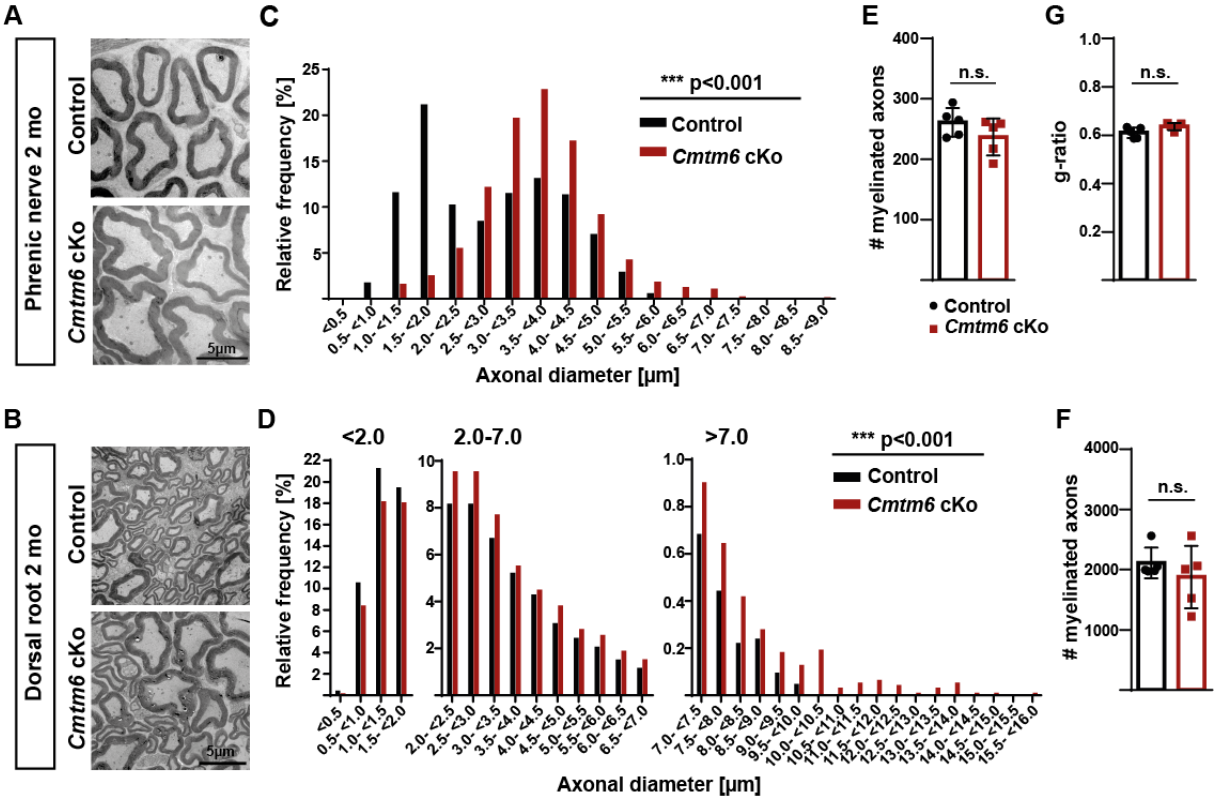

Figure 12 Diameters of myelinated axons are abnormally increased in phrenic nerves and dorsal roots when CMTM6 is lacking from Schwann cells. **A and B)** Electron micrographs of cross-sectioned phrenic nerves (A) and dorsal roots (B) of 2-month-old (2 mo) reveal increased axonal diameters in *Cmtm6* cKo compared to control mice. Scale bar, 5 µm. **C and D)** Genotype-dependent quantification of the diameters of myelinated axons on semi-thin sections reveal shift towards larger axonal diameters in *Cmtm6* mutant mice in both phrenic nerve (B) and dorsal root (F). Data are presented as frequency distribution with 0.5 µm bin width. **C)** n=1293 axons from n=5 control mice and n=1172 axons from n=5 *Cmtm6* cKo mice; Mean axonal diameter $_{(control+/-Cmtm6\text{-}cKo)}$ = 2.87 µm+0.84 µm; P=2.2e^{-16} by two-sided Kolmogorow-Smirnow test; **D)** n=10387 axons from n=5 control mice and n=9298 axons from n=5 *Cmtm6* cKo mice; Mean axonal diameter $_{(control+/-Cmtm6\text{-}cKo)}$ = 2.47 µm+0.27 µm; P=2.2e^{-16} by two-sided Kolmogorow-Smirnow test. **E and F)** Quantification of the number of myelinated axons on semi-thin sections shows no change between control and mutant mice in both phrenic nerves (**C**) and dorsal roots (**G**). Data are presented as mean +/- SD; n=5 mice per genotype. **E** P=0.1929; **F** P=0.3894; by Two-tailed Student`s t-test. **G)** g-ratio analysis

of electron micrographs from phrenic nerves at 2 mo reveals appropriate myelin sheath thickness in *Cmtm6* cKo mice. Data are presented as mean +/- SD; n=505 axons from n=3 control mice; n=459 axons from n=3 *Cmtm6* cKo mice; P=0.0637 by Two-tailed Student`s *t*-test. n.s. = non-significant P>0.05, **P<0.01, ***P<0.001.

Next, we assessed axonal diameters in the sciatic nerves of both genotypes since the sciatic nerve is commonly used in the field, has a higher number of myelinated (sensory and motor) axons (roughly around 3000-4000), is comparably easy to dissect and used in the majority of biochemical investigations throughout this study. Indeed, genotype-dependent quantification of sciatic nerves confirmed previous findings by showing that *Cmtm6* cKo display a higher frequency of large diameter axons compared to control mice (Fig. 13A, B) without a loss of the number of myelinated axons (Fig. 13C). By analyzing the g-ratio of 180 axons per nerve in five animals per genotype on electron microscopic level, we demonstrated that the ratio between myelin sheath thickness and axonal diameter is maintained in conditional knockout mice as depicted in Figure 13D. Further, we showed on light microscopic level that the number of Schwann cell nuclei within sciatic nerves is unchanged between control and *Cmtm6* cKo (Fig. 13E). Since we have not seen any changes in the number of myelinated axons so far, we additionally quantified the percentage of degenerating axons on electron microscopic images of both genotypes. We detected no change in the number of degenerated/degenerating axonal profiles in sciatic nerves of *Cmtm6* cKo suggesting that axonal loss is not a feature in these mice (Fig. 13F).

Taken together, these results show a novel role for the SC protein CMTM6 in restricting radial growth of myelinated axonal diameters and thereby maintaining the myelin sheath thickness to axon diameter ratio. Notably, the axonal survival and integrity is not impaired upon loss of CMTM6 from SCs.

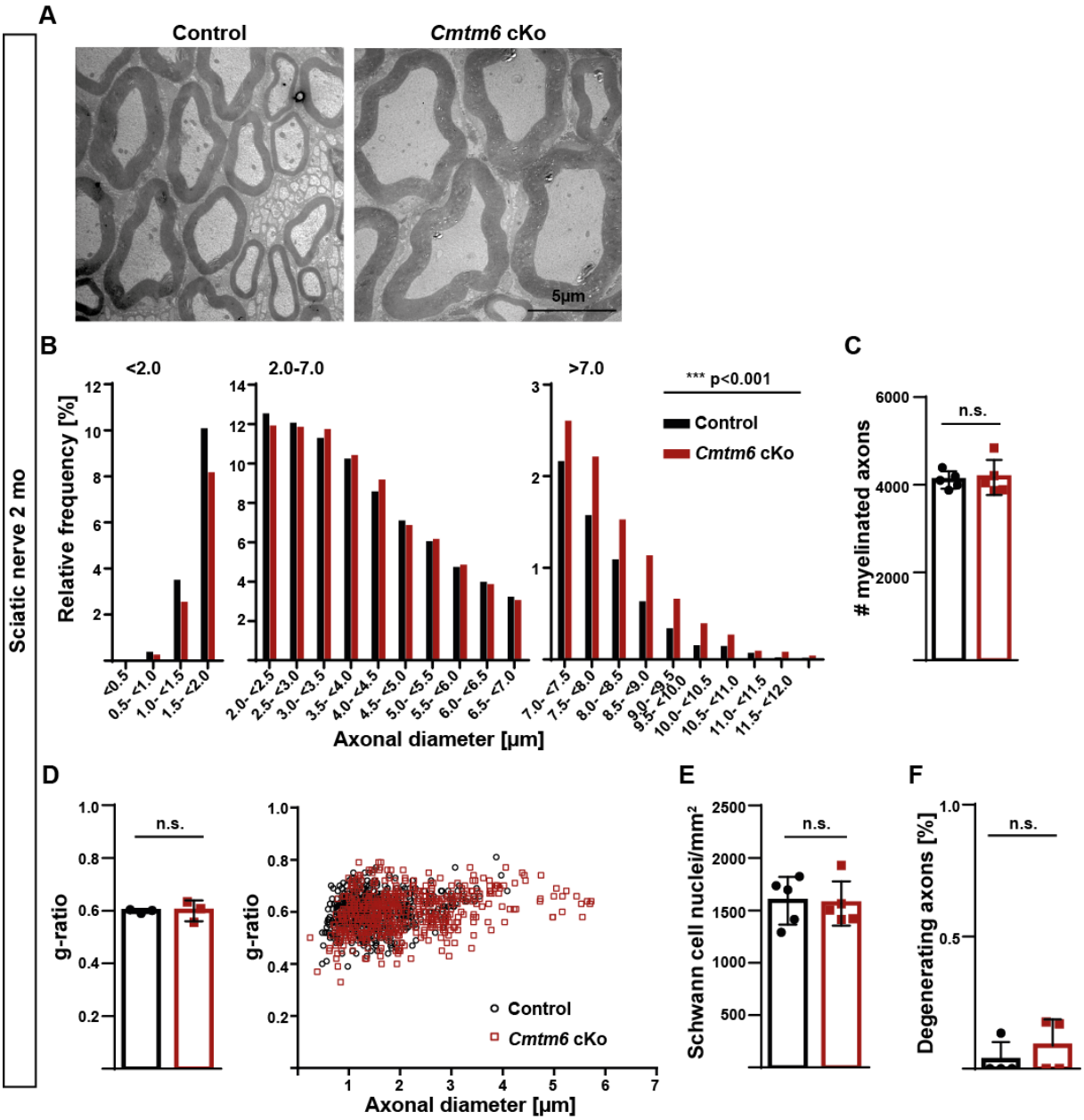

Figure 13 Axonal diameters are increased in sciatic nerves of adult Cmtm6 cKo mice without affecting myelin thickness or axonal survival. **A)** Representative electron micrographs of cross-sectioned sciatic nerves of 2-month-old control and *Cmtm6* cKo mice show increased axonal diameters. Scale bar. 5µm. **B)** Quantification of the diameters of myelinated axons on semi-thin sections shows a shift towards larger axonal diameters in sciatic nerves of *Cmtm6* cKo compared to control mice. Data are presented as frequency distribution with 0.5 µm bin width, n=19250 axons from n=5 control mice and n=18966 axons from n=5 *Cmtm6* cKo mice; Mean axonal diameter $_{(control+/-Cmtm6\text{-}cKo)}$ = 3.16 µm+0.09 µm; P=1.216e^{-5} by two-sided Kolmogorow-Smirnow test. **C)** Quantification of the number of myelinated axons within the sciatic nerve on semi-thin section reveals no change between control and *Cmtm6* cKo mice. Data are presented as mean +/- SD, n=5 mice per genotype; P=0.7781 by Two-tailed Student`s *t*-test. **D)** g-ratio analysis of electron micrographs from sciatic nerves identifies appropriate g-ratio in *Cmtm6* cKo mice. Data are presented as mean +/- SD, n=180 axons per mouse with n=3 mice per genotype; P=0.9785 by Two-tailed Student`s *t*-test. **E)** Quantitative assessment of the number of SC nuclei on sciatic nerve semi-thin sections shows normal numbers between control and *Cmtm6* cKo mice. Data are presented as mean +/- SD, n=5 mice per genotype; P=0.8557 by Two-tailed Student`s *t*-test. **F)** Genotype-dependent assessment of degenerating axonal profiles on electron micrographs of sciatic nerves reveals no significant differences in the number of degenerating-appearing axonal profiles between control and *Cmtm6* cKo mice. Data are presented as mean +/- SD in percent, n=4 mice per genotype; P=0.4132 by Two-tailed Student`s *t*-test. n.s. = non-significant P>0.05, ***P<0.001.

4.2.3 CMTM6 deletion leads to increase of non-myelinated axonal diameters but does not affect radial sorting of axons

In the peripheral nervous system, the myelination threshold for an axon to get radially sorted out of Remak bundles to be myelinated by SCs is mainly dictated by the axonal diameter and lies precisely at 1 µm (Feltri, Poitelon et al. 2016). Many of the known SC mutations and neuropathy models, but also molecules of the ECM and basal lamina, display a shift in this myelination threshold and/or affect the sorting of axons (Feltri et al., 2016; Monk et al., 2015). Thus, we analyzed the axonal diameters of non-myelinated, Remak-associated axons as well as the number of axons per bundle within sciatic nerves at P9 and of 2-month-old control and *Cmtm6* cKo mice (Fig. 14). Note that CMTM6 abundance is readily detectable in WT sciatic nerve lysates at around P10 (Fig 8B). To our surprise the axonal diameters of non-myelinated, Remak-associated axons are already increased in *Cmtm6* cKo compared to control mice at P9 (Fig. 14A, B) which becomes even more prominent at 2 mo (Fig. 14E, F). Further, we did not detect a difference in the number of axons per bundle at both time points suggesting normal sorting (Fig. 14C, G). In addition, when focusing at the axonal diameter of each quantified, unsorted axon we detected no Remak-associated axon larger than 1 µm (Fig. 14D, H). This implies that CMTM6 is additionally restricting diameters of non-myelinated axons already during development without impairing the proceeding sorting and myelination process.

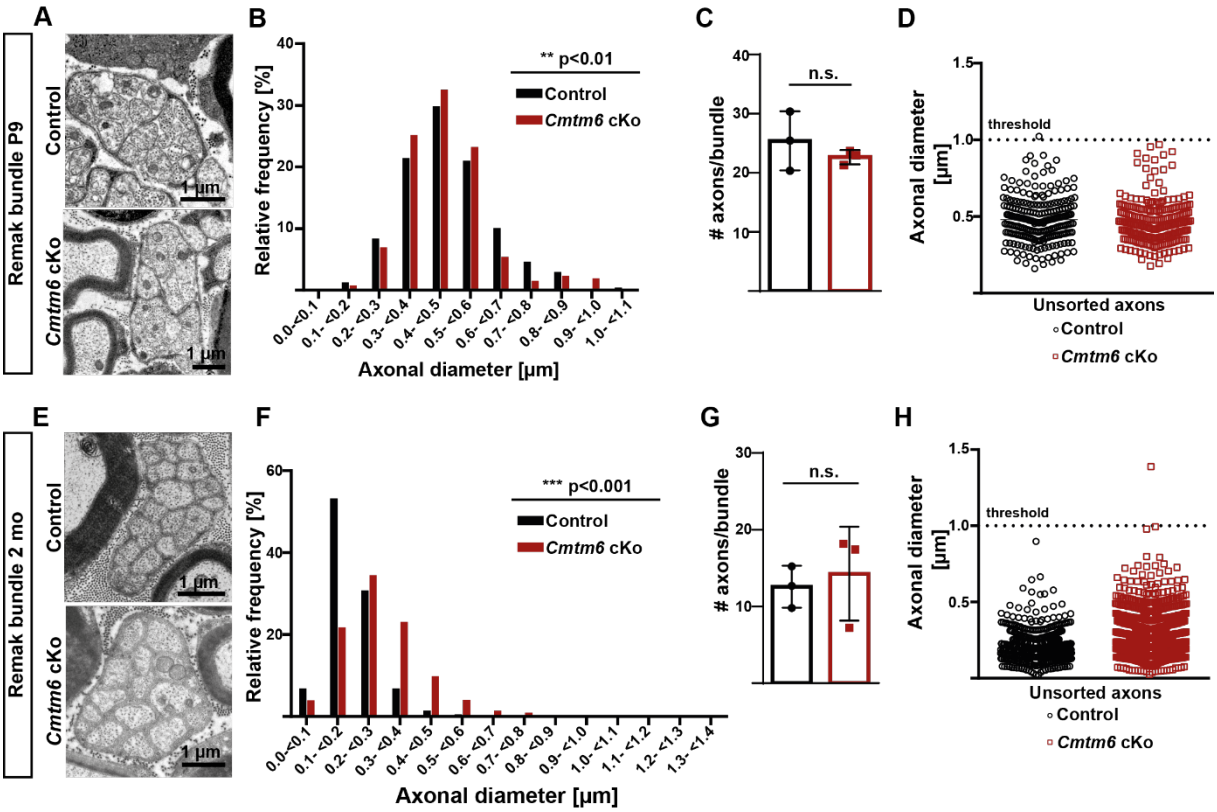

Figure 14 Non-myelinated axons are abnormally increased but radial sorting is normal when CMTM6 is lacking from Schwann cells. **A and E)** Electron micrographs show Remak bundles in sciatic nerves at P9 (**A)** and 2 mo **(E)** old control and *Cmtm6* cKo mice. Scale bar, 1 µm. **B and F)** Frequency distributions of genotype-dependent quantification reveals increased diameters of non-myelinated, Remak-associated axons in *Cmtm6* cKo compared to control mice at P9 (B) and 2 mo (F). Data are presented as frequency distribution with 0.1 µm bin width; **B)** n=690 axons from n=3 control mice and n=709 axons from n=3 *Cmtm6* cKo mice; Mean axonal diameter $_{(control+/-Cmtm6\text{-}cKo)}$ = 0.46 µm+0.02 µm; P=0.002 by two-sided Kolmogorow-Smirnow test; **F)** n=2522 axons from n=3 control mice and n=2377 axons from n=3 *Cmtm6* cKo mice; Mean axonal diameter $_{(control+/-Cmtm6\text{-}cKo)}$ = 0.19µm+0.08 µm; P=2.2e^{-16} by two-sided Kolmogorow-Smirnow test. **C and G)** Genotype-dependent quantification reveals unchanged number of non-myelinated, Remak-associated axons per bundle between P9 (C) and 2 mo (G) old *Cmtm6* cKo and control mice, implying normal radial sorting during development. Data are presented as mean+/-SD; n=3 mice per genotype; e P= 0.4057 f P= 0.683; by Two-tailed Student`s *t*-test. **D and H)** Quantification of diameters of non-myelinated, Remak-associated axons shows normal threshold diameter (1 µm) in *Cmtm6* cKo mice also implying normal radial sorting. Data are presented as data clouds; **D)** n=690 axons from 3 control mice and n=709 axons from 3 *Cmtm6* cKo mice **H)** n=2522 axons from 3 control mice and n=2377 axons from 3 *Cmtm6* cKo mice. n.s. = non-significant P>0.05, **P<0.01, ***P<0.001.

4.2.4 Development and aging in *Cmtm6* cKo mice

Since previous results of this study imply an involvement of CMTM6 in regulating diameters of non-myelinated, Remak-associated axons early during postnatal development (P9) we further investigated at which time-point larger diameters arise in myelinated axons of *Cmtm6* mutant mice. Therefore, we measured the diameters of myelinated axons within sciatic nerves at P9 and in 1-month-old control and *Cmtm6* cKo mice. Interestingly, the diameters of myelinated axons did not differ between control and *Cmtm6* cKo mice at P9 (Fig. 15A, B) and the change towards larger diameter axons in *Cmtm6* cKo becomes significant only at 1 mo of age (Fig. 15E, F).

Notably, genotype-dependent assessment of the number of myelinated axons indicates no change between genotypes at both time points (Fig. 15C, G). Since previous results revealed no impairment of sorting of axons we next quantified the number of sorted and non-myelinated axons larger than 1µm, which are termed promyelinated axons (Fig. 15D). However, we did not detect significant differences between control and *Cmtm6* cKo mice.

Results imply that CMTM6 restricts axonal diameters of non-myelinated, but not myelinated axons, early in development and that the phenotype of accelerated radial growth emerges in myelinated axons by 1 mo of age.

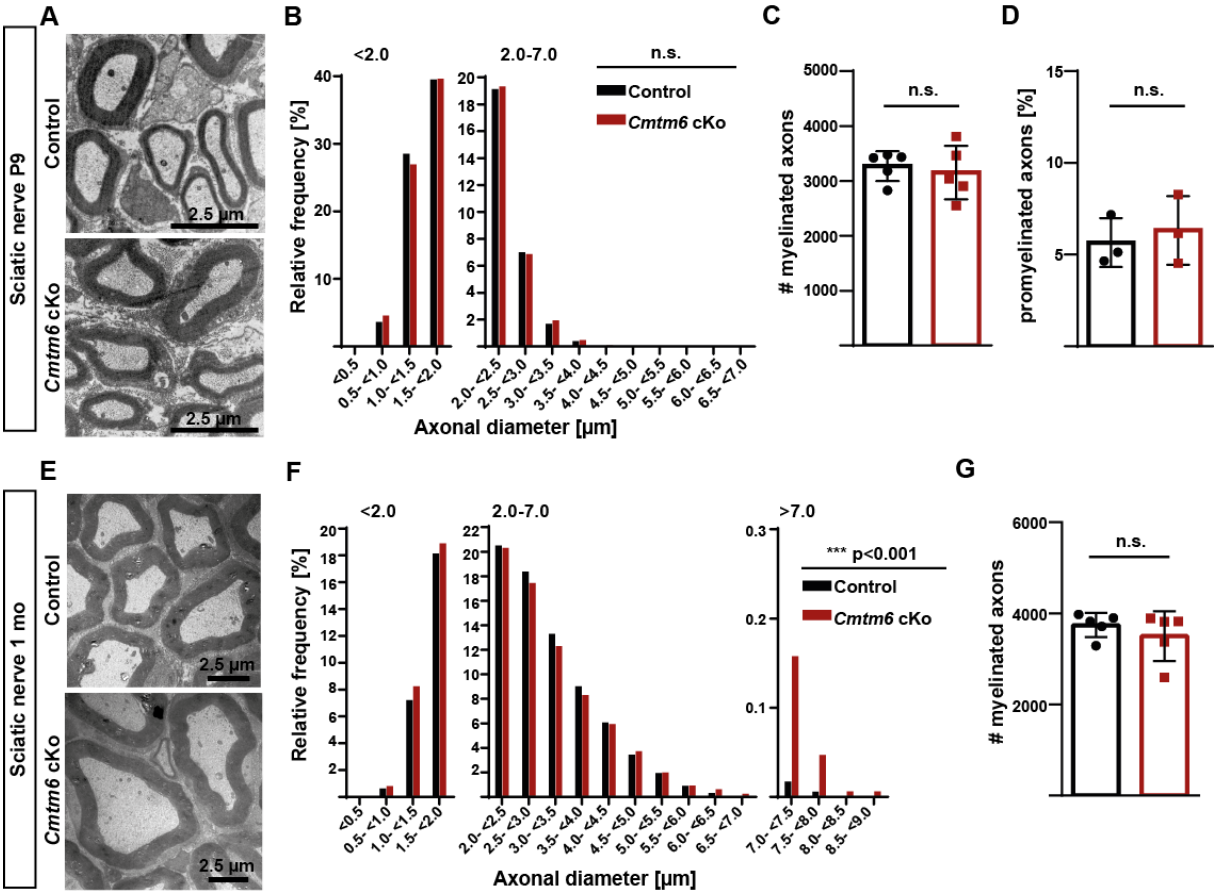

Figure 15 Increased diameters of myelinated axons in Cmtm6 cKo mice arise later in development. **A and E)** Representative electron micrographs illustrate cross-sectioned sciatic nerves at P9 (A) and 1 mo (E) of control and *Cmtm6* cKo mice. Scale bar, 2.5 µm. **B)** Genotype-dependent quantification of the diameters of myelinated axons in sciatic nerves at P9 reveals no significant difference between control and *Cmtm6* cKo mice. Data are presented as frequency distribution with 0.5 µm bin width; n=16350 axons from n=5 control mice and n=15775 axons from n=5 *Cmtm6* cKo mice; Mean axonal diameter $_{(control+/-Cmtm6\text{-}cKo)}$ = 1.77 µm+0.005 µm; P=0.3648 by Two-tailed Student`s *t*-test. **C and D)** Quantification of the number of myelinated axons (B) and pro-myelinated axons (C) on semi-thin sections of sciatic nerves indicates no change between control and *Cmtm6* cKo mice. Data are presented as mean +/- SD, **C** n=5 mice per genotype, P=0.6579; **D** n=3 mice per genotype, P=0.6424; by Two-tailed Student`s *t*-test. **F)** Genotype-dependent assessment of the diameters of myelinated axons in sciatic nerves at 1mo reveals shift towards larger axonal diameters in *Cmtm6* cKo compared to control mice. Data are presented as frequency distribution with 0.5 µm bin width; n=17578 axons from n=5 control mice and n=16966 axons from n=5 *Cmtm6* cKo mice; Mean axonal diameter $_{(control+/-Cmtm6\text{-}cKo)}$ = 2.68 µm+0.12 µm; P=2.2e^{-16} by two-sided

Kolmogorow-Smirnow test. **G)** The number of myelinated axons in sciatic nerves of 1 mo old control and *Cmtm6* cKo mice is unchanged. Data are presented as mean +/- SD, n=5 mice per genotype, P=0.4036 by Two-tailed Student`s *t*-test. n.s.=non-significant P>0.05, ***P<0.001.

Next, we wanted to assess the role of CMTM6 in aged nerves. For the PNS it was shown, that axonal diameters increase up to 12 months of age and slightly decrease afterwards (Chase, Engelhardt et al. 1992, Verdú, Butí et al. 1996, Ceballos, Cuadras et al. 1999, Verdú, Ceballos et al. 2000). When analyzing the diameters of myelinated axons in sciatic nerves of control mice from 1 month up to 20 months we confirmed these findings (Fig. 16A). The frequency distribution clearly showed a higher frequency for smaller diameter axons (1-3µm) for 1- to 2-month-old mice whereas the frequency of axons larger than 6µm is higher in mice older than 6 months. Note that no statistical tests were performed since data was generated only to confirm previously published results with our more intense way of assessing axonal diameters. We further measured the axonal diameters in sciatic nerves of 6-month-old (Fig. 16B) and 1-year-old (Fig. 16D) control and *Cmtm6* cKo mice. Whereas *Cmtm6* cKo mice exhibit larger axons at 6 months of age the significant genotype-dependent difference was surprisingly absent at the 1-year time-point, suggesting that control axons catch up to the accelerated radial axonal growth seen in *Cmtm6* cKo. Again, no significant difference in the number of myelinated axons was detected at both time-points irrespective of the genotype (Fig. 16C, E). Surprisingly, when immunoblotting sciatic nerve lysates of 1-, 2-, 4-, 6- and 12-month-old WT mice we saw a decreasing abundance of CMTM6 from 6-month of age on, while MAG was readily detectable independent of age (Fig. 16F).

These results imply that I) CMTM6 restricts the diameters of non-myelinated axons early in development, II) this precedes the establishment of larger diameters in myelinated axons which only arise at 1 month-of age and III) the abundance of CMTM6 decreases with aging resulting in no genotype-dependent difference in axonal diameters at 1 year of age.

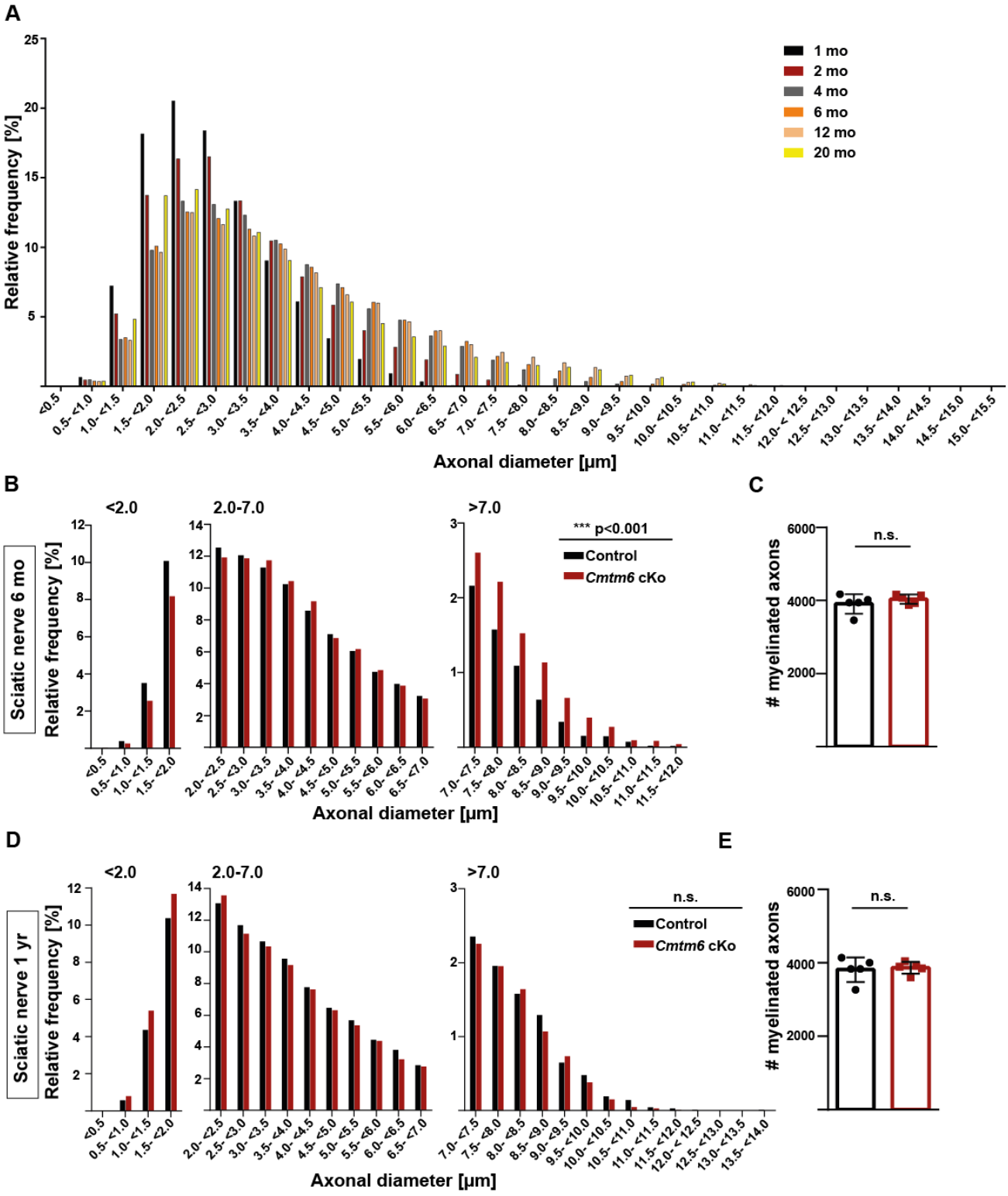
A
Relative frequency [%]
1 mo
2 mo
4 mo
6 mo
12 mo
20 mo
Axonal diameter [µm]
B
Sciatic nerve 6 mo
Relative frequency [%]
<2.0
2.0-7.0
>7.0
*** p<0.001
Control
Cmtm6 cKo
Axonal diameter [µm]
C
myelinated axons
n.s.
D
Sciatic nerve 1 yr
Relative frequency [%]
<2.0
2.0-7.0
>7.0
n.s.
Control
Cmtm6 cKo
Axonal diameter [µm]
E
myelinated axons
n.s.
F
Sciatic nerve lysate
1 mo
2 mo
4 mo
6 mo
1 yr
kDa
MAG
CMTM6
Actin
100
25
55

Figure 16 Diameters of myelinated axons in Cmtm6 cKo mice upon aging. **A)** Assessment of diameters of myelinated axons in sciatic nerves of wild-type mice at different time-points (1 mo, 2 mo, 4 mo, 6 mo, 12 mo and 20 mo) illustrate a persistent growth in axonal diameter over time. n=5 for 1-12 mo; n=4 for 20 mo) **B)** Genotype-dependent quantification of diameters of myelinated axons in sciatic nerves dissected from control and *Cmtm6* cKo mice at 6 mo display increased axonal diameters in mice lacking CMTM6 from Schwann cells. Data are presented as frequency distribution with 0.5 µm bin width; n=17665 axons from n=5 control mice and n=19196 axons from n=5 *Cmtm6* cKo mice; Mean axonal diameter $_{(control+/-Cmtm6\text{-}cKo)}$ = 3.84 µm+0.2 µm; P=2.7e^{-12} by two-sided Kolmogorow-Smirnow test. **C)** The number of myelinated axons is unchanged in sciatic nerves of *Cmtm6* cKo compared to control mice at 6 mo. Data are presented as mean +/- SD, n=5 mice per genotype, P=0.3661 by Two-tailed Student`s *t*-test. **D)** Genotype-dependent assessment of myelinated axon diameters in sciatic nerves of 1-year old control and *Cmtm6* cKo mice shows no significant differences between genotypes. Data are presented as frequency distribution with 0.5 µm bin width; n=17646 axons from n=5 control mice and n=17321 axons from n=5 *Cmtm6* cKo mice; Mean axonal diameter $_{(control+/-Cmtm6\text{-}cKo)}$ = 4.02 µm-0.01 µm; P=0.596 by two-sided Two-tailed Student`s *t*-test. **E)** Quantification of the number of myelinated axons within the sciatic nerve on semi-thin section of 1-year old control and *Cmtm6* cKo mice reveals no significant differences. Data are presented as mean +/- SD, n=5 mice per genotype; P=0.7563 by Two-tailed Student`s *t*-test. **F)** Immunoblot-analysis in sciatic nerve lysates shows decreasing abundance of CMTM6 upon aging, whereas MAG abundance is unchanged. Actin serves as loading control. Blot shows n=2 mice per time-point. n.s.=non-significant P>0.05, ***P<0.001.

4.2.5 Accelerated sensory nerve conduction velocity in *Cmtm6* cKo mice

Rushton proposed in the 1950`s that nerve conduction velocity (NCV) is roughly linear proportional to axonal diameter and myelin sheath thickness which was validated in experimental studies more previously (Rushton 1951, Hartline and Colman 2007, Li 2015). Considering that deletion of CMTM6 leads to increased axonal diameters without impairing myelin or axonal integrity, we asked if nerve conduction velocity in our mouse model is changed. Thus, we measured NCV in the tails of adult control and *Cmtm6* cKo mice. As hypothesized, we detected a significant increase in sensory nerve action potentials (SNAP) and an accelerated sensory nerve conduction velocity (SNCV) in *Cmtm6* cKo mice (Fig. 17A, B). Notably, the compound muscle action potential (CMAP) and resulting motor nerve conduction velocity (NCV) is unchanged between genotypes (Fig. 17C, D).

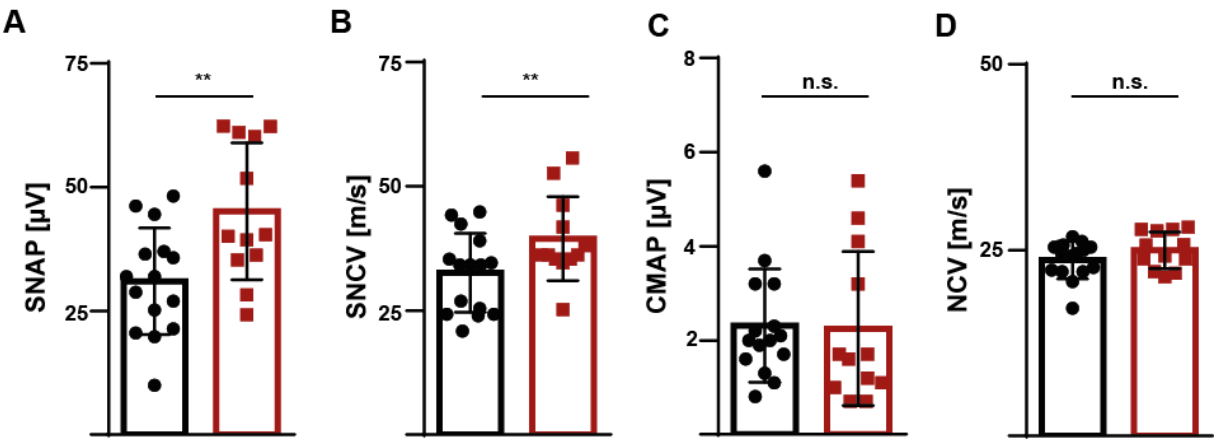

Figure 17 Sensory, but not motor nerve conduction velocity is increased in mice lacking CMTM6 from Schwann cells. **A and B)** Electrophysiological measurement reveals a higher sensory nerve action potential (SNAP) and accelerated sensory nerve conduction velocity (SNCV) in the tails of adult *Cmtm6* cKo mice compared

to controls. **C and D)** Electrophysiological measurements of the compound motor action potential (CMAP) and nerve conduction velocity (NCV) at the tails of control and *Cmtm6* cKo mice shows no significant differences between genotypes. Data are presented as mean +/- SD, n=15 control and n=12 *Cmtm6* cKo mice; **A** P=0.0061 **B** P=0.0386 **C** P=0.9089 **D** P=1819; by Two-tailed Student`s *t* test. n.s.=non-significant P>0.05, ** P<0.01.

Since alterations in nerve conduction velocity can also be influenced by nodal and paranodal parameter changes we assessed nodal and paranodal dimensions (Fig. 18) (Arancibia-Cárcamo, Ford et al. 2017). Therefore, immunohistochemistry on sciatic nerve teased fibers of adult control and *Cmtm6* cKo mice was performed visualizing paranodes by labeling CASPR (red) and nodes on Ranvier by labeling Nav1.6 (green). Paranode and nodal dimension (length and diameter) were measured using ImageJ as displayed in Figure 18A, right image. The quantification showed no difference between control and *Cmtm6* cKo for neither paranode length nor diameter (Fig. 18C, D) nor node length and diameter (Fig. 18E, F). Further, the ratio between paranode length to diameter (Fig. 18G) and the ratio between node length to diameter (Fig. 18H) is not altered between genotypes. Notably, when assessing nodal ultrastructure on electron microscopic levels of longitudinal sciatic nerve sections of both genotypes, we did not observe differences in the ultrastructure of node of Ranvier organization (Fig. 18B). In addition, we performed immunohistochemistry on sciatic nerve teased fiber preparations of both genotypes visualizing nodes with Nav1.6 and the internodes with MAG to judge if the longitudinal dimensions are affected by CMTM6 deletion. By quantifying the entire length of individual internodes we did not find genotype-dependent differences (Fig. 18I).

Thus, CMTM6 deletion does not affect nodal or paranodal dimensions as well as internodal length, implying that the accelerated sensory nerve conduction velocity is indeed owing to increased axonal diameters and thicker myelin sheaths.

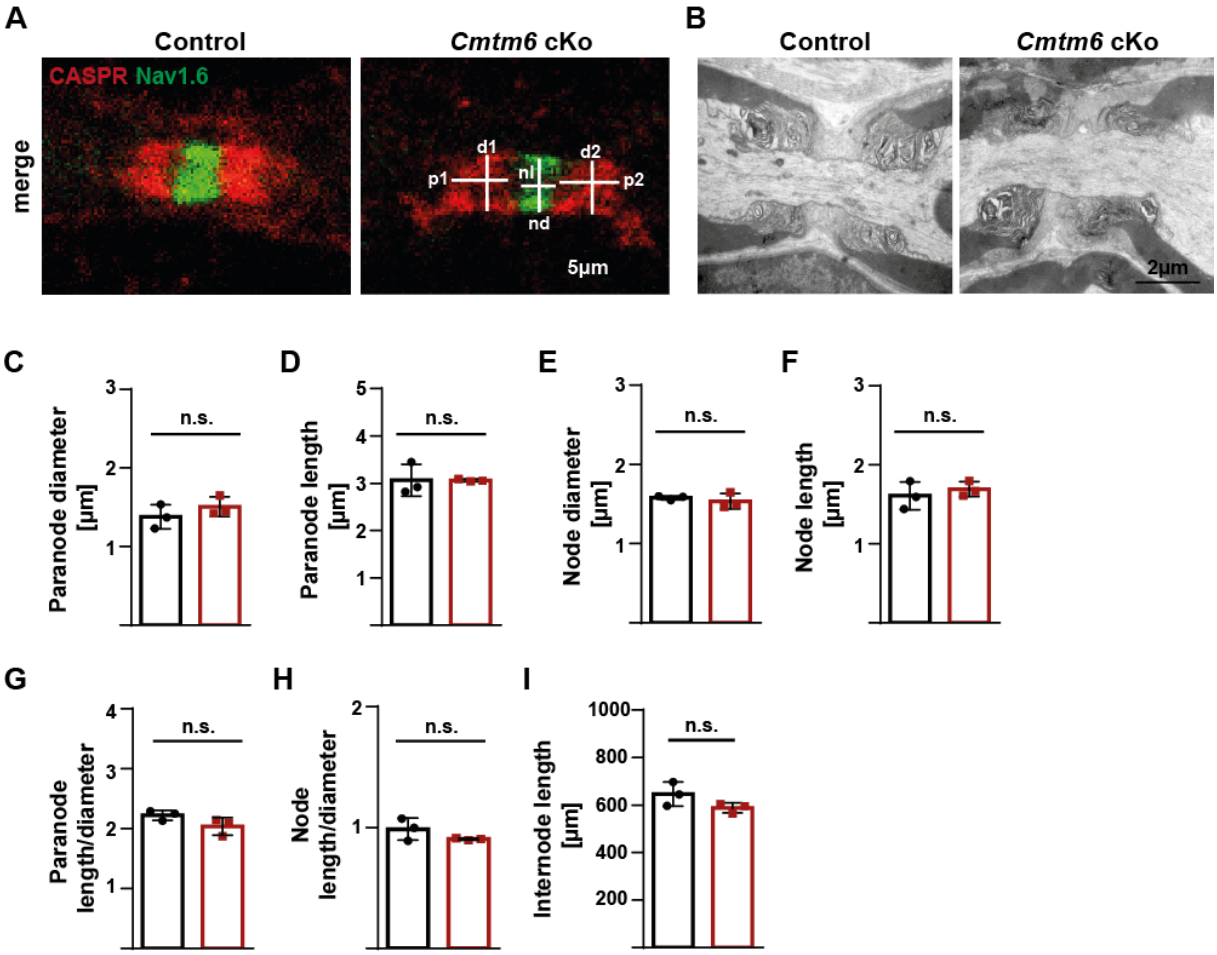

Figure 18 Loss of CMTM6 from Schwann cells does not affect nodal and paranodal dimensions or internodal length. **A)** Immunolabeling of markers for the nodes of Ranvier (Nav1.6; sodium channels, green) and paranodes (CASPR, red) on sciatic nerve teased fiber preparations from 2 mo old control and *Cmtm6* cKo mice. Merged image of *Cmtm6* cKo shows the parameters measured in **C** to **H**. p1=paranode length 1; p2=paranode length 2; d=diameter; nd=node diameter; nl=node length. Scale bar, 5µm. **B)** Representative electron micrographs illustrate longitudinal-sectioned nodes of Ranvier within sciatic nerves of 2 mo-old control and *Cmtm6* cKo mice. Scale bar, 2.0 µm **C and D)** Genotype dependent assessment of paranode diameter (**C**) and length (**D**) on sciatic nerve teased fiber preparations shows normal paranode structure when comparing control and *Cmtm6* cKo mice. Data are presented as mean +/- SD, n>130 paranodes per mouse with n=3 mice per genotype; **C** P=0.3173 **D** P=0.9809; by Two-tailed Student`s *t*-test. **E and F)** Genotype dependent quantification of node diameter (**E**) and length (**F**) on sciatic nerve teased fiber preparations display normal nodal dimensions in *Cmtm6* cKo. Data are presented as mean +/- SD, n>130 nodes per mouse with n=3 mice per genotype; **E** P=0.5089 **F** P=0.4868; by Two-tailed Student`s *t*-test. **G and H)** Assessment of the Ratio of paranode length and diameter (**G**) or node length and diameter (**H**) on sciatic nerve teased fiber preparations reveals no difference between control and *Cmtm6* cKo mice. Data are presented as mean +/- SD, n>130 paranodes/nodes per mouse with n=3 mice per genotype; **G** P=0.1251 **H** P=0.1999; by Two-tailed Student`s *t*-test. **I)** Genotype dependent quantification of internodal length on sciatic nerve teased fiber preparations display no differences in internodal length between control and *Cmtm6* cKo. Data are presented as mean +/- SD; n=490 internodes from n=3 control mice and n=437 internodes from n=3 *Cmtm6* cKo mice; P=0.1393 by Two-tailed Student`s *t*-test. n.s. = non-significant P>0.05

4.2.6 Altered behavioral performance of *Cmtm6* cKo mice

To investigate if the observed alterations in axonal diameter, myelin sheath thickness and sensory nerve conduction velocity influence *Cmtm6* cKo mice functionally, we examined motor and sensory capabilities using different behavioral assays. Within the hotplate assay (Fig. 19A) *Cmtm6* cKo displayed a significantly

smaller retraction latency indicating faster sensory responses upon a heat-stimulus. When assessing mice on a grid test we detected an increased number of fore and hind limb slips in *Cmtm6* cKo compared to control mice indicating slight difficulties in motor coordination. Nonetheless, when evaluating the motor capabilities of both genotypes on a rotating rod or with the open field assay, no differences between control and *Cmtm6* cKo mice were observed. Mice of both genotypes showed similar results in the latency to fall of the rod (Fig. 19C) or in speed (Fig. 19D) and distance (Fig. 19E) mice covered within the open field set-up. Additionally, control mice and *Cmtm6* cKo mice did neither differ in the time they spent in the center of the open-field box nor in the number of visits to the center. When considering increased axonal diameters within the phrenic nerve of *Cmtm6* cKo mice, one of the vital nerves of the PNS controlling respiration, we hypothesized that differences in the breathing behavior of control and *Cmtm6* cKo mice may occur. Thus, we decided to assess the breathing behavior of adult control and *Cmtm6* cKo mice using plethysmography (performed by Swen Hülsmann). It is known from literature, that wild-type C57BL/6N-mice display prolonged and more frequent breathing pauses which are also termed spontaneous apnea (Stettner, Zanella et al. 2008). Surprisingly, the presence of these spontaneous apnea was completely absent in *Cmtm6* cKo mice (Fig. 19H) which might indicate a more precise coordination.

Together, deletion of CMTM6 from SCs and the resulting increase in axonal diameters does not only lead to increased sensory nerve conduction velocity but also alters the behavioral phenotype of *Cmtm6* cKo mice to some extent.

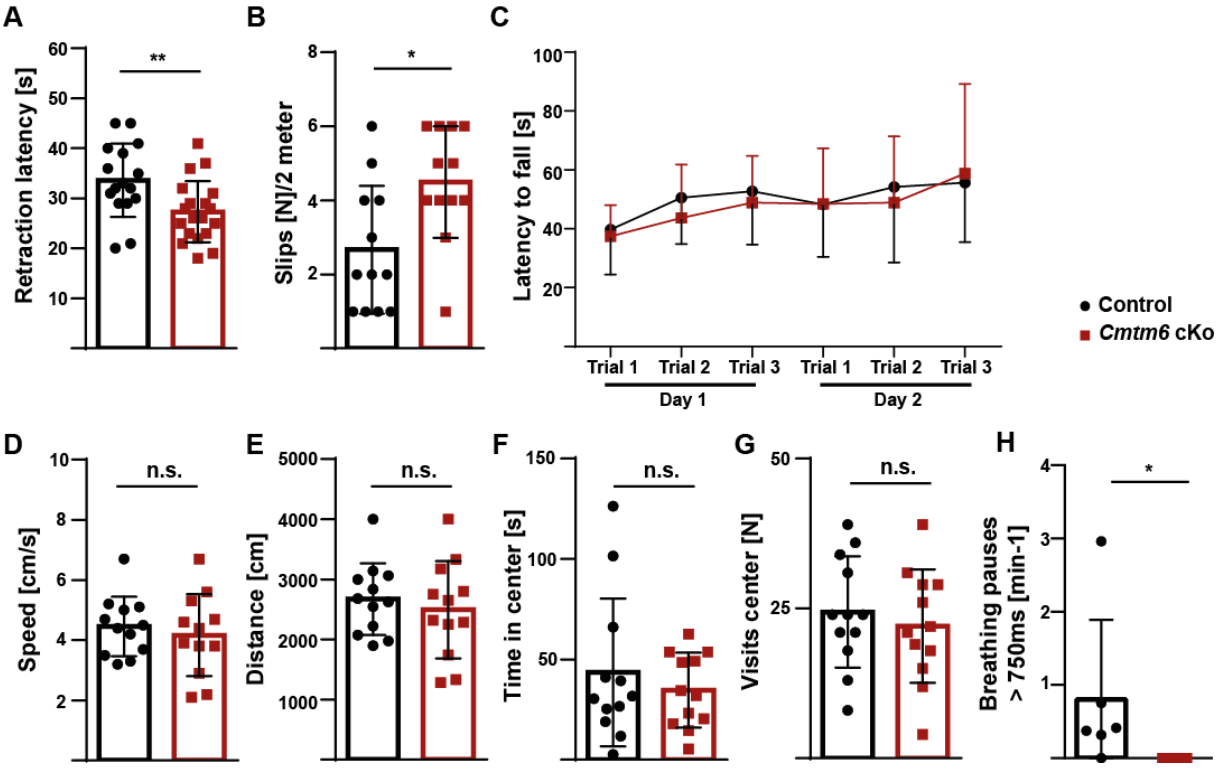

Figure 19 Behavioral performance of mice lacking CMTM6 from Schwann cells. **A)** The latency of retracting a hindlimb upon a heat stimulus is significantly reduced in *Cmtm6* cKo mice compared to control mice when using a Hotplate assay for sensory evaluation. Data are presented as mean +/- SD; n=16 control mice and n=19 *Cmtm6* cKo mice; P=0.0089 by Two-tailed Student`s *t*-test. **B)** Grid-test analysis of adult control and *Cmtm6* cKo mice reveals that *Cmtm6* cKo display an increased number of fore- and hindlimb slips while traveling a distance of 2 m on a regular grid. Data are presented as mean +/- SD; n=12 mice per genotype; P=0.0111 by Two-tailed Student`s *t*-test. **C)** Genotype-dependent assessment of the latency of control and *Cmtm6* cKo mice to fall from a rotating rod using the Rotarod assay shows no significant difference over 2 days of testing. Data are presented as mean +/- SD; n=12 mice per genotype; P=0.6737 by 2way ANOVA. **D to G)** Analyzing Speed (**D**), Distance (**E**), Time spent in center (**F**) and visits to the center (**G**) of adult control and *Cmtm6* cKo mice in the open field assay reveals no significant differences between both genotypes. **H)** Genotype-dependent assessment of breathing pauses during the plethysmography assay shows that *Cmtm6* cKo have fewer (virtually none) breathing pauses longer than 750 ms compared to control mice. Data are presented as mean +/- SD; n=6 mice per genotype; P=0.0152 by Mann Whitney Rank Sum test. n.s.=non-significant P>0.05, * P<0.05, ** P<0.01

4.2.7 Neurofilament density and phosphorylation are unaffected by CMTM6 loss

Radial axonal growth is thus far associated with changes in neurofilament (NF) density and phosphorylation (de Waegh, Lee et al. 1992, Hsieh, Kidd et al. 1994). Therefore, we evaluated if the observed increase in axonal diameters results from NF changes (Fig. 20). Quantification of NF profiles on electron micrographs of cross-sectioned sciatic nerves showed unchanged numbers of NF profiles/0.2µm^2 between control and *Cmtm6* cKo mice (Fig. 20A, B) (for more details on quantification see Material and Methods, chapter 2.2.7.4). Further, investigating the phosphorylation status of Neurofilament-heavy chain (NEFH) via immunoblotting of sciatic nerve lysate of respective genotypes (Fig. 20C) and quantification of the abundances and ratio of

phosphorylated NEFH to NEFH (Fig. 20D-F) revealed no change in abundance for neither NEFH nor phosphorylated NEFH.

Concluding, *Cmtm6* cKo mice show unaltered neurofilament density and phosphorylation which implies that the increased axonal diameter growth upon CMTM6 loss is independent of NF status and may underlie different mechanisms.

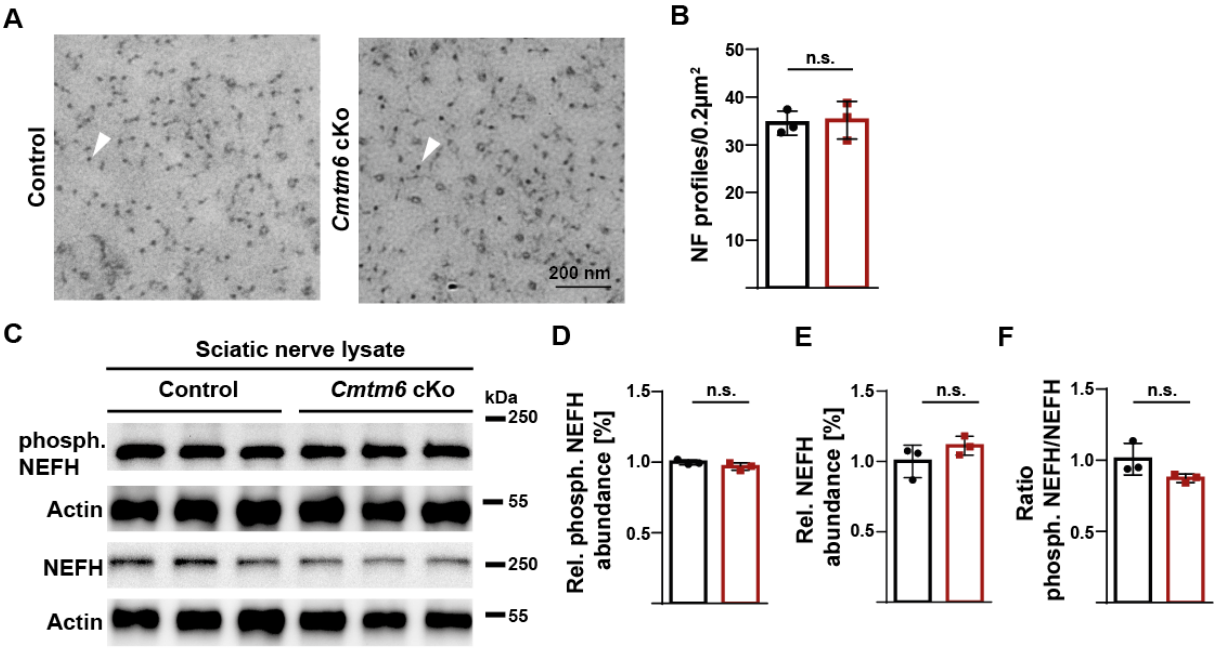

Figure 20 Sciatic nerves of Cmtm6 cKo display normal neurofilament density and phosphorylation. **A)** Representative electron micrographs of axonal neurofilament profiles (white arrowhead) in cross-sectioned sciatic nerves of control and *Cmtm6* cKo mice. Scale bar, 200 nm. **B)** Genotype dependent quantification of the number of neurofilament profiles per 0.2µm^2 on cross-sectioned sciatic nerves implies normal neurofilament density in 2 mo old *Cmtm6* cKo compared to control mice. Data are presented as mean +/- SD; Mean neurofilament number was assessed in n=30 axons per mouse with n=3 mice per genotype; P=0.8408 by Two-tailed Student`s *t*-test. **C)** Immunoblot-analysis of sciatic nerves lysates of 2 mo old control and *Cmtm6* cKo mice detecting phosphorylated NEFH and non-phosphorylated NEFH. Actin serves as control. Blot shows n=3 mice per genotype. **D-E)** Genotype-dependent quantification of immunoblots in **C** display unchanged abundances for phosphorylated NEFH (**D**) and non-phosphorylated NEFH (**E**) between control and *Cmtm6* cKo mice. Phosphorylated NEFH and non-phosphorylated NEFH were normalized to actin. Data are presented as mean +/- SD; n=3 mice per genotype; **D** P=0.1693 **E** P=0.2212 by Two-tailed Student`s *t*-test. **F)** Genotype dependent quantification of the ratio of phosphorylated NEFH and NEFH shows no difference between control and *Cmtm6* cKo mice. Data are presented as mean +/- SD; n=3 mice per genotype***;*** **F** P= 0.1142, by Two-tailed Student`s *t*-test. n.s.=non-significant P>0.05.

4.2.8 CMTM6 restricts axonal diameters after developmental myelination

Results thus far presented in this study, were obtained with mice in which CMTM6 was conditionally ablated early during SC development by using the *Dhh*^{Cre} recombinase. To investigate if CMTM6 deletion in adult mice recapitulates previous findings, we generated mice using *Plp*^{CreERT2} for tamoxifen induced recombination in myelinating glia cells of adult mice. Both control (*Cmtm6*$^{flox/flox}$) and

Cmtm6$^{flox/flox}$;*Plp*^{CreERT2} (further referred to as *Cmtm6* iKo) were administered with tamoxifen at P56 for 10 consecutive days with 2 days break in between (scheme see Fig. 21A). After 2- and 6-month post-tamoxifen injection sciatic nerves of respective mice were dissected and axonal diameters were quantified. Indeed, *Cmtm6* iKo also display increased axonal diameters at both time-points compared to control mice (Fig. 21B, C). Notably, the number of myelinated axons within sciatic nerves of both genotypes did not differ at 2 and 6 months after tamoxifen injection (Fig. 21D, E).

Thus, CMTM6 continues to restrict growth of axonal diameters also after developmental myelination.

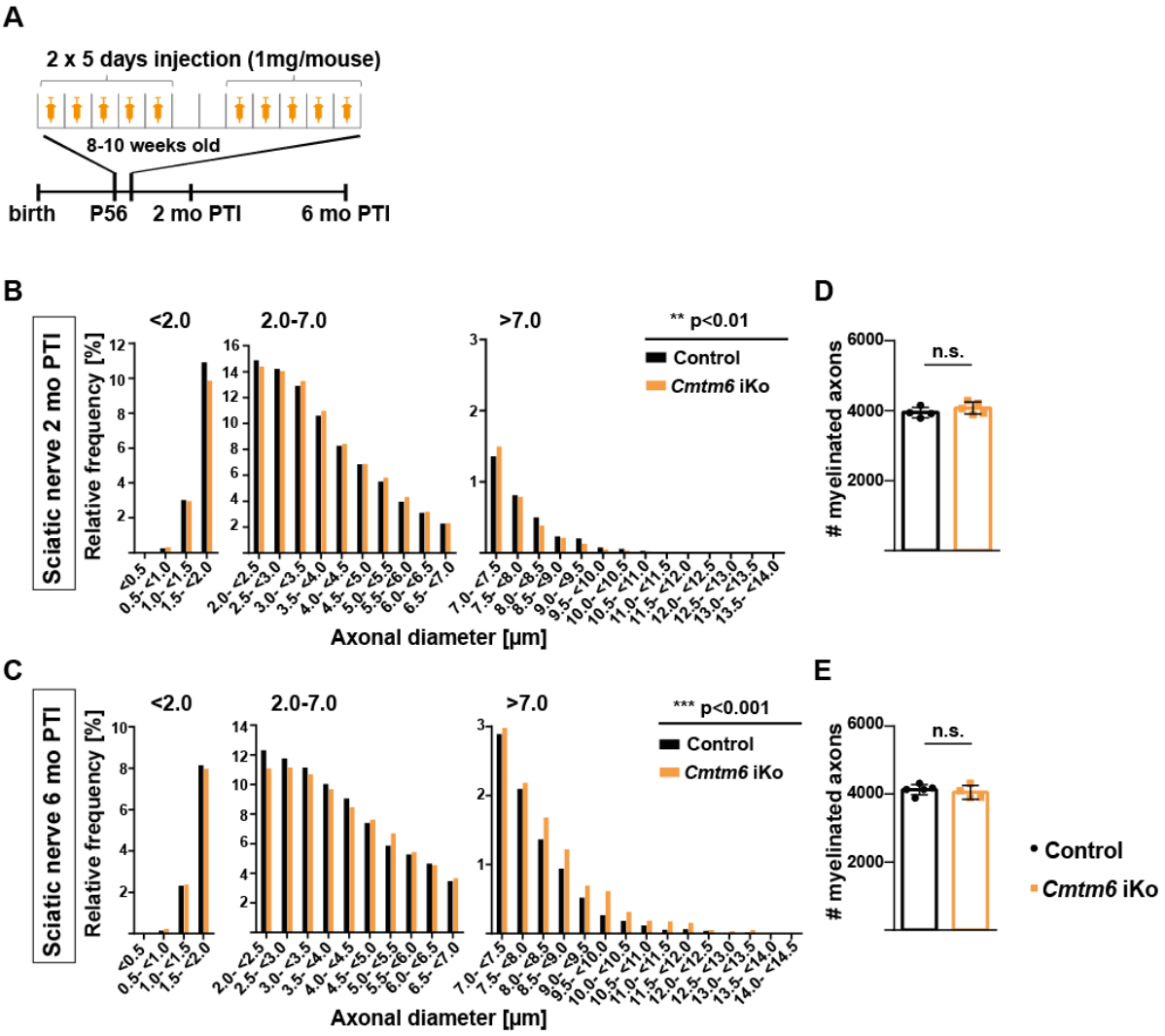

Figure 21 Adult deletion of CMTM6 from Schwann cells increases axonal diameters. **A)** Scheme for tamoxifen injection and analysis time points post-tamoxifen injection (PTI) for control mice (genotype *Cmtm6*$^{flox/flox)}$ and *Cmtm6* iKo mice (genotype Cmtm6$^{flox/flox}$;Plp^{CreERT2}). **B and C)** Genotype-dependent quantification of diameters of myelinated axons on semi-thin section of sciatic nerves dissected from control and *Cmtm6* iKo at both 2 mo PTI (**B**) and 6 mo PTI (**C**). Data indicates increased axonal diameters in *Cmtm6* iKo mice at both time-point PTI. Data are presented as frequency distribution with 0.5 µm bin width; **B** n=14814 axons from n=4 control mice and n=20067

axons from n=5 *Cmtm6* iKo mice; Mean axonal diameter $_{(control+/-Cmtm6\text{-}iKo)}$ =3.57 µm+0.03 µm; P=0.002 by two-sided Kolmogorow-Smirnow test; **C** n=19025 axons from n=5 control mice and n=15047 axons from n=4 *Cmtm6* iKo mice; Mean axonal diameter $_{(control+/-Cmtm6\text{-}iKo)}$ =4.05µm+0.17 µm; P=2.98e^{-10} by two-sided Kolmogorow-Smirnow test. **D and E)** Quantifications of the number of myelinated axons on semi-thin sections shows no change between control and *Cmtm6* iKo mice at 2 mo PTI (**D**) and 6 mo PTI (**E**). Data are presented as mean +/- SD, **D** n=4 control and n=5 *Cmtm6* iKo mice, P=0.2771 **E** n=5 control and n=4 *Cmtm6* iKo mice, P=0.5394; by Two-tailed Student`s *t*-test. n.s.=non-significant P>0.05, **P<0.01, ***P<0.001.

4.3 Investigation of possible interaction partners of CMTM6

How does the novel, adaxonal Schwann cell protein CMTM6 mediate its function towards the axon and what are possible interaction partners of CMTM6? Little is known about the signaling cascade of CMTM family members. To shed some light on this issue, the following two chapters will describe two chosen lines of research to further investigate possible CMTM6 interaction partners.

4.3.1 Axogliasome-enriched fraction of *Cmtm6* cKo mice

To closer investigate quantitative changes of protein abundances in mice lacking CMTM6 from SCs and detect relevant molecules that might mediate Schwann cell to axon signaling dependent on the presence or absence of CMTM6, we biochemically enriched and assessed the axogliasome-enriched fraction purified from P75 old control and *Cmtm6* cKo sciatic nerves. The procedure was performed as previously described under Methods chapter 3.2.5.2 and AEF fractions purified from pools of sciatic nerves of both genotypes were subjected to quantitative mass spectrometry, performed by Stefan Tenzer from the University of Mainz. In total 2869 proteins were identified in the unfiltered dataset. Heatmaps in Figure 22A illustrate log_2fold change (log_2FC) of markers from various compartments, which are unchanged in abundance between control and *Cmtm6* cKo mice. Amongst those are myelin proteins, markers of the adaxonal and axonal membrane but also protein family members of the integrin-, ankyrin-, 4.1 protein-, spectrin family and marker proteins of the ECM. Cytoskeleton proteins such as septins and neurofilaments as well as known cell adhesion molecules are also unchanged between genotypes. This implies that deletion of CMTM6 in Schwann cells and the resulting increase in axonal diameters does not result in major changes in the protein composition of the aforementioned subcompartments.

Interestingly, MS based quantitative proteome analyses of the purified AEF fractions also displayed differentially regulated proteins between genotypes. Notably,

only proteins with a threshold of over 100 ppm per sample were included. Figure 22B depicts the seven proteins which are at least 0.5-fold reduced in abundance in AEF purified from *Cmtm6* cKo sciatic nerves compared to control sciatic nerves amongst which CAGE1 shows the highest difference between the two genotypes. When focusing on proteins, which are at least 2.0-fold increased in abundance (Fig. 22C) a total of four proteins are differentially regulated with KIF20B showing the strongest increase in AEF purified from *Cmtm6* cKo compared to AEF from control mice. For further information about differentially changed proteins refer to discussion chapter 5.4. Note, that CMTM6 itself was detected in control but not *Cmtm6* cKo samples at low levels. However, it was excluded from the present analysis since the detection of CMTM6 using the applied filters was at a low level and including it would have affected the current dataset.

Concluding, the results of the quantitative mass spectrometric analyses of AEF purified from sciatic nerves of control and *Cmtm6* cKo mice imply that a deletion of CMTM6 from SCs does not impair the abundances of marker proteins of the axonal membrane, adaxonal membrane and myelin proteins, constituents of the ECM and cell adhesion proteins. The detected normality implies that increased axonal diameters observed in *Cmtm6* cKo mice are an effect of CMTM6 itself instead of resulting from compositional changes of the axon/myelin unit. Nevertheless, by scanning existing literature and databases, the differentially up- and downregulated proteins did not prompt us to further investigate a possible interaction with CMTM6 (as discussed in chapter 5.4).

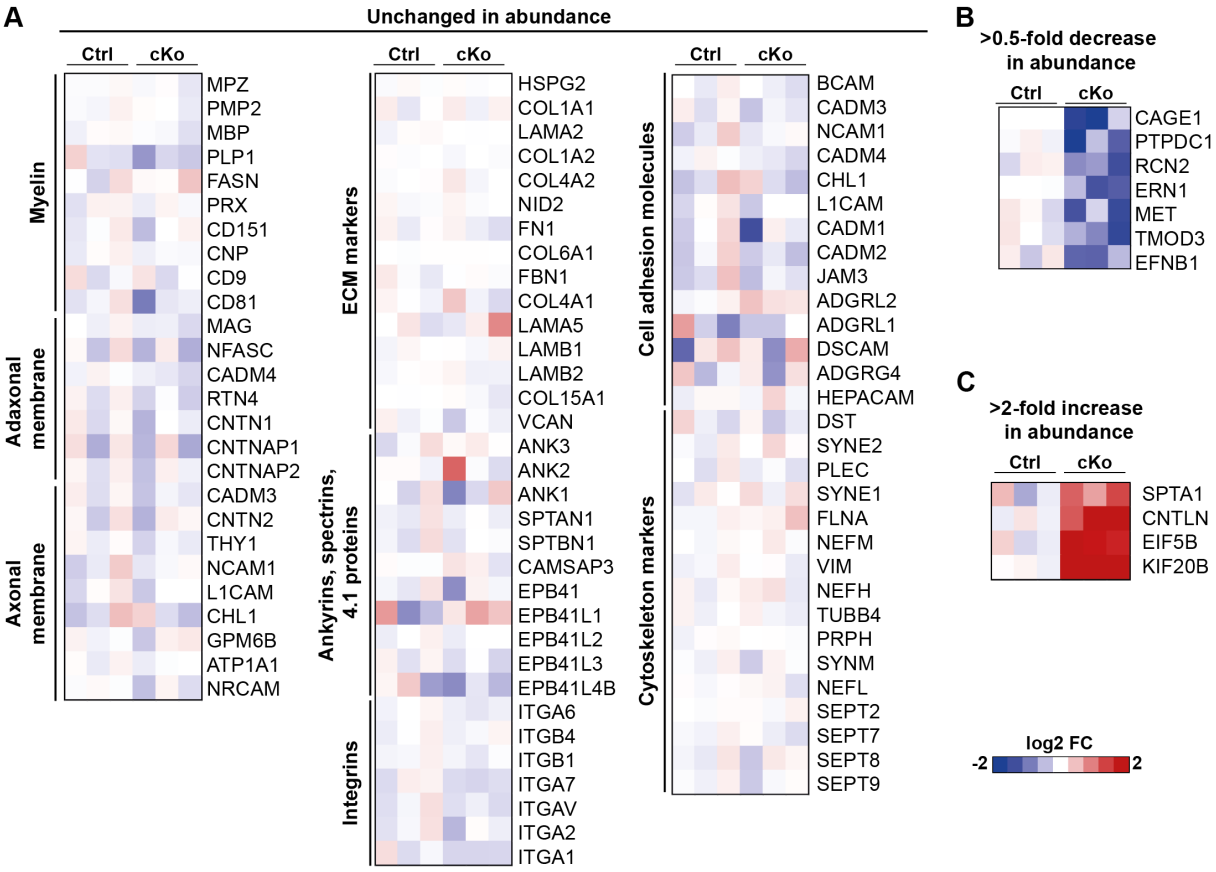

Figure 22 Mass spectrometric analysis of the axogliasome-enriched fraction (AEF) purified from sciatic nerves of Cmtm6 cKo. Quantitative mass spectrometric analysis was performed on purified AEF from sciatic nerves of adult control and *Cmtm6* cKo mice. Heatmap displays the log2-transformed fold-change (log_2FC) of proteins in *Cmtm6* cKo AEF compared to control AEF. Each line corresponds to the average fold change and the different samples (n=3 per genotype) are illustrated in corresponding columns. Note that FC values were plotted on a log2 color scale with blue representing diminishment and red enrichment. **A)** Selected subsets of proteins which are unchanged in abundance between genotypes are displayed. Proteins were chosen regarding the compartment or protein family they belong to. **B)** Differential proteome analysis reveals 7 proteins being reduced in abundance below 0.5-fold in *Cmtm6* cKo compared to control mice. **C)** Heatmap displays the 4 proteins that are increased above 2-fold in abundance in the AEF purified from *Cmtm6* cKo compared to control sciatic nerves.

4.3.2 CD274 as a possible interaction partner of CMTM6

It was previously reported by *in vitro* studies that expression of CMTM6 affects the cell surface maintenance of programmed death-ligand 1 (PDL1/CD274) in a tumor environment as a possible mechanism of regulating anti-tumor immunity (Burr, Sparbier et al. 2017, Mezzadra, Sun et al. 2017). To assess if CMTM6 regulates CD274 in non-tumorigenic SCs *in vivo* we investigated changes of CD274 abundance in lysates of sciatic nerves, ventral and dorsal roots of 2-month old control and *Cmtm6* cKo mice. However, by immunoblotting we did not detect any changes of CD274 abundance upon deletion of CMTM6 within various peripheral nerve lysates (Fig. 23A-C). In addition, immunolabeled cross-sectioned sciatic nerves of control and *Cmtm6* cKo mice revealed unaltered, preferentially abaxonal, localization of CD274 (red) in

both control and *Cmtm6* cKo nerves (Fig. 23D). *Vice versa*, we did not detect changes of CMTM6 abundance in *Cd274* Ko sciatic nerve lysates assessed via immunoblotting (Fig. 23E). Note, that MAG abundance is unchanged in both *Cmtm6* cKo and *Cd274* Ko nerve lysates.

From our *in vivo* data we conclude that CD274 most likely does not interact with CMTM6 in the peripheral nervous system and that CMTM6 does not maintain the cell surface expression of CD274 at the SC surface. To investigate how the function of CMTM6 is mediated further studies using different methodology need to be conducted.

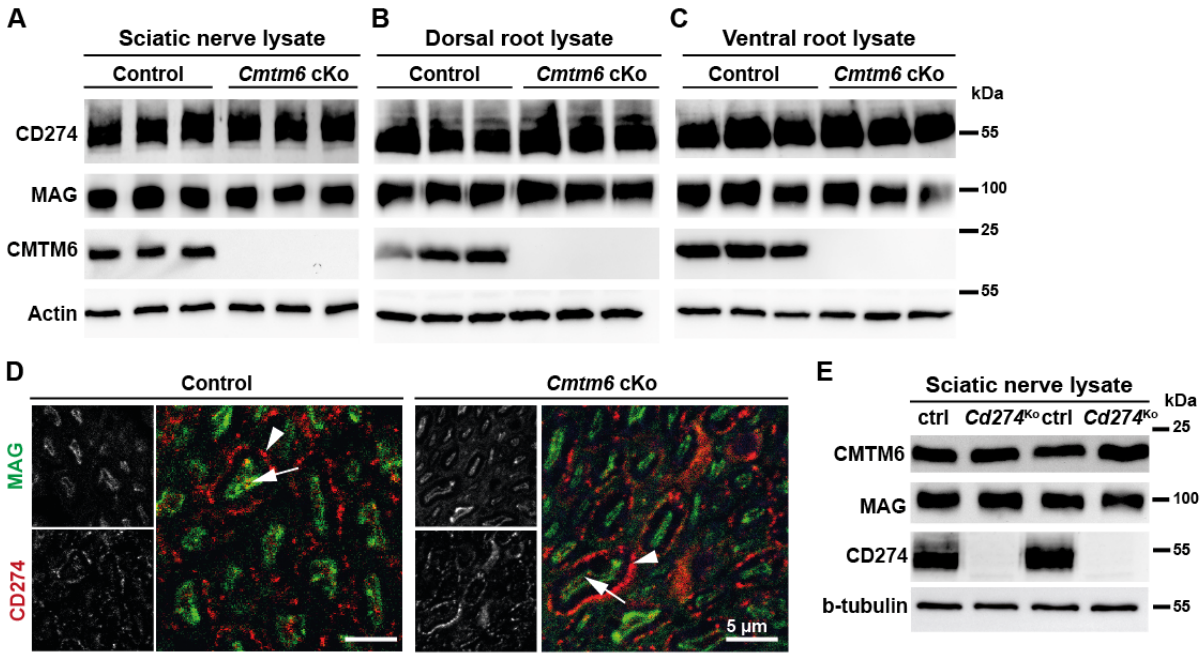

Figure 23 Abundance and localization of CD274 in the PNS is independent of CMTM6. **A to C)** Immunoblot-analysis of sciatic nerve lysate (**A**), dorsal root lysate (**B**) and ventral root lysate (**C**) from 2 mo old control and *Cmtm6* cKo mice reveals no change in CD274 and MAG abundance. CMTM6 was detected as genotype control; Actin serves as loading control. Blots show n=3 mice per genotype. **D)** Immunolabeling of cross-sectioned sciatic nerves from control and *Cmtm6* cKo mice at 2 mo indicated no changes in preferably abaxonal localization of CD274 (red, arrowheads). MAG (green, arrows) serves as marker for non-compact myelin preferentially labeling adaxonal myelin. Scale bars, 5 µm. **E)** Immunoblot-analysis of sciatic nerves lysates from adult control and *Cd274* Ko mice shows no change in CMTM6 and MAG abundance upon loss of CD274. Beta-tubulin serves as loading control. Blot shows n=2 mice per genotype in alternating order.

4.4 Mediating radial axon growth: CMTM6 and MAG

With our study we have demonstrated that CMTM6 is the first Schwann cell molecule known to restrict axonal diameters. In the past it was reported that mice lacking another SC protein, namely MAG, have smaller axonal diameters proposing a role for MAG in supporting the radial growth of axons in the PNS (Yin, Crawford et al. 1998). The following chapters will focus on the possible interaction of the two adaxonal SC molecules that either increase (MAG) or restrict (CMTM6) radial growth of axons.

4.4.1 Confirmation of MAG phenotype

To confirm the previously reported phenotype of *Mag* Ko mice we re-assessed axonal diameters in adult control and *Mag* Ko mice based on our way of quantifying nearly all myelinated axons on semi-thin section of sciatic nerves of respective mice. Indeed, we observed a significant shift towards a higher frequency of smaller diameter axons in *Mag* Ko compared to control mice (Fig. 24A) without any loss of myelinated axons (Fig. 24B).

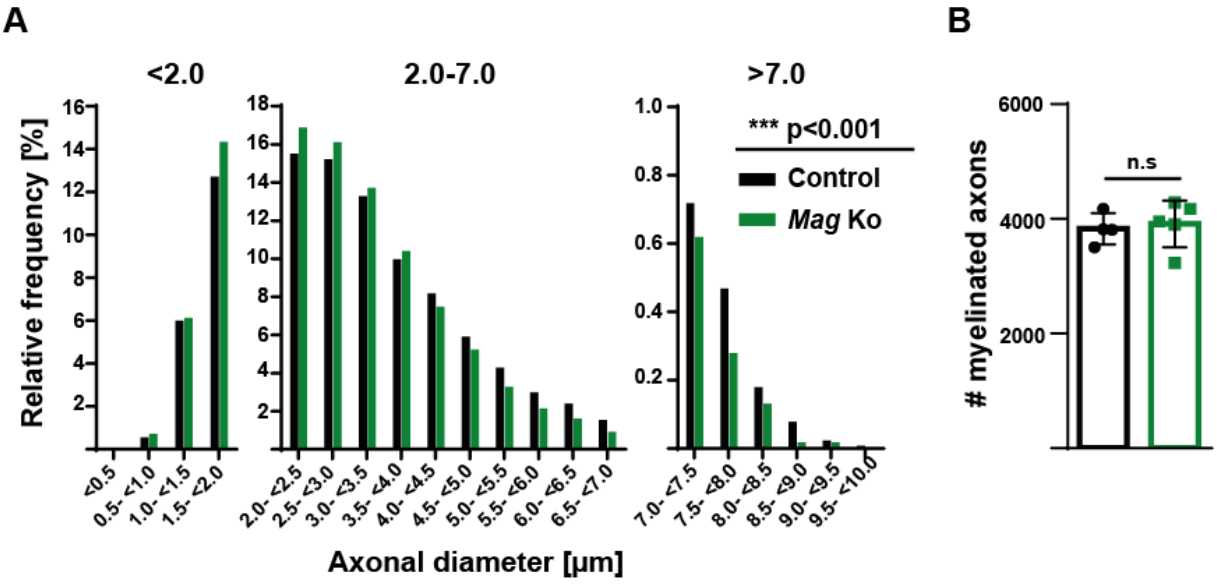

Figure 24 Axonal diameters are reduced in the absence of MAG. **A)** Genotype-dependent quantification of the diameter of myelinated axons in sciatic nerves confirms reduced axonal diameters in *Mag* Ko mice compared to control mice. Data are presented as frequency distribution with 0.5 µm bin width; n=12793 axons from n=4 control mice and n=16790 axons from n=5 *Mag* Ko mice; Mean axonal diameter $_{(control+/-Mag-Ko)}$ = 3.26µm-0.17µm; $P<2.2e^{-16}$ by two-sided Kolmogorow-Smirnow test. **B)** Quantification of the number of myelinated axons on semi-thin sections shows no change between control and *Mag* Ko sciatic nerves. Data are presented as mean +/- SD, n=4 control and n=5 *Mag* Ko mice; n.s.=non-significant (P=0.7413) by Two-tailed Student`s *t* test. n.s.=non-significant P>0.05, ***P<0.001.

4.4.2 CMTM6-loss is overriding MAG-loss regarding axonal diameters

Considering that CMTM6 and MAG may functionally interact we investigated the abundance and localization of both in the respective absence of the other. By immunoblotting and immunohistochemistry (Fig. 10) as well as in the proteomic analyses of AEF fractions of control and *Cmtm6* cKo mice (Fig. 22) it was shown that abundance and localization of MAG is independent of CMTM6. However, immunolabeling of CMTM6 (red) and MAG (green) on adult control and *Mag* Ko sciatic nerve teased fiber preparation showed a preferentially perinuclear localization of CMTM6 in Schwann cells upon deletion of MAG (Fig. 25A). By quantifying this we indeed detected a higher percentage of perinuclear CMTM6 accumulation in *Mag* Ko compared to control mice (Fig. 25B). In addition, the abundance of CMTM6 is strongly reduced in *Mag* Ko mice as shown by immunoblotting of sciatic nerve lysates of respective mice. This may indicate a transport problem of CMTM6 upon MAG loss and implies a possible function for MAG in facilitating normal CMTM6 abundance and localization in Schwann cells.

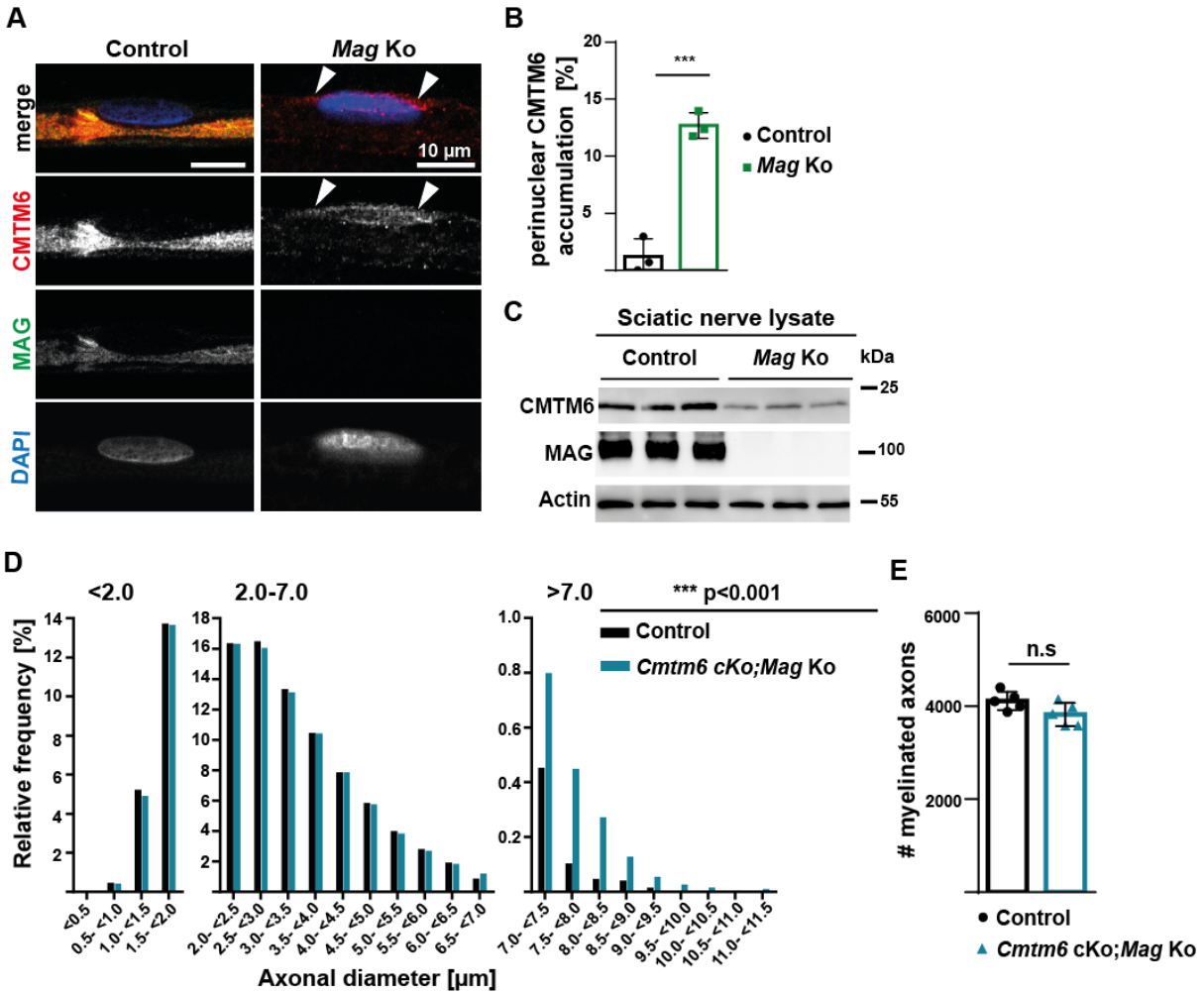

Figure 25 Axonal diameters are increased in the absence of both CMTM6 and MAG. **A)** Immunolabeling of teased fiber preparations from adult control and *Mag* Ko sciatic nerves depicts accumulation of CMTM6 (red) when MAG (green) is lacking. Nuclei were labeled with DAPI (blue). Scale bar, 10 µm. **B)** Genotype-dependent quantification on sciatic nerve teased fiber preparations from control and *Mag* Ko reveals increased CMTM6 accumulation in *Mag* Ko nerves. Data are presented as mean +/- SD; n=3 mice per genotype; P=0.0005 by Two-tailed Student`s t-test. **C)** Immunoblot-analysis of sciatic nerve lysates from control and *Mag* Ko mice at P75 shows decreased CMTM6 abundance upon loss of MAG. Actin serves as loading control. Blots shows n=3 mice per genotype. **D)** Genotype-dependent quantification of the diameters of myelinated axons from sciatic nerves reveals abnormally increased axonal diameters in adult *Cmtm6* cKo;*Mag* Ko double mutant mice compared to control mice at 2 mo. Data are presented as frequency distribution with 0.5 µm bin width; n=19108 axons from n=5 control mice and n=18003 axons from n=5 *Cmtm6* cKo;*Mag* Ko double-knockout mice; Mean axonal diameter $_{(\text{control+/- } Cmtm6\text{-cKo;}Mag\text{-Ko double-knockout})}$ = 3.13µm+0.09µm; P=0.0001 by two-sided Kolmogorow-Smirnow test. **E)** Quantification of the number of myelinated axons on semi-thin sections of dissected sciatic nerves shows no difference between *Cmtm6* cKo;*Mag* Ko double mutant compared to control mice. Data are presented as mean +/- SD, n=5 per genotype; P=0.0761 by Two-tailed Student`s *t*-test. n.s.=non-significant P>0.05, ***P<0.001.

Considering the proposed interaction of CMTM6 and MAG and to further assess the opposing function of both SC proteins in regulating axon diameter growth we generated *Cmtm6* cKo;*Mag* Ko double-knockout mice (termed *Cmtm6* cKo;*Mag* Ko) and quantified genotype-dependent differences of axonal diameters in sciatic nerves. Strikingly, frequency distributions displayed higher number of large axonal diameters in *Cmtm6* cKo;*Mag* Ko sciatic nerves compared to control mice similar to *Cmtm6* single-knockout mice (Fig. 25D). Note, that the number of myelinated axons is unchanged between genotypes. This interesting result implies that loss-of CMTM6 function overrides loss-of MAG function on regulating axonal diameters.

Concluding, these results indicate an interaction of CMTM6 and MAG in which I) MAG is facilitating normal CMTM6 abundance and localization and II) CMTM6 loss-of-function is overriding MAG loss-of-function regarding axonal diameters. Taken together, we propose a model in which Schwann cells regulate radial growth of peripheral axons via adaxonal proteins with CMTM6 restricting and MAG increasing axonal diameters (see model in Figure 26).

5 Discussion

5.1 Can we identify novel proteins at the axon-myelin interface?

Saltatory signal propagation in the PNS as well as trophic support of axons by myelinating glia cells require the close cellular association between axons and myelinating Schwann cells (Feltri, Poitelon et al. 2016). In addition, complex molecular interactions between axons, Schwann cells and the ECM mediate the development of a functional axon/myelin unit and many have been identified (Feltri, Poitelon et al. 2016, Mogha, D'Rozario et al. 2016) (see Introduction chapter 2.2 and 2.3). One such example is MAG, a SC protein known to increase the radial growth of axons (Yin, Crawford et al. 1998). However, a SC factor restricting axonal diameters is yet unknown. In this study we show that CMTM6 is a novel SC protein at the axon/myelin interface and restricts the radial growth of myelinated and non-myelinated axons in the PNS.

For identifying novel myelin proteins in the PNS Patzig et al. established proteomic analysis of purified myelin from wild-type sciatic nerves (Patzig, Jahn et al. 2011). They were the first to study the PNS myelin composition at proteome level and identified 36 known PNS myelin proteins and over 500 proteins which were previously not associated with PNS myelin (Patzig, Jahn et al. 2011). Nevertheless, due to its high lipid content, compact myelin membranes accumulate at lower sucrose densities with only few co-purifying axolemmal proteins. Aiming to study interactions between myelinating glial cells and axons in more detail, purification of the membrane interface, in particular the adaxonal membrane, axolemma and non-compact myelin is crucial. For the CNS this was previously achieved in two separate studies, which investigated either purified human myelin and “axogliasome” from white matter CNS regions (Dhaunchak, Huang et al. 2010) or murine “myelin-axolemmal complex” of 21-days old mouse brains (Menon, Rasband et al. 2003). Both studies demonstrated that the adaxonal membrane and axolemma of the axon/myelin interface can be sheared away from compact myelin membranes due to its higher protein-to-lipid ratio and can be used for systemic biochemical assessment. Dhaunchak et al. found a 28% overlap of the proteins identified in human axogliasome fraction and in purified axogliasome of rodent optic nerves, suggesting conservation of some proteins at the axon/myelin interface (Ogawa and Rasband 2009, Dhaunchak, Huang et al. 2010).

Yet, no study so far approached biochemical characterization of the axon/myelin interface of the peripheral nervous system. Thus, we adapted the preexisting CNS protocols to biochemically enrich the axogliasome from murine sciatic nerves and performed mass spectrometry to investigate if we can detect novel proteins mediating axon-to-SC or SC-to-axon signaling. Classical and known markers of the purified axogliasome, including carrier proteins, signaling and cell adhesion molecules as well as channel proteins were identified in our dataset (see addendum Fig. 27 and Table 2). Enrichment of axolemma and adaxonal marker proteins (MAG, NFASC and ATP1A1) were validated by immunoblots. Unexpectedly, proteins of the ECM, the basal lamina, compact myelin and proteins of the axonal cytoskeleton were also identified in our dataset (Fig. 6 and Fig. 27). For CNS myelin a purity of >90% can be expected indicating only little contamination by proteins of other cell types and mitochondria (de Monasterio-Schrader et al., 2012; Erwig et al., 2019). Further, the aforementioned studies also show an overlap of the proteins identified in myelin and axogliasome proteome, suggesting both fractions have distinct but also common features (Menon, Rasband et al. 2003, Dhaunchak, Huang et al. 2010). Our proteomic approach now identifies marker proteins of various sub-compartments to be present in the purified fraction. This prompted us to rename the fraction to “axogliasome-enriched fraction” (AEF) instead of the previously used terms “axogliasome” or “myelin-axolemmal complex”. Yet, with 755 identified proteins our dataset provides the first proteomic analysis of the axon/myelin contact zone of the peripheral nervous system and includes many proteins with yet unknown function for the PNS.

By identifying CMTM6 as a novel SC protein and characterizing its role for the PNS we can thus demonstrate that investigating the AEF can be a relevant tool for discovering new molecules involved in the axon/myelin unit.

5.2 CMTM6, a previously unknown Schwann cell protein

Combining the purification of the axogliasome-enriched fraction with proteomic analysis we identified candidate proteins previously unknown at the axon-SC interface. Applying the aforementioned selection criteria, we chose CMTM6 as a novel candidate and indeed verified its localization at the adaxonal membrane and expression in Schwann cells by using biochemical and histochemical methods (Fig. 6-8). The CMTM

family is a generic protein family consisting of eight, under investigated, Chemokine-like factor like MARVEL-domain containing proteins (Han, Ding et al. 2003). So far, no functional relevance for the nervous system for any of the eight protein family members was shown *in vivo*. The majority of studies propose a role in immune and male reproductive system as well as tumorigenesis and suggest a role for CMTM6 in mediating anti-tumor immunity (Shao, Cui et al. 2007, Wang, Li et al. 2009, Niu, Li et al. 2011, Liu, Su et al. 2015, Burr, Sparbier et al. 2017, Mezzadra, Sun et al. 2017), reviewed in (Lu, Wu et al. 2016). Noteworthy, the majority of these studies are based on *in vitro* or screening experiments. To this point the only CMTM family member known to be present in PNS myelin is CMTM5, which was previously identified as a novel compact myelin protein with yet unknown function (Patzig, Jahn et al. 2011). In an unpublished microarray dataset of murine sciatic nerves by Chris Hummels from the MPI-EM, CMTM6 was also detected with a higher mRNA abundance in adult mice compared to the other protein family members. Thus, investigating the role of our candidate CMTM6 appeared promising. We conditionally ablated its expression in Schwann cells by breeding *Cmtm6*$^{flox/flox}$ mice and *Dhh*^{Cre} driver mice (referred to as *Cmtm6* cKo), which could be verified by immunoblot and immunolabeling of teased fibers as well as on mRNA level (Fig. 9-11).

5.3 CMTM6 restricts radial axonal growth

Hypothesizing a role of CMTM6 in mediating SC and axon interactions we assessed consequences of its deletion first on light- and electron microscopic level. At first glance, it appeared that loss of CMTM6 had no influence on SC and axonal integrity. Strikingly though, we could reveal a shift towards larger axonal diameters in *Cmtm6* cKo mice within several peripheral nerves without any loss of myelinated axons or difference in degenerating axons (Fig. 12 and 13). It is thought that SCs sense Nrg1-type-III on the axonal surface as a readout of its diameter which subsequently affects the myelin sheath thickness in dependence on the axonal diameter (Michailov, Sereda et al. 2004, Taveggia, Zanazzi et al. 2005, Nave and Salzer 2006). When measuring the g-ratio in respective peripheral nerves we indeed found that *Cmtm6* cko mice display an appropriately thicker myelin sheath surrounding larger axons. Thus, the newly identified SC protein CMTM6 is the first protein known to restrict radial axonal growth without impairing axonal integrity or myelin biogenesis.

Further, the effect of axonal diameter on myelination is especially crucial during radial sorting. In general, PNS axons of a diameter <1 µm are ensheathed by Remak-type SCs and only axons upon radial growth to at least >1µm get sorted out and myelinated. However, mutations of genes encoding SC proteins, but also myelin-related proteins or proteins of the ECM in peripheral nerves, may impair radial sorting resulting in failed sorting (i.e. axons larger 1µm still associated with Remak bundles, fewer or more axons within one bundle or aberrant wrapping of either axons within Remak bundles or even myelination of the Remak bundle itself) (Feltri, Poitelon et al. 2016, Harty and Monk 2017). A broad list of mouse mutants associated with radial sorting defects is summarized in (Feltri, Poitelon et al. 2016).

Interestingly, none of the abovementioned changes are present in Remak bundles of *Cmtm6* cKo even though their axonal diameters are increased during early development (P9). This indicates that CMTM6 also restricts diameters of non-myelinated axons but is not essential for mediating radial sorting. For myelinated axons this shift towards larger diameters arises only at 1 month of age (Fig. 14-15). So far, there is a lack of exclusive markers to create cell-type specific deletions only in RSCs but not immature or myelinating SCs to separate the function of CMTM6 in those cell types. Especially since SC are plastic and both, myelinating and RSCs, play a role in regeneration post injury it would be of interest to also distinguish the function of CMTM6 in the two different cell types.

Surprisingly we demonstrated a considerable age dependent decrease of CMTM6 abundance in 1-year-old sciatic nerves (Fig. 16F). Interestingly, the diameters of myelinated axons of control and *Cmtm6* cKo mice do not differ at 1 year of age (Fig. 16). This is most likely explained by the decreased abundance of CMTM6 at 1 year, which does thus not restrict axonal diameters anymore. Previous studies investigated the morphometric changes on ultrastructural level during aging and examined nerve conduction velocity changes in different organisms such as cat, rat and mice (Chase, Engelhardt et al. 1992, Verdú, Butí et al. 1996, Painter 2017). Taken together, the majority of these studies suggest that murine peripheral nerves have a rather long postnatal maturation period up to 12 months-of age. This period is reflected by stable morphology with a steady increase in fiber size as well as nerve conduction velocity (Verdú, Butí et al. 1996, Ceballos, Cuadras et al. 1999).

With a more intensive analysis of approximately 3000 axons per sciatic nerve we could confirm the findings of increased axonal diameters up to 1 year in wild-type mice (Fig. 16 A). In mice age-related changes such as loss of myelinated and non-myelinated fibers, myelin outfoldings and smaller axonal diameters slowly establish from 1 year up to 20-months of age and become more prominent afterwards (Verdú, Ceballos et al. 2000). Chase et al. combined electrophysiological and morphological analysis in the cat masseter nerve, which is mainly comprised of motorneurons, and was able to link the decrease in nerve conduction velocity with the age-dependent decrease of axonal diameters as well as myelin sheath disruptions (Chase, Engelhardt et al. 1992). In line with this, Verdu and colleagues could demonstrate the same for mice. Their data suggests that the decrease in axonal size and loss of especially large myelinated axons are partially responsible for the changes in nerve conduction velocity and non-linearly decline at around 18-months of age (Verdú, Butí et al. 1996, Ceballos, Cuadras et al. 1999, Verdú, Ceballos et al. 2000).

Regarding axonal diameter changes in aged animals we also analyzed sciatic nerves in 20-months-old mice. Figure 16A illustrates a slightly higher number of smaller diameter axons in 20-month-old mice compared to 4-12-months old mice which is similar to previously published results. However, a more detailed comparison between large and small diameter axons as well as myelin sheath integrity was not part of our study. By the decreased abundance of CMTM6 in SCs by 1 year of age the restriction of radial axonal growth might be partially diminished. This implies that during aging other mechanisms might be involved in axonal diameter changes. This time-dependent regulation of CMTM6 suggests a role for CMTM6 in restricting radial axonal growth during development (up to 2 month) and maturation (up to 1 year) but most likely not during aging (older than 12-16 months).

By generating *Cmtm6*$^{flox/flox}$*;Plp*^{CreERT2} (*Cmtm6* iKo) mice and injecting tamoxifen at 2-months of age we could study the role of CMTM6 post development. Interestingly, when analyzing axonal diameters at 2- and 6- months post tamoxifen injection we could show an increase in axonal diameters in *Cmtm6* iKo compared to control mice (Fig. 21). Thus, CMTM6 is utilized by Schwann cells to restrict radial axonal growth not only during developmental myelination but also in adult mice.

5.4 How do axonal diameters increase in the absence of CMTM6?

Changes in the diameter of myelinated axons have thus far been associated with the density and phosphorylation of neurofilaments (NF) which are amongst the most prominent cytoskeletal constituents of larger caliber axons (Friede and Samorajski 1970, Hsieh, Kidd et al. 1994, Perrot, Lonchampt et al. 2007). Accumulation and failed transport of NF is one hallmark of diseases such as Amyotrophic Lateral Sclerosis and some forms of CMT (Dale and Garcia 2012). However, various studies suggested that phosphorylation of NF may not be achieved without intact myelin. This indicates that myelinating glia cells play an essential role for phosphorylation of NF. For example, studies in *Trembler* mice, which have a point mutation in the myelin gene *Pmp22* show demyelination, but also smaller axonal diameters correlated with impaired phosphorylation of neurofilaments (De Waegh and Brady 1990, de Waegh, Lee et al. 1992).

Further, it was shown that MAG-deficient mice have reduced axonal diameters accompanied by a hyperphosphorylation of NF-heavy (NF-H) and NF-medium (NF-M) underlining that neurofilament organization within axons is regulated by SC signals in an “outside-in” signaling cascade (Yin, Crawford et al. 1998, Garcia, Lobsiger et al. 2003). Garcia et al. further provided evidence that NF-M is the target for MAG dependent phosphorylation and thus axonal diameter increase (Garcia, Lobsiger et al. 2003) (also see Introduction chapter 2.3). Noteworthy, not all changes in neurofilament density or phosphorylation are dependent on MAG signaling. Schwann cells which lack the protein kinase mTOR display reduced axonal diameters and impaired myelin sheath postnatally. This is additionally accompanied by diminished NF phosphorylation without any changes of MAG abundance (Sherman, Krols et al. 2012).

In CMTM6 cKo mice we could not observe changes in MAG abundance and localization (Fig. 10) as well as differences in neurofilament phosphorylation (Fig. 20 C-F). Interestingly, also the neurofilament density was unchanged between *Cmtm6* cKo and control mice (Fig. 20 A-B). Thus, it seems that the more extensive radial growth of myelinated axons in maturing and adult *Cmtm6* cKo mice is independent of changes in neurofilament density and phosphorylation. Further investigating axonal cytoskeleton changes in *Cmtm6* cKo has the potential to provide novel insight in how SCs can influence the axonal cytoskeleton and axonal growth independent of

neurofilaments. With emerging super-resolution techniques, the axonal cytoskeleton can be observed in more detail. For example, Leite et al could demonstrate that the actin cytoskeleton is comprised of actin rings which are capped by α-Adducin. These actin rings have a dynamic periodic distribution along the axons and are linked by spectrin tetramers (Leite, Sampaio et al. 2016). Further, they show that axonal α-Adducin is essential for controlling the actin ring diameters, and subsequently axonal-diameters, without affecting the periodicity of actin rings. Notably, this does not only lead to increased axons within the optic nerve, spinal cord and sciatic nerve but also to progressive axonal degeneration (Leite, Sampaio et al. 2016). However, this study does not suggest an active involvement of SC in regulating changes of actin-ring diameter or adducin capping. Our own preliminary immunoblot experiments with a lower n number did not indicate α-Adducin but slight β-Adducin changes in *Cmtm6* cKo nerves (data not shown).

How the dynamic actin microfilament organization within axons changes upon tension and contractility is currently under investigation in other labs. Hopefully it will be unraveled in the near feature, how the actin cytoskeleton is involved in regulating axonal diameters as well as neuronal architecture (Leterrier, Dubey et al. 2017, Costa, Pinto-Costa et al. 2018). If the actin-ring diameter is changed in CMTM6 mutant mice or if other axonal cytoskeleton changes are affected by CMTM6 remains unknown within the timeframe of this thesis. Since the abundance of typical known cytoskeletal proteins is unchanged within the purified AEF from *Cmtm6* cKo mice, differences in the axonal cytoskeleton of larger axons might originate from yet unknown or so far undetected molecules (Fig. 22).

Taken together, the increased axonal diameters in *Cmtm6* cKo mice do not result from changes in neurofilament density and/or phosphorylation. However, the axonal actin cytoskeleton may play a role in increasing the axonal diameters in *Cmtm6* cKo mice.

5.5 How can CMTM6 mediate its function towards the axon?

CMTM6 belongs to the CKLF-like-MARVEL transmembrane domain-containing member family which was first reported in 2003 and renamed from CKLFSF1-8 to

CMTM1-8 later on (Han, Ding et al. 2003). All members contain the MARVEL domain which has been previously identified in proteins of the myelin and lymphocyte (MAL) protein superfamily. Since the family members contain four transmembrane domains they are maybe involved in cell-cell signaling. Still, a functional signaling domain within members of the CMTM family has not been described so far, and possible downstream pathways or signaling cascades are unknown. To identify how CMTM6 mediates its function remains to be elucidated.

By purifying and assessing the AEF, we have shown that it is possible to identify novel interesting signaling molecules mediating glia to axon interaction (Fig. 6). This prompted us to purify the AEF from sciatic nerves of control and *Cmtm6* cKo mice. We were able to successfully show similar abundance for axonal proteins, myelin proteins as well as ECM and cell adhesion proteins (Fig. 22A). In addition, we applied the following criteria to select interesting candidates: I) robust abundance in purified AEF samples (threshold >100ppm per sample), II) changed abundance in *Cmtm6* cKo compared to wild-type AEF with at least less 0.5 fold decrease or more than 2.0 fold increase of abundance and a significance level of $p<0.05$ based on ppm values, III) transmembrane protein, secreted factors or proteins with a possible function as ligand or receptor, IV) a possible involvement in regulation of the nervous system, specifically to myelin, axon or the ECM. For none of the in Figure 22 B and C depicted proteins all of the criteria apply. By scanning literature and existing databases such as the RNA-sequencing transcriptome and splicing database of cortical neurons, glia and vascular cells (Zhang, Chen et al. 2014, Zeisel, Munoz-Manchado et al. 2015) no candidate for mediating CMTM6 function was revealed. Nevertheless, two of the upregulated proteins are of potential interest especially when considering cytoskeletal changes and neuronal growth.

Kinesin family member 20b (KIF20B) was shown to be involved in neuronal polarization and migration in the neocortex (McNeely, Cupp et al. 2017). Beyond this, it mediates the transport of Shootin 1 (SHTN1) and thus promotes migration of cortical neurons (Sapir, Levy et al. 2013). Interestingly, SHTN1 is known to interact with L1CAM, an important neuronal cell adhesion molecule, as well as influencing phosphatidylinositol 3,4,5-triphosphate (PIP3) accumulation in the growth of hippocampal neurons (Shimada, Toriyama et al. 2008, Sapir, Levy et al. 2013). PIP3

accumulation on the other side is crucial for the development of neurites into axons and elevated PIP3 levels in the PNS lead to hypermyelination of small caliber axons and impaired radial sorting (Ménager, Arimura et al. 2004, Goebbels, Oltrogge et al. 2010). The second candidate, Centlein, is a microtubule associated protein and *in vitro* studies suggest a role in neurite outgrowth (Zeisel, Munoz-Manchado et al. 2015) by stabilizing microtubules (Jing, Yin et al. 2016). This might be of interest since microtubules are known to be involved in regulation of axonal diameters of small caliber axons which only show low levels of neurofilament expression (Friede and Samorajski 1970). Still, both candidates are possibly contamination considering that published RNAseq databases of different murine CNS areas do not suggest expression by myelinating glia cells (Zhang, Chen et al. 2014, Zeisel, Munoz-Manchado et al. 2015). Thus, KIF20B and centlein did not seem promising for mediating CMTM6 function in restricting radial axonal growth and where thus not further investigated.

Beyond our proteomic approach, we investigated CD274/PDL1 (programmed-death ligand 1) as a promising candidate for CMTM6 interaction. Previous *in vitro* studies using cancer cell lines and a CRISPR-Cas9 screening approach identified CMTM6 as a regulator of CD274 (Burr, Sparbier et al. 2017, Mezzadra, Sun et al. 2017). Further, they have shown that CMTM6 co-localizes with CD274 at the plasma membrane and is crucial for maintaining its cell surface expression on recycling endosomes, thus preventing CD274 degradation (Burr, Sparbier et al. 2017). Mezzadra et al. supported this by showing that CMTM6 regulates CD274 on protein but not mRNA level. Interestingly, they demonstrated that, in the absence of CMTM6, CMTM4 can take over this regulatory function. Apparently, none of the other tested CMTM family members share this function (Mezzadra, Sun et al. 2017). These two *in vitro* studies were the first to identify a role for CMTM6 in regulating T-cell mediated anti-tumor immunity via interacting and stabilizing CD274/PD-L1 on tumor cells recognizing a novel therapeutic target. In our study we show that CD274/PD-L1 is present in the PNS and preferably localizes to the abaxonal myelin sub-compartment. However, abundance and localization of CD274 upon CMTM6 deletion is not changed suggesting that SC expressed CMTM6 does not regulate CD274 protein levels *in vivo* in the PNS (Fig. 23). Notably also CMTM6 abundance is unchanged upon deletion of CD274. Throughout our study we did not test for CMTM4 compensation on any level

mainly because unpublished microarray mRNA data from the department does not indicate *Cmtm4* gene expression in peripheral nerves.

5.6 How do Schwann cells mediate radial axonal growth?

It is still unclear how CMTM6 might mediate its function towards the axon. Notably, it was reported that another adaxonal SC protein, namely MAG, has a role in increasing radial axonal growth in the PNS (Yin, Crawford et al. 1998). This was confirmed with our analysis of axonal diameters within sciatic nerves of control and *Mag* Ko mice (Fig. 24). Since both, CMTM6 and MAG, are localized at the adaxonal SC membrane and are involved in axon diameter regulation we hypothesize that MAG and CMTM6 might functionally interact. Upon CMTM6 deletion we could not detect any changes in protein abundance, mRNA expression or localization of MAG (Fig. 10, 11 and 22). Strikingly though, we could identify a decreased abundance of CMTM6 in *Mag* Ko sciatic nerve lysates as well as a perinuclear accumulation of CMTM6 on SC nuclei of MAG deficient mice (Fig. 25). This implies a possible intracellular transport impairment of CMTM6 when MAG is lacking and identifies a first hint towards a molecular interaction partner of CMTM6. It can be assumed that MAG is important to facilitate the correct localization or abundance of CMTM6 in Schwann cells.

Thus far, known interaction partners of MAG are the major brain gangliosides GT1b and GD1a which together with MAG mediate the periaxonal diameter of myelinated axons (Trapp and Quarles 1982, Pan, Fromholt et al. 2007). Especially for the CNS it was proposed that MAG inhibits axonal regeneration mainly involving interactions with Nogo-receptors as well as $p75^{NTR}$ and RhoA/Rock downstream signaling pathways (Filbin 2003, Palandri, Salvador et al. 2015). However, it is still not fully understood which of the proposed interaction partners indeed mediate the effects of MAG for either CNS or PNS (Schnaar and Lopez 2009). We now identified CMTM6 as a novel Schwann cell protein, which is likely stabilized by MAG.

Since both SC proteins regulate axonal diameters in opposing manner we wanted to assess the consequences of deleting both, MAG (increasing axonal diameters) and CMTM6 (restricting axonal diameters). Thus, we generated double mutant mice (*Cmtm6* cKo;*Mag* Ko). Surprisingly, we could detect a shift towards larger diameter

axons in *Cmtm6* cKo;*Mag* Ko compared to control mice appearing similar to the observed differences in single *Cmtm6* cKo mice (Fig. 25). This led us to conclude, that for the regulation of radial axonal growth in adult mice loss-of CMTM6 function is overriding the loss-of MAG function within peripheral nerves. With our study we propose a model in which proteins like MAG and CMTM6 localized at the adaxonal membrane directly influence the regulation of radial axonal growth of peripheral myelinated axons (Fig. 26A). Upon the deletion of MAG, we could validate what others previously showed: axonal diameters are smaller (Fig. 26B) (Yin, Crawford et al. 1998), whereas if SC lack CMTM6 axonal diameters are increased (Fig. 26C). If both adaxonal proteins are deleted the axonal diameters are similarly enlarged as in *Cmtm6* cKo, suggesting CMTM6 loss is overriding the loss of MAG on axonal diameter regulation (Fig. 26D).

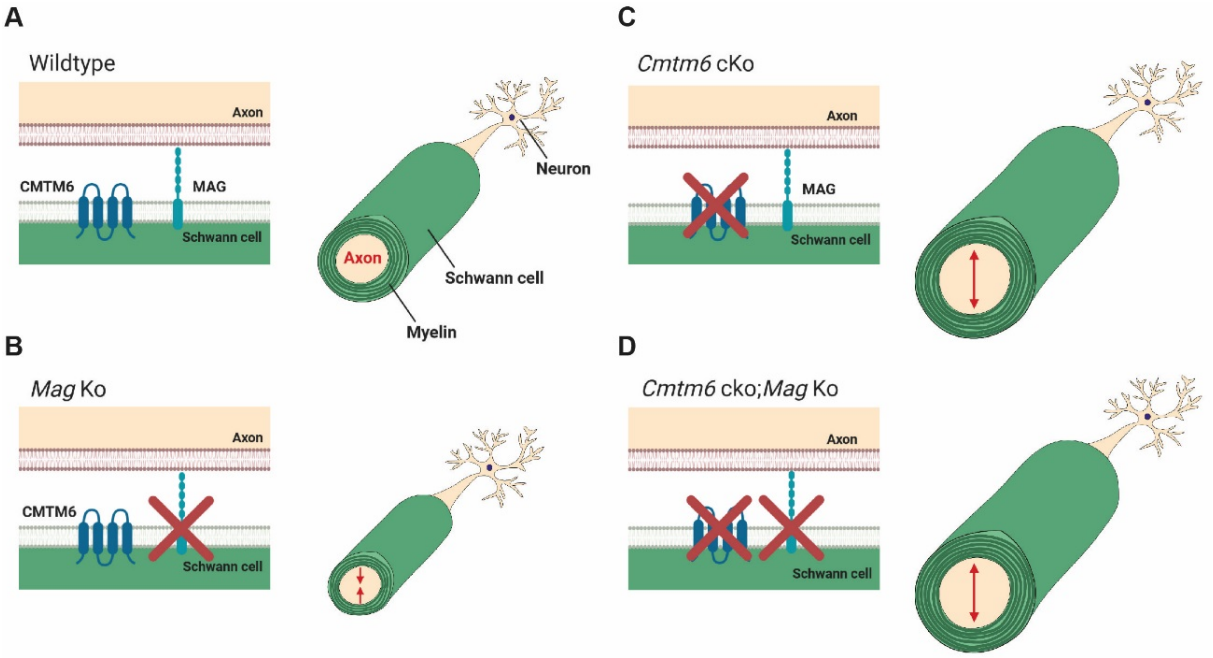

Figure 26. Model of the role of adaxonal Schwann cell proteins CMTM6 and MAG in regulation of axonal diameters in the PNS. Compared to wildtype mice (**A**) axonal diameters are reduced when MAG is lacking, as previously shown by Yin et al. 1998 (**B**) indicating that MAG mediates radial axonal growth. **C**) The diameters of Cmtm6 cKo mice are enlarged implying that CMTM6 restricts axonal diameters. **D**) Upon deletion of both, MAG and CMTM6, axonal diameters are enlarged suggesting loss of CMTM6 function overrides the loss of MAG function. We propose that Schwann cells regulate axonal diameters via adaxonal proteins including MAG and CMTM6. Scheme created with Biorender.com.

5.7 Nerve conduction velocity; a matter of size and precision

It is commonly accepted that upon myelination the internodal capacitance is reduced and upon radial axonal growth the interior resistance along internodes is

decreased, both achieving faster signal propagation along myelinated axons (Hartline and Colman 2007). Calculations in the 1950`s suggest a linear dependency of nerve conduction velocity on axonal diameters of myelinated fibers (Rushton 1951).

In our mouse model the axonal diameters within sciatic nerves are increased when CMTM6 is lacking from SC but the g-ratio remains constant. Thus, the myelin sheath increases appropriately to the larger axonal diameter. The increase of axonal diameters in *Cmtm6* cKo mice together with the appropriately increased myelin sheath thickness prompted us to analyze the nerve conduction velocity of control and *Cmtm6* cKo mice. The described morphological changes are especially prominent in the sensory dorsal roots and the phrenic nerve. As expected, both SNAP and SNCV are increased in mice lacking CMTM6 from SCs (Fig. 17). These alterations affect *Cmtm6* cKo mice functionally. Behavioral assays showed a significantly faster reaction towards a heat-stimulus and an elimination of breathing pauses, which are commonly seen in C57BL/6N mice (Fig. 19) (Stettner, Zanella et al. 2008). Notably, most behavioral experiments that were conducted in this study assessing motor capabilities showed no differences. One exception is the Grid test for which *Cmtm6* cKo mice displayed a higher number of fore- and hind limb slips. This is consistent with the observed unchanged CMAP and mNCV (Fig. 17 and 19). Concluding, the changes observed in axonal diameter and myelin sheath thickness in *Cmtm6* cKo affect preferably sensory function and alter motor function and coordination only to a minor extend. Nonetheless, we demonstrated that SC mediated alterations of axonal diameters influence the signal propagation within the PNS.

SC signals including mTOR, MAG and PMP22 initiate and/or support the continued radial growth of axons mainly via modulating the axonal cytoskeleton (de Waegh, Lee et al. 1992, Yin, Crawford et al. 1998, Sherman, Krols et al. 2012). Beyond that, studies in *shiverer* mice, which lack myelin basic protein (MBP) and thus lack compact myelin in the CNS also exhibit reduced axonal diameters in the CNS (Readhead, Popko et al. 1987, Panagopoulos, King et al. 1989, Gould, Byrd et al. 1995, Sadahiro, Yoshikawa et al. 2000, Kirkpatrick, Witt et al. 2001). The myelin compaction in the PNS in these mice is comparably normal but Panagopoulos and Gould et al. showed smaller axonal diameters in tibial and sciatic nerves of *shiverer* mice (Panagopoulos, King et al. 1989, Gould, Byrd et al. 1995). These studies together

imply that another role of myelin is to increase axonal diameters. However, the previously published assessments are not based on high numbers of both axons and mice.

Vice versa, the axonal diameter regulates the initiation of myelination in the PNS (described in more detail in introduction chapter 2.2 and previous discussion chapters). Our study now provides the first evidence of a myelin signal which represses axonal diameter growth without impairing myelination. This suggests a more complex interplay between SCs and axons than previously assumed. Not only impaired myelin or disruption of glial genes can lead to smaller axonal diameters but intrinsic glial signals restrict radial axonal growth. This leads to the following question: Why do axons need to be restricted in size?

In the CNS, Perge et al. quantified axonal diameters (myelinated and non-myelinated axons) and mitochondrial volume in 16 different fiber tracts in five different species, combined with published information about firing rates of respective axons/fiber tracts (Perge, Niven et al. 2012). Interestingly, they showed that axons vary around 100-fold in diameter amongst the different CNS fiber tracts. From this study they propose, but not experimentally validate, an evolutionary pressure towards smaller axonal diameters since axonal diameters appear to be linear to firing rates. Further, they state that to double the information rate along specific fibers an axon would need to increase its volume by 4-fold which would require high amounts of energy. They conclude that information rate processing in different tracts defines axonal diameter to improve timing precision (Perge, Niven et al. 2012). Adding to this, Hartline & Colman discuss that non-myelinated axons would need to be 100-times larger for a ten-fold increase in NCV (Hartline and Colman 2007). The emergence of myelination possibly benefitted the development of smaller axonal diameters which might have paved the way for the development of sophisticated signaling systems. Even though the majority of these studies focus on the CNS it is likely that molecular signals that restrict radial axonal growth exist throughout the whole nervous system. Since there is a variety of axonal diameters also within the PNS (e.g. observed different diameters in the control nerves of this study) it seems plausible to assume that also axonal diameter regulating proteins such as MAG or CMTM6 might be differentially

expressed in various fiber tracts such as ventral or dorsal roots, or mixed nerves like the sciatic nerve.

What else besides myelination and axonal diameter affects nerve conduction velocity? Studies by Rushton, Waxman as well as Huxley and Stämpfli already proposed that internodal length, the distance between two nodes of Ranvier, affect NCV and that a specific length or maximum value can be reached beyond which conduction velocity will not increase any further (Huxley and Stämpeli 1949, Rushton 1951, Waxman 1980). This was experimentally supported in a mouse model in which internodes were shortened during development without impaired myelination or differences in axonal diameters (Wu, Williams et al. 2012). This resulted in a decreased nerve conduction velocity and functional motor impairment of respective mice. Strikingly though, internodal length, NCV and functional readout recovered during postnatal development (Wu, Williams et al. 2012). In *Cmtm6* cKo mice, internodal distances are unchanged at least postnatally and thus do not contribute to the observed increase in nerve conduction velocity (Fig. 18).

Beyond this, increasing nodal length can potentially alter the conduction speed either via increasing the capacitance of the nodal membrane or increasing the number of Na^+ channels at the nodes. By investigating nodes of Ranvier in the rat optic nerve and cerebral cortical axons the lab of David Attwell has demonstrated that the length of nodes can vary between 4.4-8.7-fold whereas the variation is less along the same axon. By computational modelling they predict that altering nodal length can influence speed of conduction by 20 percent (depending on internodal length changes but not channel density changes) (Arancibia-Cárcamo et al., 2017). Consequently, nodal length is another parameter to affect nerve conduction velocity. This prompted us to also investigate nodal and paranodal ultrastructure as well as measuring length and diameter for which we did not detect changes in *Cmtm6* cKo compared to control mice (Fig. 18). The observed increase in nerve conduction velocity in our model thus appears to originate solely from the increased axonal diameters as well as myelin sheath thickness but not from other parameters that influence the speed of signal propagation. This makes our model attractive to assess *in vivo* how axonal diameters affect nerve conduction velocity independent of other parameters of the myelinated axon unit.

The modulation of NCV by about 20 percent by nodal alterations in the study of Arancibia-Cárcamo et al. is roughly similar to what changes in adding further myelin sheaths or changes in internodal length may achieve. However, changing node length requires less addition/retraction of membrane than what would be needed for adding more myelin wraps. Thus, fine-tuning of nodes of Ranvier is perhaps a fast and more efficient way of adapting nerve conduction velocity on the specific requirements in the CNS (Arancibia-Cárcamo, Ford et al. 2017). In the PNS two independent computational modelling studies targeted the question if there is an optimum extent of constriction of axonal diameters at the nodes for proper NCV (Halter and Clark 1993, Johnson, Holmes et al. 2015). They confirm this idea and propose that mechanisms must exist which restrict axonal diameters so that optimal nodal constriction is achieved depending on the NCV required for optimal signal transmission in a particular circuit or nerve. Note that the majority of these computational models have not yet been confirmed *in vivo*. The interplay of the relevant parameters of the myelinated axon unit affecting NCV remain to be experimentally assessed for both CNS and PNS.

Together, *Cmtm6* cKo mice provide an experimental model with a specifically defined morphological change of axonal diameters but not nodal, paranodal or internodal parameters. We could experimentally assess that the increased axonal diameters in peripheral nerves and the appropriately thicker myelin sheath increase sensory nerve conduction velocity. Thus, *Cmtm6* cKo mice contribute to understanding the effects of spatial dimensions of the axon/myelin unit and how it precisely regulates nerve conduction velocity and thus nervous system function.

5.8 Conclusion

In this thesis we aimed at identifying novel proteins mediating interactions between peripheral axons and myelinating Schwann cells (SCs). Using a proteomic screen of the axogliasome-enriched fraction (AEF) purified from murine sciatic nerves we identified CMTM6 as a novel SC protein and determined its localization at the adaxonal membrane. By deleting its expression in SCs, we investigated morphological, functional and behavioral changes in *Cmtm6* cKo mice.

Strikingly, we found a considerable shift towards increased diameters of both myelinated and non-myelinated axons in various peripheral nerves when CMTM6 is lacking from SCs. Since myelination accelerates nerve conduction velocity more efficiently than increased axonal diameters, it is plausible that molecules restricting the radial expansion of axons exist. Notably, myelin biogenesis, axonal integrity and radial sorting are not impaired in CMTM6 deficient mice. In agreement with increased axonal diameters and appropriate myelin sheath thickness *Cmtm6* cKo mice exhibit faster sensory nerve conduction velocity, accelerated sensory responses and mild motor coordination changes. Since internodal, nodal and paranodal dimensions are not impaired by deficiency of CMTM6, its function in restricting radial axonal growth is highly specific.

While the adaxonal myelin protein MAG has long been known to be involved in increasing axonal size, CMTM6 is the first myelin protein to restrict radial axonal growth. By deleting both MAG and CMTM6 we demonstrate that CMTM6 loss-of function overrides MAG loss-of function. In addition, the abundance and localization of CMTM6 appears to be regulated by MAG.

In many PNS diseases or upon nerve injury the myelinated axon unit is pathologically disrupted which is sometimes accompanied by altered/reduced axonal diameters (De Waegh and Brady 1990, Vaughan 1992, Frei, Mötzing et al. 1999). Thus, as a possible preclinical application I propose that the findings of this thesis are promising toward investigating the potential beneficial role of counteracting CMTM6, e.g. in the following two scenarios:

I) Charcot-Marie-Tooth diseases (CMT) result from mutations in either axonal (CMT type 2) or SC (CMT type 1) proteins and are inherited neuropathies in which patients suffer from progressive muscle weakness caused by impaired nerve conduction owing to reduced axonal diameter, axonal loss and either hypo- or de/dysmyelination (Stassart, Möbius et al. 2018). For example, mutations affecting the major peripheral myelin protein P0/MPZ result in either CMT1B or the more severe Dejerine-Sottas syndrome (Pareyson and Marchesi 2009, Saporta and Shy 2013). Previous analyzes of established mouse models ($P0^{null/null}$ and $P0^{+/-}$) have shown decreased

axonal diameters and hypomyelination (Giese, Martini et al. 1992, Martini, Zielasek et al. 1995, Shapiro, Doyle et al. 1996, Frei, Mötzing et al. 1999, Patzig, Kusch et al. 2016). Thus, it would be of interest to examine if experimentally increasing axonal diameters by deleting CMTM6 could rescue the axonal phenotype, increase myelin sheath thickness and improve behavioral performance in these mouse models.

II) The PNS has higher regenerative capabilities compared to the CNS, mainly because Schwann cells are comparatively plastic and can dynamically act upon nerve injuries with defined steps of degeneration, myelin clearance and remyelination (Jessen and Mirsky 2016). However, full functional recovery is rarely achieved in human patients (Fu and Gordon 1997). Often times, myelin sheaths remain abnormally thin, resulting in slower nerve conduction velocity (Stassart, Fledrich et al. 2013). It would be of interest to investigate the regeneration capabilities in a nerve crush or transection model using control and *Cmtm6* cko mice to assess if an increase in axonal diameters could either speed up recovery and/or restore functionality post injury by establishing the original myelin sheath thickness.

Counteracting the function of CMTM6 in restricting axonal diameters may emerge as a promising therapeutic approach in disorders affecting the peripheral nervous system. Results of this thesis meanwhile have been published in Eichel, M. A., et al. (2020). "CMTM6 expressed on the adaxonal Schwann cell surface restricts axonal diameters in peripheral nerves." Nat Commun 11(1): 4514.

6 References

Abdo, H., L. Calvo-Enrique, J. M. Lopez, J. Song, M. D. Zhang, D. Usoskin, A. E. Manira, I. Adameyko, J. Hjerling-Leffler and P. Ernfors (2019). "Specialized cutaneous schwann cells initiate pain sensation." Science.

Adlkofer, K., R. Frei, D. H. H. Neuberg, J. Zielasek, K. V. Toyka and U. Suter (1997). "Heterozygous peripheral myelin protein 22-deficient mice are affected by a progressive demyelinating tomaculous neuropathy." Journal of Neuroscience **17**(12): 4662-4671.

Aguayo, A. J., M. Attiwell, J. Trecarten, S. Perkins and G. M. Bray (1977). Abnormal myelination in transplanted Trembler mouse Schwann cells [29].

Aguayo, A. J., J. M. Peyronnard and G. M. Bray (1973). "A quantitative ulthastructural study of regeneration from isolated proximal stumps of transected unmyelinated nerves." Journal of Neuropathology and Experimental Neurology.

Allen, M. J., J. A. Drummond and K. G. Moffat (1998). "Development of the giant fiber neuron of Drosophila melanogaster." Journal of Comparative Neurology.

Arancibia-Cárcamo, I. L., M. C. Ford, L. Cossell, K. Ishida, K. Tohyama and D. Attwell (2017). "Node of ranvier length as a potential regulator of myelinated axon conduction speed." eLife **6**: 1-15.

Arroyo, E. J. and S. S. Scherer (2000). "On the molecular architecture of myelinated fibers." Histochemistry and Cell Biology **113**(1): 1-18.

Arthur-Farraj, P. J., M. Latouche, D. K. Wilton, S. Quintes, E. Chabrol, A. Banerjee, A. Woodhoo, B. Jenkins, M. Rahman, M. Turmaine, G. K. Wicher, R. Mitter, L. Greensmith, A. Behrens, G. Raivich, R. Mirsky and K. R. Jessen (2012). "c-Jun Reprograms Schwann Cells of Injured Nerves to Generate a Repair Cell Essential for Regeneration." Neuron.

Barry, D. M., W. Stevenson, B. G. Bober, P. J. Wiese, G. S. Barry, J. M. Dale, G. S. Barry, N. S. Byers, J. D. Strope, R. Chang, D. J. Schulz, S. Shah, N. A. Calcutt, Y. Gebremichael and M. L. Garcia (2012). "Expansion of NF-M carboxy terminus increases axonal diameter independent of increases in conduction velocity or myelin thickness." J Neurosci **32**(18): 6209-6219.

Berghs, S., D. Aggujaro, R. Dirkx, E. Maksimova, P. Stabach, J. M. Hermel, J. P. Zhang, W. Philbrick, V. Slepnev, T. Ort and M. Solimena (2000). "βIV spectrin, a new spectrin localized at axon initial segments and nodes of ranvier in the central and peripheral nervous system." Journal of Cell Biology.

Birchmeier, C. (2009). "ErbB receptors and the development of the nervous system." Experimental Cell Research **315**(4): 611-618.

Birchmeier, C. and K. A. Nave (2008). "Neuregulin-1, a key axonal signal that drives schwann cell growth and differentiation." GLIA.

Bremer, J., F. Baumann, C. Tiberi, C. Wessig, H. Fischer, P. Schwarz, A. D. Steele, K. V. Toyka, K. A. Nave, J. Weis and A. Aguzzi (2010). "Axonal prion protein is required for peripheral myelin maintenance." Nature Neuroscience.

Brennan, A., C. H. Dean, A. L. Zhang, D. T. Cass, R. Mirsky and K. R. Jessen (2000). "Endothelins control the timing of Schwann cell generation in vitro and in vivo." Developmental Biology.

Britsch, S., D. E. Goerich, D. Riethmacher, R. I. Peirano, M. Rossner, K. A. Nave, C. Birchmeier and M. Wegner (2001). "The transcription factor Sox10 is a key regulator of peripheral glial development." Genes and Development.

Brown, A. M., R. D. Evans, J. Black and B. R. Ransom (2012). "Schwann cell glycogen selectively supports myelinated axon function." Annals of Neurology **72**(3): 406-418.

Burr, M. L., C. E. Sparbier, Y. C. Chan, J. C. Williamson, K. Woods, P. A. Beavis, E. Y. N. Lam, M. A. Henderson, C. C. Bell, S. Stolzenburg, O. Gilan, S. Bloor, T. Noori, D. W. Morgens, M. C. Bassik, P. J. Neeson, A. Behren, P. K. Darcy, S. J. Dawson, I. Voskoboinik, J. A. Trapani, J. Cebon, P. J. Lehner and M. A. Dawson (2017). "CMTM6 maintains the expression of PD-L1 and regulates anti-Tumour immunity." Nature **549**(7670): 101-105.

Ceballos, D., J. Cuadras, E. Verdú and Navarro (1999). "Morphometric and ultrastructural changes with ageing in mouse peripheral nerve." J. Anat.: 563-576.

Charles, P., S. Tait, C. Faivre-Sarrailh, G. Barbin, F. Gunn-Moore, N. Denisenko-Nehrbass, A. M. Guennoc, J. A. Girault, P. J. Brophy and C. Lubetzki (2002). "Neurofascin is a glial receptor for the paranodin/Caspr-contactin axonal complex at the axoglial junction." Current Biology.

Chase, M. H., J. K. Engelhardt, A. M. Adinolfi and S. S. Chirwa (1992). "Age-dependent changes in cat masseter nerve: an electrophysiological and morphological study." Brain Research.

Cheng, C. M., R. R. Reinhardt, W. H. Lee, G. Joncas, S. C. Patel and C. A. Bondy (2000). "Insulin-like growth factor 1 regulates developing brain glucose metabolism." Proceedings of the National Academy of Sciences of the United States of America.

Chiu, S. Y. and J. M. Ritchie (1984). "On the physiological role of internodal potassium channels and the security of conduction in myelinated nerve fibers." Proceedings of the Royal Society of London - Biological Sciences.

Cohen, C. C. H., M. A. Popovic, J. Klooster, M.-T. Weil, W. Möbius, K.-A. Nave and M. H. P. Kole (2019). "Saltatory Conduction along Myelinated Axons Involves a Periaxonal Nanocircuit." Cell: 311-322.

Costa, A. R., R. Pinto-Costa, S. C. Sousa and M. M. Sousa (2018). "The Regulation of Axon Diameter: From Axonal Circumferential Contractility to Activity-Dependent Axon Swelling." Frontiers in Molecular Neuroscience **11**(September): 1-7.

D'Este, E., D. Kamin, F. Balzarotti and S. W. Hell (2017). "Ultrastructural anatomy of nodes of Ranvier in the peripheral nervous system as revealed by STED microscopy." Proceedings of the National Academy of Sciences of the United States of America.

Dale, J. M. and M. L. Garcia (2012). "Neurofilament Phosphorylation during Development and Disease: Which Came First, the Phosphorylation or the Accumulation?" Journal of Amino Acids **2012**: 1-10.

Davis, J. Q., S. Lambert and V. Bennett (1996). "Molecular composition of the node of Ranvier: Identification of ankyrin- binding cell adhesion molecules neurofascin (mucin+/third FNIII domain-) and NrCAM at nodal axon segments." Journal of Cell Biology.

De Monasterio-Schrader, P., O. Jahn, S. Tenzer, S. P. Wichert, J. Patzig and H. B. Werner (2012). Systematic approaches to central nervous system myelin.

De Waegh, S. and S. T. Brady (1990). "Altered slow axonal transport and regeneration in a myelin-deficient mutant mouse: The trembler as an in vivo model for schwann cell-axon interactions." Journal of Neuroscience **10**(6): 1855-1865.

de Waegh, S. M., V. M. Y. Lee and S. T. Brady (1992). "Local modulation of neurofilament phosphorylation, axonal caliber, and slow axonal transport by myelinating Schwann cells." Cell **68**(3): 451-463.

Dere, E., L. Dahm, D. Lu, K. Hammerschmidt, A. Ju, M. Tantra, A. Kästner, K. Chowdhury and H. Ehrenreich (2014). "Heterozygous Ambra1 deficiency in mice: A genetic trait with autism-like behavior restricted to the female gender." Frontiers in Behavioral Neuroscience.

Dere, E., D. Winkler, C. Ritter, A. Ronnenberg, G. Poggi, J. Patzig, M. Gernert, C. Müller, K. A. Nave, H. Ehrenreich and H. B. Werner (2015). "Gpm6b deficiency impairs sensorimotor gating and modulates the behavioral response to a 5-HT2A/C receptor agonist." Behavioural Brain Research.

Dhaunchak, A. S., J. K. Huang, O. De Faria, A. D. Roth, L. Pedraza, J. P. Antel, A. Bar-Or and D. R. Colman (2010). "A proteome map of axoglial specializations isolated and purified from human central nervous system." Glia **58**(16): 1949-1960.

Distler, U., J. Kuharev, P. Navarro, Y. Levin, H. Schild and S. Tenzer (2014). "Drift time-specific collision energies enable deep-coverage data-independent acquisition proteomics." Nature Methods.

Distler, U., J. Kuharev, P. Navarro and S. Tenzer (2016). "Label-free quantification in ion mobility-enhanced data-independent acquisition proteomics." Nature Protocols.

Domènech-Estévez, E., H. Baloui, C. Repond, K. Rosafio, J. J. Médard, N. Tricaud, L. Pellerin and R. Chrast (2015). "Distribution of monocarboxylate transporters in the peripheral nervous system suggests putative roles in lactate shuttling and myelination." Journal of Neuroscience **35**(10): 4151-4156.

Dong, Z., A. Brennan, N. Liu, Y. Yarden, G. Lefkowitz, R. Mirsky and K. R. Jessen (1995). "Neu differentiation factor is a neuron-glia signal and regulates survival, proliferation, and maturation of rat schwann cell precursors." Neuron.

Douarin, N. L., C. Dulac, E. Dupin and P. Cameron-Curry (1991). "Glial cell lineages in the neural crest." Glia.

Drorbaugh, J. E. and W. O. Fenn (1955). "A barometric method for measuring ventilation in newborn infants." Pediatrics.

Eaton, R. C. (1984). Neural Mechanisms of Startle Behavior.

Eichel, M. A., V. I. Gargareta, E. D'Este, R. Fledrich, T. Kungl, T. J. Buscham, K. A. Luders, C. Miracle, R. B. Jung, U. Distler, K. Kusch, W. Mobius, S. Hulsmann, S. Tenzer, K. A. Nave and H. B. Werner (2020). "CMTM6 expressed on the adaxonal Schwann cell surface restricts axonal diameters in peripheral nerves." Nat Commun **11**(1): 4514.

Erwig, M. S., D. Hesse, R. B. Jung, M. Uecker, K. Kusch, S. Tenzer, O. Jahn and H. B. Werner (2019). Myelin: Methods for purification and proteome analysis.

Feltri, M. L., Y. Poitelon and S. C. Previtali (2016). How Schwann Cells Sort Axons: New concepts.

Filbin, M. T. (2003). "Myelin-associated inhibitors of axonal regeneration in the adult mammalian CNS." Nature Reviews Neuroscience.

FitzGerald, M. J. T., G. Gruener and E. Mtui (2012). Clinical neuroanatomy and neuroscience, Saunders/Elsevier.

Fledrich, R., D. Akkermann, V. Schütza, T. A. Abdelaal, D. Hermes, E. Schäffner, M. C. Soto-Bernardini, T. Götze, A. Klink, K. Kusch, M. Krueger, T. Kungl, C. Frydrychowicz, W. Möbius, W. Brück, W. C. Mueller, I. Bechmann, M. W. Sereda, M. H. Schwab, K. A. Nave and R. M. Stassart (2019). "NRG1 type I dependent autoparacrine stimulation of Schwann cells in onion bulbs of peripheral neuropathies." Nature Communications.

Fledrich, R., T. Kungl, K. A. Nave and R. M. Stassart (2019). "Axo-glial interdependence in peripheral nerve development." Development (Cambridge, England) **146**(21): 1-12.

Fledrich, R., B. Schlotter-Weigel, T. J. Schnizer, S. P. Wichert, R. M. Stassart, G. Meyer Zu Hörste, A. Klink, B. G. Weiss, U. Haag, M. C. Walter, B. Rautenstrauss, W. Paulus, M. J. Rossner and M. W. Sereda (2012). "A rat model of Charcot-Marie-Tooth disease 1A recapitulates disease variability and supplies biomarkers of axonal loss in patients." Brain.

Fledrich, R., R. M. Stassart, A. Klink, L. M. Rasch, T. Prukop, L. Haag, D. Czesnik, T. Kungl, T. A. M. Abdelaal, N. Keric, C. Stadelmann, W. Brück, K. A. Nave and M. W. Sereda (2014). "Soluble neuregulin-1 modulates disease pathogenesis in rodent models of Charcot-Marie-Tooth disease 1A." Nature Medicine **20**(9): 1055-1061.

Fontana, X., M. Hristova, C. Da Costa, S. Patodia, L. Thei, M. Makwana, B. Spencer-Dene, M. Latouche, R. Mirsky, K. R. Jessen, R. Klein, G. Raivich and A. Behrens (2012). "C-Jun in Schwann cells promotes axonal regeneration and motoneuron survival via paracrine signaling." Journal of Cell Biology.

Ford, M. C., O. Alexandrova, L. Cossell, A. Stange-Marten, J. Sinclair, C. Kopp-Scheinpflug, M. Pecka, D. Attwell and B. Grothe (2015). "Tuning of Ranvier node and internode properties in myelinated axons to adjust action potential timing." Nature Communications **6**: 1-14.

Frei, R., S. Mötzing, I. Kinkelin, M. Schachner, M. Koltzenburg and R. Martini (1999). "Loss of distal axons and sensory Merkel cells and features indicative of muscle denervation in hindlimbs of P0-deficient mice." Journal of Neuroscience **19**(14): 6058-6067.

Friede, R. L. and T. Samorajski (1970). "Axon caliber related to neurofilaments and microtubules in sciatic nerve fibers of rats and mice." The Anatomical Record **167**(4): 379-387.

Fu, S. Y. and T. Gordon (1997). "The cellular and molecular basis of peripheral nerve regeneration." Molecular Neurobiology.

Fünfschilling, U., L. M. Supplie, D. Mahad, S. Boretius, A. S. Saab, J. Edgar, B. G. Brinkmann, C. M. Kassmann, I. D. Tzvetanova, W. Möbius, F. Diaz, D. Meijer, U. Suter, B. Hamprecht, M. W. Sereda, C. T. Moraes, J. Frahm, S. Goebbels and K. A. Nave (2012). "Glycolytic oligodendrocytes maintain myelin and long-term axonal integrity." Nature.

Garcia, M. L., C. S. Lobsiger, S. B. Shah, T. J. Deerinck, J. Crum, D. Young, C. M. Ward, T. O. Crawford, T. Gotow, Y. Uchiyama, M. H. Ellisman, N. A. Calcutt and D. W. Cleveland (2003). "NF-M is an essential target for the myelin-directed "outside-in" signaling cascade that mediates radial axonal growth." Journal of Cell Biology **163**(5): 1011-1020.

Giese, K. P., R. Martini, G. Lemke, P. Soriano and M. Schachner (1992). "Mouse P0 gene disruption leads to hypomyelination, abnormal expression of recognition molecules, and degeneration of myelin and axons." Cell **71**(4): 565-576.

Glenn, T. D. and W. S. Talbot (2013). Signals regulating myelination in peripheral nerves and the Schwann cell response to injury.

Goebbels, S., J. H. Oltrogge, R. Kemper, I. Heilmann, I. Bormuth, S. Wolfer, S. P. Wichert, W. Möbius, X. Liu, C. Lappe-Siefke, M. J. Rossner, M. Groszer, U. Suter, J. Frahm, S. Boretius and K. A. Nave (2010). "Elevated phosphatidylinositol 3,4,5-trisphosphate in glia triggers cell-autonomous membrane wrapping and myelination." Journal of Neuroscience.

Gomez-Sanchez, J. A., L. Carty, M. Iruarrizaga-Lejarreta, M. Palomo-Irigoyen, M. Varela-Rey, M. Griffith, J. Hantke, N. Macias-Camara, M. Azkargorta, I. Aurrekoetxea, V. G. De Juan, H. B. J. Jefferies, P. Aspichueta, F. Elortza, A. M. Aransay, M. L. Martínez-Chantar, F. Baas, J. M. Mato, R. Mirsky, A. Woodhoo and K. R. Jessen

(2015). "Schwann cell autophagy, myelinophagy, initiates myelin clearance from injured nerves." Journal of Cell Biology.

Gomez-Sanchez, J. A., K. S. Pilch, M. Van Der Lans, S. V. Fazal, C. Benito, L. J. Wagstaff, R. Mirsky and K. R. Jessen (2017). "After nerve injury, lineage tracing shows that myelin and Remak Schwann cells elongate extensively and branch to form repair Schwann cells, which shorten radically on remyelination." Journal of Neuroscience **37**(37): 9086-9099.

Gould, R. M., A. L. Byrd and E. Barbarese (1995). "The number of Schmidt-Lanterman incisures is more than doubled in shiverer PNS myelin sheaths." J Neurocytol **24**(2): 85-98.

Griffin, J. W. and W. J. Thompson (2008). "Biology and pathology of nonmyelinating schwann cells." GLIA.

Grinspan, J. B., M. A. Marchionni, M. Reeves, M. Coulaloglou and S. S. Scherer (1996). "Axonal interactions regulate Schwann cell apoptosis in developing peripheral nerve: Neuregulin receptors and the role of neuregulins." Journal of Neuroscience.

Halter, J. A. and J. W. Clark (1993). "The influence of nodal constriction on conduction velocity in myelinated nerve fibers." NeuroReport.

Han, W., P. Ding, M. Xu, L. Wang, M. Rui, S. Shi, Y. Liu, Y. Zheng, Y. Chen, T. Yang and D. Ma (2003). "Identification of eight genes encoding chemokine-like factor superfamily members 1-8 (CKLFSF1-8) by in silico cloning and experimental validation." Genomics **81**(6): 609-617.

Hartline, D. K. and D. R. Colman (2007). "Rapid Conduction and the Evolution of Giant Axons and Myelinated Fibers." Current Biology **17**(1): 29-35.

Harty, B. L. and K. R. Monk (2017). "Unwrapping the unappreciated: recent progress in Remak Schwann cell biology." Current Opinion in Neurobiology **47**(Figure 1): 131-137.

Hildebrand, C., C. M. Bowe and I. N. Remahl (1994). "M Y E L I N A T I O N A N D M Y E L I N SHEATH R E M O D E L L I N G IN N O R M A L A N D P A T H O L O G I C A L PNS N E R V E FIBRES." **43**.

Hodgkin, A. L. (1954). "A note on conduction velocity." The Journal of Physiology.

Höke, A. (2006). Mechanisms of Disease: What factors limit the success of peripheral nerve regeneration in humans?

Hsieh, S.-T., G. J. Kidd, T. Crawford, Z. Xu, W.-M. Lin, B. D. Trapp, D. W. Cleveland and J. W. Griffinv (1994). "Regional Modulation of Neurofilament Organization by Myelination in Normal Axons." Journal of Neuroscience(November): 6392-6401.

Huxley, A. F. and R. Stämpeli (1949). "Evidence for saltatory conduction in peripheral myelinated nerve fibres." The Journal of Physiology.

Huxley, A. F. and R. Stämpfli (1949). "Evidence for saltatory conduction in peripheral myelinated nerve fibres." The Journal of Physiology.

Huxley, A. F. and R. Stämpfli (1951). "Direct determination of membrane resting potential and action potential in single myelinated nerve fibres." The Journal of Physiology.

Jahn, O., S. Tenzer and H. B. Werner (2009). Myelin proteomics: Molecular anatomy of an insulating sheath.

Jessen, K. R. and R. Mirsky (1999). "Schwann cells and their precursors emerge as major regulators of nerve development." Trends in Neurosciences **22**(9): 402-410.

Jessen, K. R. and R. Mirsky (2005). The origin and development of glial cells in peripheral nerves.

Jessen, K. R. and R. Mirsky (2008). "Negative regulation of myelination: Relevance for development, injury, and demyelinating disease." GLIA.

Jessen, K. R. and R. Mirsky (2016). "The repair Schwann cell and its function in regenerating nerves." Journal of Physiology **594**(13): 3521-3531.

Jessen, K. R. and R. Mirsky (2019). "Schwann cell precursors; multipotent glial cells in embryonic nerves." Frontiers in Molecular Neuroscience **12**(March): 1-16.

Jessen, K. R., R. Mirsky and A. C. Lloyd (2015). "Schwann cells: Development and role in nerve repair." Cold Spring Harbor Perspectives in Biology **7**(7): 1-15.

Jing, Z., H. Yin, P. Wang, J. Gao and L. Yuan (2016). "Centlein, a novel microtubule-associated protein stabilizing microtubules and involved in neurite formation." Biochemical and Biophysical Research Communications.

Johnson, C., W. R. Holmes, A. Brown and P. Jung (2015). "Minimizing the caliber of myelinated axons by means of nodal constrictions." Journal of Neurophysiology **114**(3): 1874-1884.

Kegel, L., M. Jaegle, S. Driegen, E. Aunin, K. Leslie, Y. Fukata, M. Watanabe, M. Fukata and D. Meijer (2014). "Functional phylogenetic analysis of LGI proteins identifies an interaction motif crucial for myelination." Development (Cambridge).

Kirkpatrick, L. L., A. S. Witt, H. R. Payne, H. D. Shine and S. T. Brady (2001). "Changes in microtubule stability and density in myelin-deficient shiverer mouse CNS axons." Journal of Neuroscience.

Kordeli, E., J. Davis, B. Trapp and V. Bennett (1990). "An isoform of ankyrin is localized to nodes of Ranvier in myelinated axons of central and peripheral nerves." Journal of Cell Biology.

Küffer, A., A. K. K. Lakkaraju, A. Mogha, S. C. Petersen, K. Airich, C. Doucerain, R. Marpakwar, P. Bakirci, A. Senatore, A. Monnard, C. Schiavi, M. Nuvolone, B. Grosshans, S. Hornemann, F. Bassilana, K. R. Monk and A. Aguzzi (2016). "The prion protein is an agonistic ligand of the G protein-coupled receptor Adgrg6." Nature.

Lee, Y., B. M. Morrison, Y. Li, S. Lengacher, M. H. Farah, P. N. Hoffman, Y. Liu, A. Tsingalia, L. Jin, P. W. Zhang, L. Pellerin, P. J. Magistretti and J. D. Rothstein (2012).

"Oligodendroglia metabolically support axons and contribute to neurodegeneration." Nature.

Leite, S. C., P. Sampaio, V. F. Sousa, J. Nogueira-Rodrigues, R. Pinto-Costa, L. L. Peters, P. Brites and M. M. Sousa (2016). "The Actin-Binding Protein α-Adducin Is Required for Maintaining Axon Diameter." Cell Reports **15**(3): 490-498.

Lenz, P. H., D. K. Hartline and A. D. Davis (2000). "The need for speed. I. Fast reactions and myelinated axons in copepods." Journal of Comparative Physiology - A Sensory, Neural, and Behavioral Physiology.

Leone, D. P., S. Genoud, S. Atanasoski, R. Grausenburger, P. Berger, D. Metzger, W. B. Macklin, P. Chambon and U. Suter (2003). "Tamoxifen-inducible glia-specific Cre mice for somatic mutagenesis in oligodendrocytes and Schwann cells." Molecular and Cellular Neuroscience.

Leterrier, C., P. Dubey and S. Roy (2017). The nano-architecture of the axonal cytoskeleton.

Li, C., M. B. Tropak, R. Gerlai, S. Clapoff, W. Abramow-Newerly, B. Trapp, A. Peterson and J. Roder (1994). "Myelination in the absence of myelin-associated glycoprotein." Nature.

Li, J. (2015). "Molecular regulators of nerve conduction - Lessons from inherited neuropathies and rodent genetic models." Experimental Neurology **267**: 209-218.

Liu, B., Y. Su, T. Li, W. Yuan, X. Mo, H. Li, Q. He, D. Ma and W. Han (2015). "CMTM7 knockdown increases tumorigenicity of human nonsmall cell lung cancer cells and EGFR-AKT signaling by reducing Rab5 activation." Oncotarget **6**(38): 41092-41107.

Lu, J., Q. Q. Wu, Y. B. Zhou, K. H. Zhang, B. X. Pang, L. Li, N. Sun, H. S. Wang, S. Zhang, W. J. Li, W. Zheng and W. Liu (2016). "Cancer research advances regarding the CKLF-like MARVEL transmembrane domain containing family." Asian Pacific Journal of Cancer Prevention **17**(6): 2741-2744.

Mager, G. M., R. M. Ward, R. Srinivasan, S. W. Jang, L. Wrabetz and J. Svaren (2008). "Active gene repression by the Egr2·NAB complex during peripheral nerve myelination." Journal of Biological Chemistry.

Martini, R. and M. Schachner (1997). "Molecular bases of myelin formation as revealed by investigations on mice deficient in glial cell surface molecules." Glia **19**(4): 298-310.

Martini, R., J. Zielasek, K. V. Toyka, K. P. Giese and M. Schachner (1995). "Protein zero (P0)-deicient mice show myelin degradation in peripheral nerves characteristic of inherited human nueropathies." Nature **2**(11): 983-989.

McNeely, K. C., T. D. Cupp, J. N. Little, K. M. Janisch, A. Shrestha and N. D. Dwyer (2017). "Mutation of Kinesin-6 Kif20b causes defects in cortical neuron polarization and morphogenesis." Neural Development.

Mei, L. and K. A. Nave (2014). "Neuregulin-ERBB signaling in the nervous system and neuropsychiatric diseases." Neuron **83**(1): 27-49.

Meier, C., E. Parmantier, A. Brennan, R. Mirsky and K. R. Jessen (1999). "Developing schwann cells acquire the ability to survive without axons by establishing an autocrine circuit involving insulin-like growth factor, neurotrophin-3, and platelet-derived growth factor-BB." Journal of Neuroscience.

Meintanis, S., D. Thomaidou, K. R. Jessen, R. Mirsky and R. Matsas (2001). "The neuron-glia signal β-neuregulin promotes Schwann cell motility via the MAPK pathway." GLIA.

Ménager, C., N. Arimura, Y. Fukata and K. Kaibuchi (2004). "PIP3 is involved in neuronal polarization and axon formation." Journal of Neurochemistry.

Menon, K., M. N. Rasband, C. M. Taylor, P. Brophy, R. Bansal and S. E. Pfeiffer (2003). "The myelin-axolemmal complex: Biochemical dissection and the role of galactosphingolipids." Journal of Neurochemistry.

Meyer, D. and C. Birchmeier (1995). "Multiple essential functions of neuregulin in development." Nature.

Mezzadra, R., C. Sun, L. T. Jae, R. Gomez-Eerland, E. De Vries, W. Wu, M. E. W. Logtenberg, M. Slagter, E. A. Rozeman, I. Hofland, A. Broeks, H. M. Horlings, L. F. A. Wessels, C. U. Blank, Y. Xiao, A. J. R. Heck, J. Borst, T. R. Brummelkamp and T. N. M. Schumacher (2017). "Identification of CMTM6 and CMTM4 as PD-L1 protein regulators." Nature **549**(7670): 106-110.

Michailov, G. V., M. W. Sereda, B. G. Brinkmann, T. H. Fischer, B. Haug, C. Birchmeier, L. Role, C. Lai, M. H. Schwab and K. A. Nave (2004). "Axonal Neuregulin-1 Regulates Myelin Sheath Thickness." Science.

Mogha, A., M. D'Rozario and K. R. Monk (2016). "G Protein-Coupled Receptors in Myelinating Glia." Trends in Pharmacological Sciences **37**(11): 977-987.

Monk, K. R., M. L. Feltri and C. Taveggia (2015). "New insights on schwann cell development." Glia **63**(8): 1376-1393.

Moore, J. W., R. W. Joyner, M. H. Brill, S. D. Waxman and M. Najar-Joa (1978). "Simulations of conduction in uniform myelinated fibers. Relative sensitivity to changes in nodal and internodal parameters." Biophysical Journal.

Mukouyama, Y. S., H. P. Gerber, N. Ferrara, C. Gu and D. J. Anderson (2005). "Peripheral nerve-derived VEGF promotes arterial differentiation via neuropilin 1-mediated positive feedback." Development.

Mullis, K., F. Faloona, S. Scharf, R. Saiki, G. Horn and H. Erlich (1992). "Specific enzymatic amplification of DNA in vitro: the polymerase chain reaction. 1986." Biotechnology (Reading, Mass.).

Murinson, B. B. and J. W. Griffin (2004). "C-Fiber Structure Varies with Location in Peripheral Nerve." Journal of Neuropathology and Experimental Neurology.

Nave, K.-A. and B. D. Trapp (2008). "Axon-Glial Signaling and the Glial Support of Axon Function." Annual Review of Neuroscience **31**(1): 535-561.

Nave, K.-A. and H. B. Werner (2014). "Myelination of the Nervous System: Mechanisms and Functions." Annual Review of Cell and Developmental Biology **30**(1): 503-533.

Nave, K. A. (2010). "Myelination and support of axonal integrity by glia." Nature **468**(7321): 244-252.

Nave, K. A. (2010). Myelination and the trophic support of long axons.

Nave, K. A. and J. L. Salzer (2006). "Axonal regulation of myelination by neuregulin 1." Current Opinion in Neurobiology **16**(5): 492-500.

Netrakanti, P. R., B. H. Cooper, E. Dere, G. Poggi, D. Winkler, N. Brose and H. Ehrenreich (2015). "Fast Cerebellar Reflex Circuitry Requires Synaptic Vesicle Priming by Munc13-3." Cerebellum.

Niu, J., H. Li, Y. Zhang, J. Li, M. Xie, L. Li, X. Qin, Y. Qin, X. Guo, Q. Jiang, Y. Liu, S. Chen, X. Huang, W. Han and G. Ruan (2011). "Aberrant expression of CKLF-like MARVEL transmembrane member 5 (CMTM5) by promoter methylation in myeloid leukemia." Leukemia Research **35**(6): 771-776.

Norton, W. T. and L. A. Autilio (1965). "THE CHEMICAL COMPOSITION OF BOVINE CNS MYELIN." Annals of the New York Academy of Sciences.

Norton, W. T. and S. E. Poduslo (1973). "MYELINATION IN RAT BRAIN: CHANGES IN MYELIN COMPOSITION DURING BRAIN MATURATION." Journal of Neurochemistry.

Ogawa, Y. and M. N. Rasband (2009). "Proteomic analysis of optic nerve lipid rafts reveals new paranodal proteins." Journal of Neuroscience Research.

Paavola, K. J., H. Sidik, J. B. Zuchero, M. Eckart and W. S. Talbot (2014). "Type IV collagen is an activating ligand for the adhesion G protein-coupled receptor GPR126." Science Signaling.

Painter, M. W. (2017). "Aging Schwann cells: mechanisms, implications, future directions." Current Opinion in Neurobiology **47**: 203-208.

Palandri, A., V. R. Salvador, J. Wojnacki, A. L. Vivinetto, R. L. Schnaar and P. H. H. Lopez (2015). "Myelin-associated glycoprotein modulates apoptosis of motoneurons during early postnatal development via NgR/p75 NTR receptor-mediated activation of RhoA signaling pathways." Cell Death and Disease **6**.

Pan, B., S. E. Fromholt, E. J. Hess, T. O. Crwaford, J. W. Griffin, K. A. Sheikh and R. L. Schnaar (2007). "Myelin-associated glycoprotein and complementary axonal ligands, gangliosides, mediate axon stability in the CNS and PNS: Neuropathology and behavioral deficits in single- and double-null mice." Exp. Neurol. **195**(1): 208-217.

Panagopoulos, G., R. H. M. King, G. Gabriel, C. Stolinski, D. Sofer, F. Lachapelle and P. K. Thomas (1989). "Morphometric and freeze-fracture studies on peripheral nerve in shiverer mice." Journal of Comparative Neurology **286**(3): 337-344.

Pareyson, D. and C. Marchesi (2009). "Diagnosis, natural history, and management of Charcot-Marie-Tooth disease." The Lancet Neurology **8**(7): 654-667.

Parkinson, D. B., A. Bhaskaran, A. Droggiti, S. Dickinson, M. D'Antonio, R. Mirsky and K. R. Jessen (2004). "Krox-20 inhibits Jun-NH2-terminal kinase/c-Jun to control Schwann cell proliferation and death." Journal of Cell Biology.

Parmantier, E., B. Lynn, D. Lawson, M. Turmaine, S. S. Namini, L. Chakrabarti, A. P. McMahon, K. R. Jessen and R. Mirsky (1999). "Schwann cell-derived desert hedgehog controls the development of peripheral nerve sheaths." Neuron.

Patzig, J., O. Jahn, S. Tenzer, S. P. Wichert, P. de Monasterio-Schrader, S. Rosfa, J. Kuharev, K. Yan, I. Bormuth, J. Bremer, A. Aguzzi, F. Orfaniotou, D. Hesse, M. H. Schwab, W. Möbius, K. A. Nave and H. B. Werner (2011). "Quantitative and integrative proteome analysis of peripheral nerve myelin identifies novel myelin proteins and candidate neuropathy loci." Journal of Neuroscience.

Patzig, J., K. Kusch, R. Fledrich, M. A. Eichel, K. A. Lüders, W. Möbius, M. W. Sereda, K. A. Nave, R. Martini and H. B. Werner (2016). "Proteolipid protein modulates preservation of peripheral axons and premature death when myelin protein zero is lacking." Glia **64**(1): 155-174.

Peles, E., M. Nativ, M. Lustig, M. Grumet, J. Schilling, R. Martinez, G. D. Plowman and J. Schlessinger (1997). "Identification of a novel contactin-associated transmembrane receptor with multiple domains implicated in protein-protein interactions." EMBO Journal.

Pellerin, L., G. Pellegri, P. G. Bittar, Y. Charnay, C. Bouras, J. L. Martin, N. Stella and P. J. Magistretti Evidence supporting the existence of an activity-dependent astrocyte-neuron lactate shuttle.

Pereira, J. A., F. Lebrun-Julien and U. Suter (2012). Molecular mechanisms regulating myelination in the peripheral nervous system.

Perge, J. A., J. E. Niven, E. Mugnaini, V. Balasubramanian and P. Sterling (2012). "Why do axons differ in caliber?" Journal of Neuroscience **32**(2): 626-638.

Perrot, R., P. Lonchampt, A. C. Peterson and J. Eyer (2007). "Axonal neurofilaments control multiple fiber properties but do not influence structure or spacing of nodes of Ranvier." Journal of Neuroscience **27**(36): 9573-9584.

Pertusa, M., C. Morenilla-Palao, C. Carteron, F. Viana and H. Cabedo (2007). "Transcriptional control of cholesterol biosynthesis in schwann cells by axonal neuregulin 1." Journal of Biological Chemistry.

Petersen, S. C., R. Luo, I. Liebscher, S. Giera, S. J. Jeong, A. Mogha, M. Ghidinelli, M. L. Feltri, T. Schöneberg, X. Piao and K. R. Monk (2015). "The Adhesion GPCR GPR126 Has Distinct, Domain-Dependent Functions in Schwann Cell Development Mediated by Interaction with Laminin-211." Neuron.

Poliak, S. and E. Peles (2003). "The local differentiation of myelinated axons at nodes of ranvier." Nature Reviews Neuroscience **4**(12): 968-980.

Poliak, S., D. Salomon, H. Elhanany, H. Sabanay, B. Kiernan, L. Pevny, C. L. Stewart, X. Xu, S. Y. Chiu, P. Shrager, A. J. W. Furley and E. Peles (2003). "Juxtaparanodal clustering of Shaker-like K+ channels in myelinated axons depends on Caspr2 and TAG-1." Journal of Cell Biology.

Price, R. L., P. Paggi, R. J. Lasek and M. J. Katz (1988). "Neurofilaments are spaced randomly in the radial dimension of axons." Journal of Neurocytology.

Readhead, C., B. Popko, N. Takahashi, H. David Shine, R. A. Saavedra, R. L. Sidman and L. Hood (1987). "Expression of a myelin basic protein gene in transgenic shiverer mice: Correction of the dysmyelinating phenotype." Cell **48**(4): 703-712.

Rich, L. R. and A. M. Brown (2018). "Fibre sub-type specific conduction reveals metabolic function in mouse sciatic nerve." Journal of Physiology **596**(10): 1795-1812.

Riethmacher, D., E. Sonnenberg-Riethmacher, V. Brinkmann, T. Yamaai, G. R. Lewin and C. Birchmeier (1997). "Severe neuropathies in mice with targeted mutations in the ErbB3 receptor." Nature.

Rushton, W. A. H. (1951). "From the Physiological Laboratory , University of Cambridge." J. Physiol.

Sadahiro, S., H. Yoshikawa, N. Yagi, Y. Yamamoto, T. Yanagihara, M. Kimura and S. Sakoda (2000). "Morphometric analysis of the myelin-associated oligodendrocytic basic protein-deficient mouse reveals a possible role for myelin-associated oligodendrocytic basic protein in regulating axonal diameter." Neuroscience **98**(2): 361-367.

Saiki, R. K., D. H. Gelfand, S. Stoffel, S. J. Scharf, R. Higuchi, G. T. Horn, K. B. Mullis and H. A. Erlich (1988). "Primer-directed enzymatic amplification of DNA with a thermostable DNA polymerase." Science.

Salzer, J. L. (2003). Polarized domains of myelinated axons.

Salzer, J. L., P. J. Brophy and E. Peles (2008). "Molecular domains of myelinated axons in the peripheral nervous system." GLIA.

Sapir, T., T. Levy, A. Sakakibara, A. Rabinkov, T. Miyata and O. Reiner (2013). "Shootin1 acts in concert with KIF20B to promote polarization of migrating neurons." Journal of Neuroscience.

Saporta, M. A. and M. E. Shy (2013). Inherited peripheral neuropathies.

Schnaar, R. L. and P. H. H. Lopez (2009). Myelin-associated glycoprotein and its axonal receptors.

Shah, N. M., M. A. Marchionni, I. Isaacs, P. Stroobant and D. J. Anderson (1994). "Glial growth factor restricts mammalian neural crest stem cells to a glial fate." Cell.

Shao, L., Y. Cui, H. Li, Y. Liu, H. Zhao, Y. Wang, Y. Zhang, M. N. Ka, W. Han, D. Ma and Q. Tao (2007). "CMTM5 exhibits tumor suppressor activities and is frequently silenced by methylation in carcinoma cell lines." Clinical Cancer Research **13**(19): 5756-5762.

Shapiro, L., J. P. Doyle, P. Hensley, D. R. Colman and W. A. Hendrickson (1996). "Crystal structure of the extracellular domain from P0, the major structural protein of peripheral nerve myelin." Neuron **17**(3): 435-449.

Sherman, D. L., M. Krols, L. M. N. Wu, M. Grove, K. A. Nave, Y. G. Gangloff and P. J. Brophy (2012). "Arrest of myelination and reduced axon growth when Schwann cells lack mTOR." Journal of Neuroscience.

Shimada, T., M. Toriyama, K. Uemura, H. Kamiguchi, T. Sugiura, N. Watanabe and N. Inagaki (2008). "Shootin1 interacts with actin retrograde flow and L1-CAM to promote axon outgrowth." Journal of Cell Biology.

Silva, J. C., M. V. Gorenstein, G.-Z. Li, J. P. C. Vissers and S. J. Geromanos (2006). "Absolute Quantification of Proteins by LCMS E." Molecular & Cellular Proteomics.

Stassart, R. M., R. Fledrich, V. Velanac, B. G. Brinkmann, M. H. Schwab, D. Meijer, M. W. Sereda and K. A. Nave (2013). "A role for Schwann cell-derived neuregulin-1 in remyelination." Nature Neuroscience **16**(1): 48-54.

Stassart, R. M., W. Möbius, K. A. Nave and J. M. Edgar (2018). "The Axon-Myelin unit in development and degenerative disease." Frontiers in Neuroscience **12**(JUL).

Stettner, G. M., S. Zanella, P. Huppke, J. Gärtner, G. Hilaire and M. Dutschmann (2008). "Spontaneous central apneas occur in the C57BL/6J mouse strain." Respiratory Physiology and Neurobiology.

Stewart, H. J. S., A. Brennan, M. Rahman, G. Zoidl, P. J. Mitchell, K. R. Jessen and R. Mirsky (2001). "Developmental regulation and overexpression of the transcription factor AP-2, a potential regulator of the timing of Schwann cell generation." European Journal of Neuroscience.

Suter, U., J. J. Moskow, A. A. Welcher, G. J. Snipes, B. Kosaras, R. L. Sidman, A. M. Buchberg and E. M. Shooter (1992). "A leucine-to-proline mutation in the putative first transmembrane domain of the 22-kDa peripheral myelin protein in the trembler-J mouse." Proceedings of the National Academy of Sciences of the United States of America **89**(10): 4382-4386.

Suter, U., A. A. Welcher, G. J. Snipes and A. A. Welcher (1993). "Progress in the molecular understanding of hereditary peripheral neuropathies reveals new insights into the biology of the peripheral nervous system." **22**(Mdl).

Syroid, D. E., P. R. Maycox, P. G. Burrola, N. Liu, D. Wen, K. F. Lee, G. Lemke and T. J. Kilpatrick (1996). "Cell death in the Schwann cell lineage and its regulation by neuregulin." Proceedings of the National Academy of Sciences of the United States of America.

Szaro, B. G., M. H. Whitnall and H. Gainer (1990). "Phosphorylation-Dependent epitopes on neurofilament proteins and neurofilament densities differ in axons in the corticospinal and primary sensory dorsal column tracts in the rat spinal cord." Journal of Comparative Neurology.

Tait, S., F. Gunn-Moore, J. M. Collinson, J. Huang, C. Lubetzki, L. Pedraza, D. L. Sherman, D. R. Colman and P. J. Brophy (2000). "An oligodendrocyte cell adhesion molecule at the site of assembly of the paranodal axo-glial junction." Journal of Cell Biology.

Tasaki, I. (1939). "THE ELECTRO-SALTATORY TRANSMISSION OF THE NERVE IMPULSE AND THE EFFECT OF NARCOSIS UPON THE NERVE FIBER." American Journal of Physiology-Legacy Content.

Taveggia, C., G. Zanazzi, A. Petrylak, H. Yano, J. Rosenbluth, S. Einheber, X. Xu, R. M. Esper, J. A. Loeb, P. Shrager, M. V. Chao, D. L. Falls, L. Role and J. L. Salzer (2005). "Neuregulin-1 type III determines the ensheathment fate of axons." Neuron.

Traka, M., L. Goutebroze, N. Denisenko, M. Bessa, A. Nifli, S. Havaki, Y. Iwakura, F. Fukamauchi, K. Watanabe, B. Soliven, J. A. Girault and D. Karagogeos (2003). "Association of TAG-1 with Caspr2 is essential for the molecular organization of juxtaparanodal regions of myelinated fibers." Journal of Cell Biology.

Trapp, B. D. and R. H. Quarles (1982). "Presence of the myelin-associated glycoprotein correlates with alterations in the periodicity of peripheral myelin." Journal of Cell Biology **92**(3): 877-882.

Vaughan, D. W. (1992). "Effects of advancing age on peripheral nerve regeneration." J Comp Neurol **323**(2): 219-237.

Verdú, E., M. Butí and X. Navarro (1996). "Functional changes of the peripheral nervous system with aging in the mouse." Neurobiology of Aging.

Verdú, E., D. Ceballos, J. J. Vilches and X. Navarro (2000). "Influence of aging on peripheral nerve function and regeneration." Journal of the Peripheral Nervous System **5**(4): 191-208.

Wang, Y., J. Li, Y. Cui, T. Li, M. N. Ka, H. Geng, H. Li, X. S. Shu, H. Li, W. Liu, B. Luo, Q. Zhang, T. S. K. Mok, W. Zheng, X. Qiu, G. Srivastava, J. Yu, J. J. Y. Sung, A. T. C. Chan, D. Ma, Q. Tao and W. Han (2009). "CMTM3, located at the critical tumor suppressor locus 16q22.1, is silenced by CpG methylation in carcinomas and inhibits tumor cell growth through inducing apoptosis." Cancer Research **69**(12): 5194-5201.

Warner, L. E., M. J. Hilz, S. H. Appel, J. M. Killian, E. H. Kolodny, G. Karpati, S. Carpenter, G. V. Watters, C. Wheeler, D. Witt, A. Bodell, E. Nelis, C. Van Broeckhoven and J. R. Lupski (1996). "Clinical phenotypes of different MPZ (P0) mutations may include Charcot-Marie-Tooth type 1B, Dejerine-Sottas, and congenital hypomyelination." Neuron.

Waxman, S. G. (1980). "Determinants of conduction velocity in myelinated nerve fibers." Muscle & Nerve **3**(2): 141-150.

Webster, H. d. F., J. R. Martin and M. F. O'Connell (1973). "The relationships between interphase Schwann cells and axons before myelination: A quantitative electron microscopic study." Developmental Biology.

Werner, H. B., K. Kuhlmann, S. Shen, M. Uecker, A. Schardt, K. Dimova, F. Orfaniotou, A. Dhaunchak, B. G. Brinkmann, W. Möbius, L. Guarente, P. Casaccia-Bonnefil, O. Jahn and K. A. Nave (2007). "Proteolipid protein is required for transport of sirtuin 2 into CNS myelin." Journal of Neuroscience.

Wiśniewski, J. R., A. Zougman, N. Nagaraj and M. Mann (2009). "Universal sample preparation method for proteome analysis." Nature Methods.

Woldeyesus, M. T., S. Britsch, D. Riethmacher, L. Xu, E. Sonnenberg-Riethmacher, F. Abou-Rebyeh, R. Harvey, P. Caroni and C. Birchmeier (1999). "Peripheral nervous system defects in erbB2 mutants following genetic rescue of heart development." Genes and Development.

Wu, L. M. N., A. Williams, A. Delaney, D. L. Sherman and P. J. Brophy (2012). "Increasing internodal distance in myelinated nerves accelerates nerve conduction to a flat maximum." Current Biology **22**(20): 1957-1961.

Yin, X., T. O. Crawford, J. W. Griffin, P. H. Tu, V. M. Y. Lee, C. Li, J. Roder and B. D. Trapp (1998). "Myelin-associated glycoprotein is a myelin signal that modulates the caliber of myelinated axons." Journal of Neuroscience **18**(6): 1953-1962.

Zeisel, A., A. B. Munoz-Manchado, S. Codeluppi, P. Lonnerberg, G. La Manno, A. Jureus, S. Marques, H. Munguba, L. He, C. Betsholtz, C. Rolny, G. Castelo-Branco, J. Hjerling-Leffler and S. Linnarsson (2015). "Brain structure. Cell types in the mouse cortex and hippocampus revealed by single-cell RNA-seq." Science **347**(6226): 1138-1142.

Zhang, Y., K. Chen, S. A. Sloan, M. L. Bennett, A. R. Scholze, S. O'Keeffe, H. P. Phatnani, P. Guarnieri, C. Caneda, N. Ruderisch, S. Deng, S. A. Liddelow, C. Zhang, R. Daneman, T. Maniatis, B. A. Barres and J. Q. Wu (2014). "An RNA-sequencing transcriptome and splicing database of glia, neurons, and vascular cells of the cerebral cortex." Journal of Neuroscience.

Zollinger, D. R., K. L. Baalman and M. N. Rasband (2015). "The Ins and Outs of Polarized Axonal Domains." Annual Review of Cell and Developmental Biology **31**(1): 647-667.

7 Addendum

7.1 R Script for statistical assessment of axonal diameters

```
setwd("~/")

library("xlsx")
library("lmtest")
library("ggplot2")

cn <- read.xlsx("Ctrl.xlsx", 1)
ck <- read.xlsx("cko.xlsx", 1)
View(McNeely, Cupp et al.)
View(ck)

cn <- data.frame(cn = cn)
names(McNeely, Cupp et al.) <- c("1","2","3","4","5")
cn1 <- c(na.omit(cn[,1]), na.omit(cn[,2]), na.omit(cn[,3]),
         na.omit(cn[,4]), na.omit(cn[,5]))

ck <- data.frame(ck = ck)
names(ck) <- c("1","2","3","4","5")
ck1 <- c(na.omit(ck[,1]), na.omit(ck[,2]), na.omit(ck[,3]),
         na.omit(ck[,4]), na.omit(ck[,5]))

a <- data.frame(y = cn1)
a$x <- "control"
b <- data.frame(y = ck1)
b$x <- "cko"
d <- rbind(a,b)

d$x <- as.factor(d$x)
levels(d$x)
d$x <- relevel(d$x, ref = "control")

View(d)

head(cn1)
length(cn1)
mean(cn1)
var(cn1)
head(ck1)
length(ck1)
mean(ck1)
var(ck1)

t.test(d$y[d$x == "control"], d$y[d$x == "cko"])
```

```
t.test(d$y[d$x == "control"], d$y[d$x == "cko"], alternative =
 "less")

lm1 <- lm(d$y ~ d$x)
summary(lm1)

ks.test(d$y[d$x == "control"], d$y[d$x == "cko"])

ks.test(d$y[d$x == "control"], d$y[d$x == "cko"],
        alternative = "less")
ks.test(d$y[d$x == "control"], d$y[d$x == "cko"],
        alternative = "greater")

m <- as.matrix(summary(lm1)$coeff)
m1 <- as.data.frame(m)
write.xlsx(m1, "Name.xlsx")
```

7.2 Statistical analysis of axonal diameters

Table 1 Statistical analysis of axonal diameters throughout this study. Data depicts the statistical analysis performed with R including type of nerve, age, p-values for t-Test and Kolmogorow-Smirnow test, the Mean of axonal diameter in control group +/- mean of axonal diameter change in mutant mice (averaged for each axon) as well as the number of axons in total which were analyzed and statistically assessed in respect to axonal diameter distribution. Note that the total number of myelinated axons differs and is not included in this table but in respective graphs. Most of the data come from n=5 biological replicates unless indicated otherwise in respective figure legends.

Ctrl vs. *Cmtm6* cKo	**Age**	**tTest**	**Mean+/-**	**K&S Test**	**Axon# Ctrl**	**Axon # cKo**
Sciatic nerve	P9	0,3648	1,77+0.0005	0.0246	16350	15775
	1 mo	<2.2e-16	2,68+0.12	<2.2e-16	17578	16966
	2 mo	9.56e-12	3.16+0.09	1.22e-5	19250	18966
	6 mo	<2.2e-16	3.84+0.2	2.76e-12	17665	19196
	1 yr	0.5961	4.02-0.01	0.64	17646	17321
Phrenic nerve	2 mo	<2.2e-16	2.84+0.84	2.2e-16	1293	1172
Dorsal root	2 mo	<2.2e-16	2.47+0.27	<2.2e-16	10387	9298
Non-myelinated axons	P9	0.001048	0.46+0.02	0.002	690	709
	2 mo	<2.2e-16	0.19+0.08	<2.2e-16	2522	2377
Ctrl vs. *Cmtm6* iKo	2 mo p.T.i.	0.02616	3.57+0.03	0.0027	14814	20067

	6 mo p.T.i.	4.74e-16	4.05+0.17	2.98e-10	19025	15047
Ctrl vs *Mag* Ko	P75	2.2e-16	3.26-0.17	2.2e-16	12793	16790
Ctrl vs. *Cmtm6* cKo;*Mag* Ko	2 mo	1.16e-11	3.13+0.09	0.000146	19108	18003

7.3 Supplementary data Fig. 6: Proteomic analysis of AEF purified from murine wild-type sciatic nerves

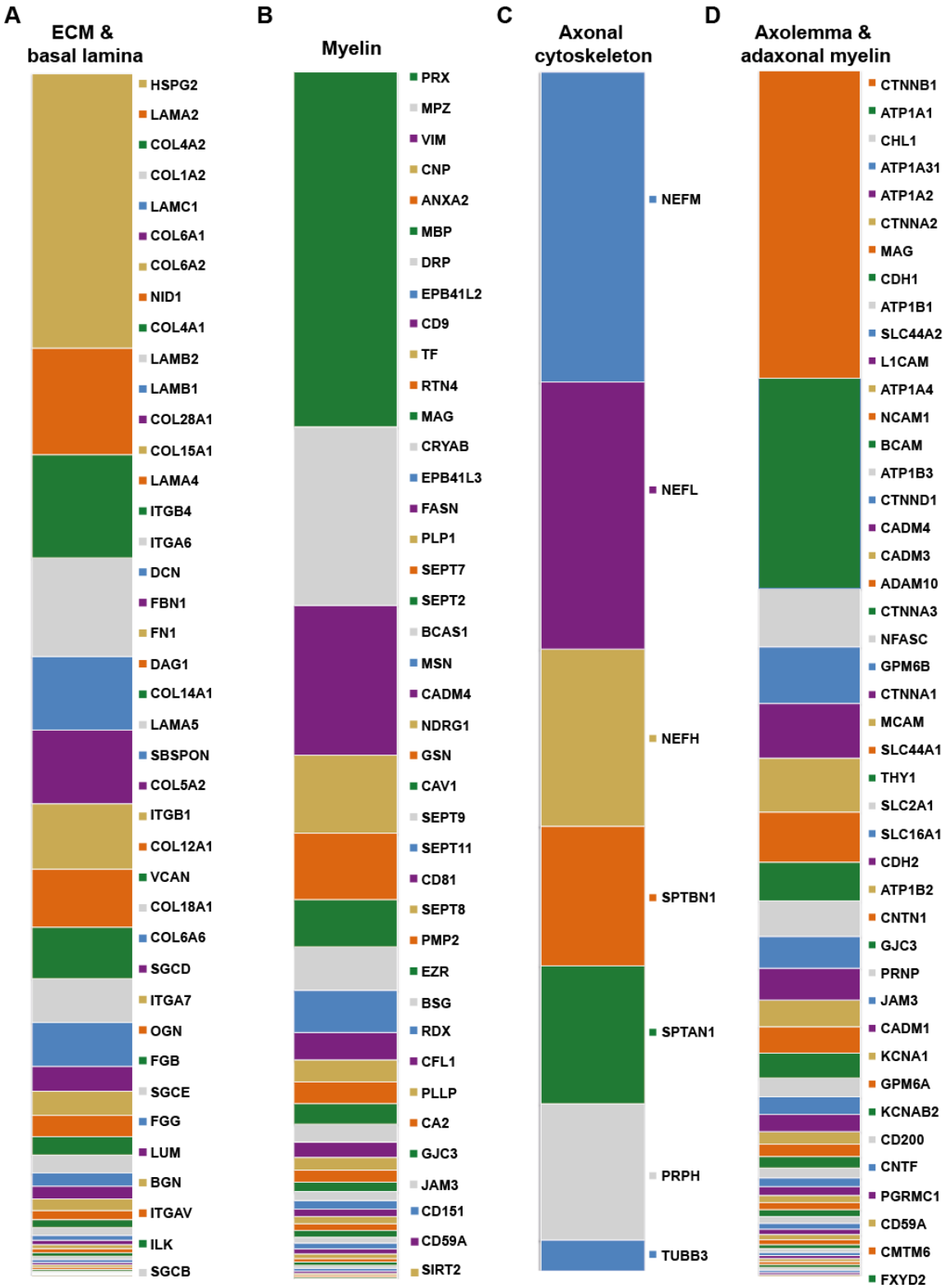

Figure 27 Protein composition of ECM and basal lamina, axolemma and adaxonal myelin, axonal cytoskeleton and myelin in the axolemma and adaxonal myelin enriched fraction (AEF). Bar charts showing protein composition of selected extracellular matrix (ECM) and basal lamina proteins (A), axolemma and adaxonal myelin proteins (B), axonal cytoskeleton proteins (C) and myelin protein (D) of the axolemma and adaxonal myelin enriched fraction (AEF) purified from sciatic nerves of adult WT mice.

Table 2 Exact ppm and CT% values for selected proteins of ECM and basal lamina, axolemma and adaxonal myelin, axonal cytoskeleton and myelin in the AEF purified from wild-type sciatic nerves.

ECM and basal lamina

	average ppm	% CV bio
Sgcb	135,89183	0,113962
Ilk	182,667263	0,129023
Itgav	189,402495	0,189051
Bgn	223,384794	0,240537
Lum	224,684682	0,212287
Fgg	241,390119	0,232638
Sgce	321,057068	0,147409
Fgb	427,839989	0,157002
Ogn	590,217732	0,427397
Itga7	598,892953	0,393118
Sgcd	607,354287	0,170341
Col6a6	764,753625	0,273905
Col18a1	851,145503	0,142925
Vcan	907,625518	0,14923
Col12a1	1049,54141	0,143786
Itgb1	1051,16667	0,142545
Col5a2	1157,26364	0,220454
Sbspon	1205,20023	0,209203
Lama5	2038,02194	0,153614
Col14a1	2069,06601	0,19157
Dag1	2310,27251	0,128199
Fn1	2993,43186	0,624693
Fbn1	3329,23384	0,193414
Dcn	3375,67808	0,161078
Itga6	4627,34376	0,122106
Itgb4	4741,42849	0,110315
Lama4	5496,33498	0,119854
Col15a1	6185,51556	0,152919
Col28a1	6441,11594	0,278102
Lamb1	11301,386	0,123273
Lamb2	11325,7392	0,136897
Col4a1	13282,0528	0,132358
Nid1	14943,9659	0,105614
Col6a2	16857,2731	0,123211
Col6a1	18965,5814	0,110399
Lamc1	19005,263	0,137865
Col1a2	25406,7564	0,158392
Col4a2	26638,514	0,106823
Lama2	27462,8959	0,129781
Hspg2	70740,5781	0,134567

Myelin Proteins

	average ppm	% CV bio
Sirt2	50,16176289	0,152546463
Cd59a	58,01241045	0,246093416
Cd151	66,28546641	0,276992245
Jam3	94,76414084	0,161354875
Gjc3	112,5116991	0,21362747
Ca2	119,2071063	0,512541552
Pllp	128,018304	0,165191284
Cfl1	134,2386432	0,424760258
Rdx	172,5524876	0,230556505
Bsg	199,7850582	0,114987668
Ezr	203,961151	0,175454327
Pmp2	228,8893647	0,37700527
Sept8	253,60735	0,148565673
Cd81	333,9421426	0,221461301
Sept11	360,5763571	0,190257841
Sept9	410,6476359	0,132186274
Cav1	414,7150393	0,14209295
Gsn	480,5432284	0,12159615
Ndrg1	482,2795149	0,204305188
Cadm4	502,5320723	0,14096139
Msn	537,0560236	0,161170558
Bcas1	596,2956786	0,138941965
Sept2	649,7104519	0,101041993
Sept7	661,9538265	0,150244754
Plp1	859,2663176	0,469931691
Fasn	911,5485422	0,128023366
Epb41l3	1080,86852	0,181654002
Cryab	1277,359248	0,157435333
Mag	1468,248431	0,157039018
Rtn4	1541,618539	0,229125323
Tf	1568,668341	0,247962743
Cd9	1945,205517	0,143380936
Epb41l2	3012,414103	0,072333961
Drp2	3079,005705	0,120468577
Mbp	3363,328242	0,289778442
Anxa2	4733,872151	0,151631308
Cnp	5548,888292	0,130625233
Vim	10648,12063	0,297614705
Mpz	12703,09565	0,134573383
Prx	25263,04526	0,039101204

Axonal Cytoskeleton

	average ppm	% CV bio
Tubb3	1847,72639	0,218839
Prph	8034,58039	0,204542
Sptan1	8137,92327	0,168215
Sptbn1	8238,80024	0,129321
Nefh	10440,0326	0,265167
Nefl	15757,4292	0,162812
Nefm	18286,3202	0,165102

Axolemma & adaxonal myelin

	average ppm	% CV bio
CTNNB1	9026,027046	0,210466826
ATP1A1	6172,300681	0,127409442
CHL1	1719,233255	0,185765695
ATP1A3	1666,224258	0,245775628
ATP1A2	1603,237128	0,123111861
CTNNA2	1586,58679	0,314305973
MAG	1468,248431	0,157039018
CDH1	1144,14384	0,138853218
ATP1B1	1038,420249	0,221322929
SLC44A2	937,0069446	0,073277556
L1CAM	935,2063333	0,139780157
ATP1A4	780,2376304	0,3185284
NCAM1	772,6473398	0,105418984
BCAM	731,5198814	0,090812128
ATP1B3	557,0547265	0,111605009
CTNND1	516,9010873	0,10111346
CADM4	502,5320723	0,14096139
CADM3	366,9706671	0,161235036
ADAM10	365,5711336	0,141634801
CTNNA3	332,7907845	0,142217402
NFASC	291,5000563	0,201199343
GPM6B	260,9654156	0,290787792
CTNNA1	256,2057785	0,1384878
MCAM	208,6050642	0,072454452
SLC44A1	207,8883171	0,128536805
THY1	203,1638096	0,215022852
SLC2A1	202,0143289	0,209280292
SLC16A1	168,3203607	0,117570766
ATP1B2	150,2252331	0,160742297
CNTN1	146,3377667	0,210713043
GJC3	112,5116991	0,21362747
PRNP	111,4582746	0,264381373
JAM3	94,76414084	0,161354875
CADM1	90,55277051	0,101715066
KCNA1	86,56533465	0,221670794
GPM6A	85,64992542	0,089638203
KCNAB2	85,28320366	0,449012248
CD200	79,31774023	0,098833235
CNTF	69,18055765	0,160306479
PGRMC1	65,47020815	0,13486754
CD59A	58,01241045	0,246093416
CMTM6	49,52970659	0,10281971
FXYD2	9,538251399	0,172219527

8 Curriculum Vitae